

Texas Southern University

Digital Scholarship @ Texas Southern University

Dissertations (2016-Present)

Dissertations

12-2023

Discovery Of Novel Hit Molecules Targeting Parp1 Using Structure-Based Design

Shahrazad Polk

Texas Southern University

Follow this and additional works at: <https://digitalscholarship.tsu.edu/dissertations>

 Part of the [Pharmacy and Pharmaceutical Sciences Commons](#)

Recommended Citation

Polk, Shahrazad, "Discovery Of Novel Hit Molecules Targeting Parp1 Using Structure-Based Design" (2023). *Dissertations (2016-Present)*. 89.

<https://digitalscholarship.tsu.edu/dissertations/89>

This Dissertation is brought to you for free and open access by the Dissertations at Digital Scholarship @ Texas Southern University. It has been accepted for inclusion in Dissertations (2016-Present) by an authorized administrator of Digital Scholarship @ Texas Southern University. For more information, please contact haiying.li@tsu.edu.

DISCOVERY OF NOVEL HIT MOLECULES TARGETING PARP1 USING STRUCTURE-
BASED DESIGN

DISSERTATION

Presented in Partial Fulfilment of the Requirements for the Degree, Doctor of Philosophy in the
Graduate School of Texas Southern University

By

Shahrazad M.K. Polk, B.S.

Texas Southern University

2023

Approved By

Dr. Selvam Chelliah

Chairperson, Dissertation Committee

Dr. Mahesh Vanjani

Dean, The Graduate School

Approved By

Dr. Selvam Chelliah
Chairperson, Dissertation Committee

9/18/23
Date

Dr. Shirlette Milton
Committee Member

9/18/23
Date

Dr. Kasturi Ranganna
Committee Member

9/18/23
Date

Dr. Hector Miranda
Committee Member

9/18/23
Date

© Copyright by Shahrazad Polk 2023

All Rights Reserved

DISCOVERY OF NOVEL HIT MOLECULES TARGETING PARP1 USING STRUCTURE-BASED DESIGN

By

Shahrazad M.K. Polk, B.S.

Texas Southern University, 2023

Professor Selvam Chelliah, Advisor

In the United States of America alone, cancer is the second highest cause of death. While there have been many remarkable breakthroughs in cancer research, there is still a need for the development of new therapies that target the different mechanisms of cancer cells. Therefore, the focus of our research is identifying novel hit molecules targeting Poly (ADP-ribose) polymerase 1.

Poly (ADP-ribose) polymerase 1 (PARP1) is an enzyme that has many distinct functions in the body. PARP1 has four domains: zinc fingers also known as the DNA binding domain, BRCT domain, WGR domain, and the ART catalytic domain. Its most notable function is in DNA repair, which is possible because of its DNA binding domain. PARP1 helps catalyze the DNA repair pathway of single-strand breaks.

Some of the deadliest cancers upregulate Poly (ADP-ribose) polymerase 1 to escape cell death, making it a suitable target for drug discovery. This study uses a combination of virtual high throughput screening, structure-based drug design, molecular dynamics, and inhibitor screening to identify molecules targeting Poly (ADP-ribose) polymerase 1. Herein we discovered Hit 10, Hit 17, Hit 22, and Hit 24 in our PARP1 inhibitory screening and Hit 2, Hit 8, Hit 13, Hit 18, and Hit 22 from our molecular dynamics study, and Hit 22 showed good results in molecular dynamics and screening with the PARP1

colorimetric kit with an IC_{50} value of 1.476 at 50 μ M. It also has a novel structure that has never been reported for PARP1 inhibition.

Based on our findings, Hit 22 could be a viable candidate for hit-to-lead characterization and could be evaluated further as a PARP1 inhibitor.

Keywords: DNA repair, cancer, PARP1

TABLE OF CONTENTS

	Page
LIST OF FIGURES	vi
LIST OF TABLES	viii
VITA	ix
DEDICATION	x
ACKNOWLEDGEMENTS	xi
CHAPTERS	
1. INTRODUCTION	1
2. LITERATURE REVIEW	5
2.01 Hallmarks of Cancer	5
2.02 New Approaches to Cancer Treatment	11
2.03 The PARP Family	13
2.04 PARPs in Hallmark Cancer Traits	18
2.05 PARP1 Structure	22
2.06 The Multifunctionality of PARP1	24
2.07 PARP1 and Neurodegenerative Diseases	28
2.08 PARPi Mechanism of Action	29

2.09	Overview of FDA-Approved PARPi	31
2.10	PARPi Resistance	32
2.11	Promising Novel PARPi	33
2.12	PARP1 Assay Method	34
2.13	Clinical Trials	35
2.14	Screening Libraries	38
2.15	Criteria of Drug Target Identification and Validation	38
2.16	Lipinski's Rule of Five	39
2.17	Virtual High Throughput Screening	42
2.18	Drug Design and its Methods	44
2.19	Methods of Virtual High Throughput Screening	46
2.20	Molecular Dynamics	49
3.	DESIGN OF STUDY	50
3.01	Central Hypothesis and Aims	50
3.02	Materials, Compounds, and Chemicals	51
3.03	Methods	53
4.	RESULTS	60

4.01	Protein-Ligand Interaction	60
4.02	Receptor File Generation	65
4.03	Hits' Chemical Classification	91
4.04	MD Simulations of Protein-Ligand Complexes	96
4.05	PARP Colorimetric Assay	102
5.	SUMMARY AND CONCLUSION	110
	REFERENCES	113

LIST OF FIGURES

Figure		Page
1	Estimated New Cases and Estimated Death for 20232	2
2	Rate of Incidence of cancer for males and females	3
3	Hallmarks of Cancer	5
4	PARP Family Functions	22
5	Molecular Mechanism of PARP1 in Neurodegeneration	28
6	PARPi Trapping Mechanism	29
7	Potency and Structure of FDA-Approved Inhibitors	31
8	Differences Between Synthetic and Natural Screening Sets	38
9	Rule of Five, Molecular Weight	40
10	Rule of Five, Hydrogen Bonds	40
11	Rule of Five, Hydrogen Bond Acceptors	41
12	Rule of Five, LogP	41
13	High Throughput Screening vs. <i>in silico</i> High Throughput Screening	42
14	The Four Major Class of Drug Design Methods	44
15	Structure-Based High Throughput Screening	46
16	Methods of Virtual Screening	47
17	Schematic Representation of PARP1 Colorimetric Assay	58
18	Protein-Ligand Interactions	61
19	Crucial Interactions between PARP1 and Marketed Drugs	62
20	Crucial Interactions between PARP1 and Marketed Drugs	63
21	Summary of Crucial Interactions	64

22	Receptor File Generation	65
23	Results from FRED Docking	66
24	Schematic Representation of Molecular Dynamics Study	96
25	Chemical Structure of Five Hits for Molecular Dynamics Study	97
26	Results from RMSD Analysis	98
27	Results from RMSF Analysis	99
28	Results from Rg Analysis	100
29	Results from H-bonding Analysis	101
30	Schematic Representation of PARP1 <i>in vitro</i> study	103
31	Chemical Structures and Interactions of Top hits from PARP1 inhibitory study	106
32	IC ₅₀ Graph of Selected Hits	108
33	Summary of Virtual Screening Results	109

LIST OF TABLES

Table		Page
1	Features of the PARP Family	21
2	Overview of Clinical Trials using PARPi	35
3	Classification of Chemical Structure Based on Heterocyclic Ring	91
4	Chemical Structure and ClogP of Top 25 Hits	92
5	Summary of MM/PBSA Calculations	102
6	PARP1 Inhibitory Activity	104
7	The IC ₅₀ values of selected hits, chemical structure, and heterocyclic ring classification	107

VITA

2017

Bachelor of Science,
College of Science, Engineering, and Technology
Texas Southern University

2018-2023

Graduate Research Assistant
College of Pharmacy and Health Science
Texas Southern University

Major Field

Pharmaceutical Sciences

DEDICATION

To

The unconditional love and support of my parents,

Jaqueline Thomas and Ernest Polk

My siblings,

Ernest Polk II, Kandaka Polk, and Jamal Polk

My nephew,

Romeo Polk,

My Aunt,

Yolanda Lumar,

And

My Grandparents,

Dorothy Thomas, Robert Thomas, Tom Polk, and Margurite Berry

ACKNOWLEDGEMENTS

I would like to first acknowledge God who led me on this path of scholarly knowledge and provided me with favor and understanding. I would also like to acknowledge my family who has been there for me, encouraging me all these years. Mom and Dad, your patience and love do not go unnoticed. My siblings Ernest, Kandaka, and Jamal, thank you for listening to me ramble on and on about chemistry, biology, and pharmaceutical sciences.

I want to thank the LSAMP program at TSU for taking me under their wing molding me into a researcher and always setting the bar high. A special thanks to Ms. Tolbert for keeping me on the right path to reach my goals.

I would like to thank my previous advisor Dr. Matin for teaching me so much in the little time we were together. I would like to special thanks to Jyotsna, a fellow PhD candidate who helped me learn various biology techniques. Thanks for your patience.

I would like to acknowledge and thank my current mentor and advisor, Dr. Chelliah for helping me reach the end of my education and preparing me for the next steps. I am glad to have been mentored by such a wonderful person.

I would like to thank Openeye Inc. for providing the academic license to use the virtual screening tools, and I would also like to acknowledge Sridhar Priyanka and Dr. Prakash for their work in our molecular dynamics study. We acknowledge the Center for Bioinformatics, the University of Hamburg for the online PoseView tool.

CHAPTER 1: INTRODUCTION

Despite advancements in cancer treatments such as innovative therapies, early detection methods, and precision medicine, the mortality rate of certain cancers remains high. After two decades of decline, prostate cancer incidence increased by 3% annually from 2014 through 2019, translating to an additional 99,000 new cases. African American men have the highest mortality rate (227.3 per 100,000) while Asian/Pacific Islander women have the lowest (85.6 per 100,000) (*Cancer Statistics - NCI, 2015*). From 2014 through 2018 there was an increase in female breast cancer and remained stable for prostate cancer (Siegel et al., 2022). However, lung cancer in women reduced at a slower than men (1.1% vs. 2.6% annually) from 2015 through 2019. Also, for women, liver, melanoma, breast, and uterine cancer increased over the studied period. While these cancers become more stabilized in men over 50 years old, the rate of incidence declines in younger men (Siegel et al., 2023). In 2020, approximately 16,850 children and adolescents aged 0 to 19 are expected to be diagnosed with cancer and 1,730 are predicted to die from it (*Cancer Statistics - NCI, 2015; Siegel et al., 2022*). There are over one million new cancer cases and 609,360 cancer deaths predicted to occur in the United States alone (Siegel et al., 2023). It is definitely mind-boggling. This includes over 300 deaths per day from lung cancer, which is the most diagnosed cancer in 2022 (Siegel et al., 2022). Because of the COVID-19 pandemic, there has been a dip in the diagnosis and treatment of cancer. This is from reduced access to care and lead to a temporary drop in cancer incidence followed by an increase in advanced-stage cancer (Yabroff et al., 2022). Every year the American Cancer Society publishes estimated cancer diagnoses and deaths of the ten most common cancers (Figure 1). Prostate and breast cancer has the highest diagnosis from 1975 to 2019, and both of these cancers are expected to be in the top 2 for estimated new cases and estimated deaths for 2023 (Siegel et al., 2023). The rate of incidence for prostate cancer and breast

cancer has stayed high from 1975-2019 (figure 2). It's concerning that individuals with a germline mutation in the breast cancer susceptibility genes BRCA1 or BRCA2 have a high risk of developing breast or ovarian cancer and are sensitive to DNA-damaging agents.

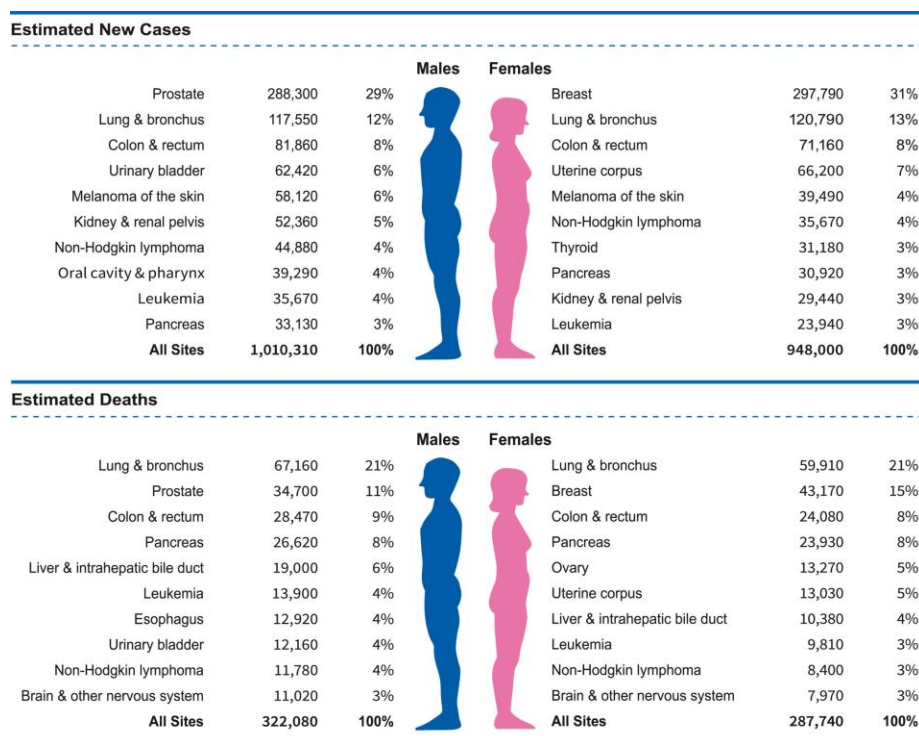


Figure 1: Estimated New Cases and Estimated Deaths for 2023

Reprinted from “Cancer statistics, 2023”, by Rebecca Siegal et. al., 2023 retrieved from

<https://doi.org/10.3322/caac.21763>

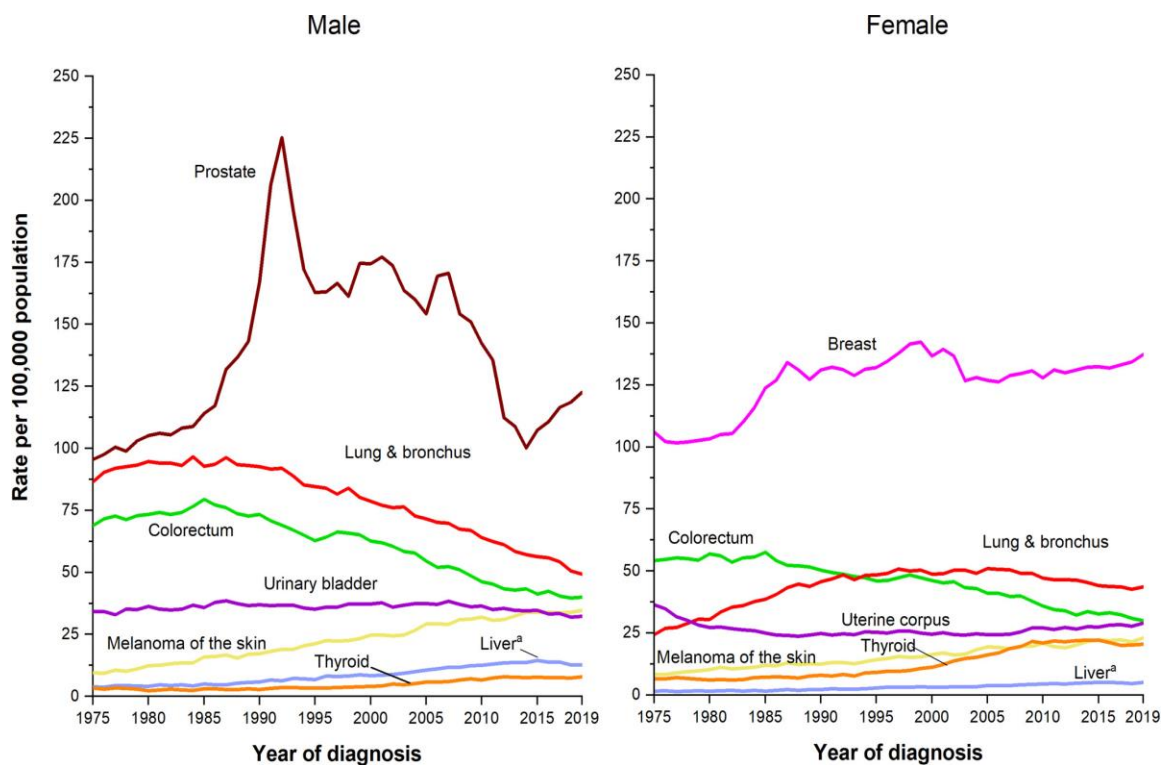


Figure 2: Rate of Incidence of cancer for males and females

Reprinted from “Cancer statistics, 2023”, by Rebecca Siegal et. al., 2023 retrieved from

<https://doi.org/10.3322/caac.21763>

DNA damage can occur from “dietary mutagenic chemicals, ultraviolet and ionizing radiation, and heavy metals” (Tice et al., 2000). These unrepaired or inaccurately repaired double-strand breaks (DSB) lead to the accumulation of damage to DNA. This manifests as genomic instability and drives carcinogenesis and disease progression. Homologous recombination defect (HRD) is identifiable in many cancers. A total of 50% have HRD, (Andrikopoulou et al., 2022; Lheureux et al., 2019; Stewart et al., 2022). Similarly, gBRCA1/2 mutations are approximately 15% of triple-negative breast cancers (TNBC) and a further 40% have HRD in the absence of gBRCA1/2 mutations (Barchiesi et al., 2021; Stewart et al.,

2022). In advanced prostate cancers, 10%–12% of patients have germline or somatic BRCA2 inactivation and up to 25% contain a DNA damage repair defect (Shah et al., 2021; Stewart et al., 2022). This just shows how prevalent HRD is in cancers. This mutation leads to an overexpression of enzymes like PARP1, which plays a crucial role in activating the DNA repair system.

CHAPTER 2
LITERATURE REVIEW

2.01 Hallmarks of Cancer

There are ten identified hallmarks, or characteristics of cancer. These include; “evading growth suppressors, avoiding immune destruction, enabling replicative immortality, tumor promoting inflammation, activating invasion and metastasis, inducing angiogenesis, genome instability and mutation, resisting cell death, deregulating cellular energetics, and sustaining proliferative signaling” (Figure 3) (Hanahan & Weinberg, 2011). Evading the body’s checkpoints, cancer cells can grow and thrive, so addressing these hallmarks are pertinent to cancer treatment.

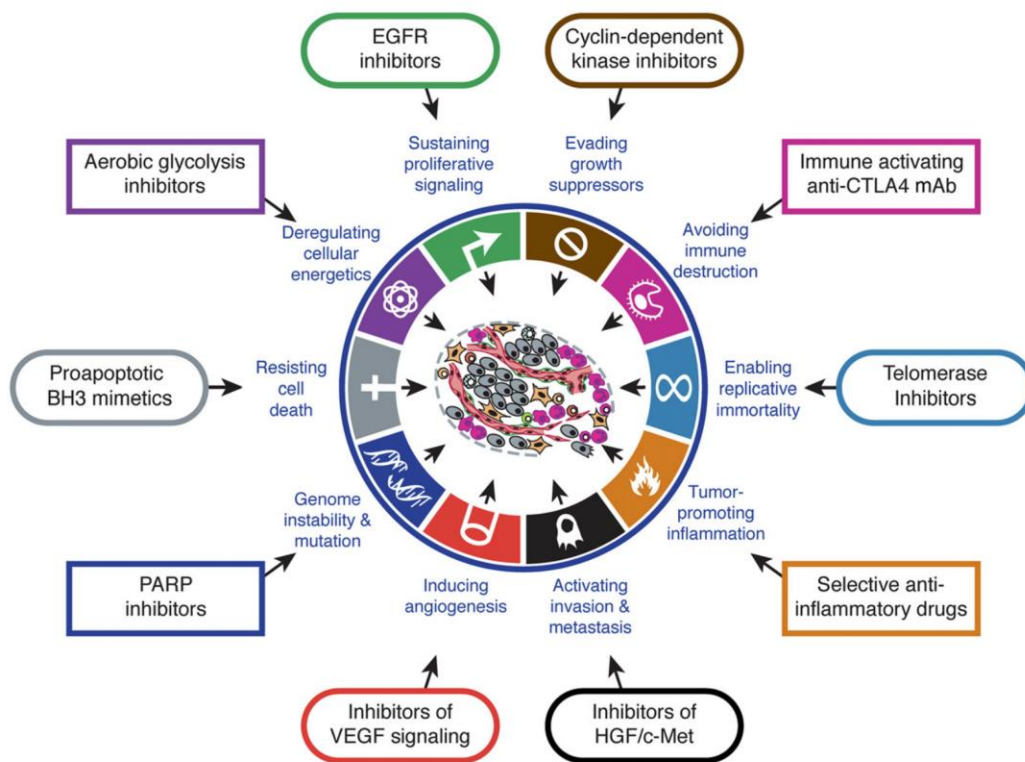


Figure 3: Hallmarks of Cancer

Reprinted from “Hallmarks of Cancer: Next Generation”, by Douglass Hanahan and Robert Weinberg, 2011, retrieved from [https://www.cell.com/fulltext/S0092-8674\(11\)00127-9](https://www.cell.com/fulltext/S0092-8674(11)00127-9)

Evading Growth Suppressors. For cancer cells to thrive, they need to not only maintain continuous proliferation but also evade the growth-suppressing mechanisms that regulate proliferation. Multiple tumor suppressors play a role in limiting cell growth and proliferation in cancer cells, with TP53 and retinoblastoma-associated proteins being the prototypical examples. These two proteins act as control centers, each contributing to complementary cellular regulatory pathways involved in proliferation, senescence activity, and apoptosis (Burkhart & Sage, 2008; Deshpande et al., 2005; Sherr & McCormick, 2002).

TP53, often referred to as the cell's inner operating system, receives inputs from sensors that detect stress and abnormalities. Upon detecting these signals, TP53 halts cell-cycle progression until suitable conditions such as growth-promoting signals, oxygenation, and glucose levels are restored to normal (Hanahan & Weinberg, 2011).

On the other hand, the RB protein integrates signals from various sources, both inside and outside the cell. The response of RB to these signals, particularly those originating from the extracellular environment, determines whether a cell should proceed with the growth and division cycle (Hanahan & Weinberg, 2011). This "gatekeeper" function is impaired in cancer cells, resulting in persistent cell proliferation.

Avoiding Immune Destruction. Cancer cells possess remarkable strategies to evade immune destruction, enabling their survival and proliferation within the body. One mechanism involves the downregulation or alteration of molecules on the cancer cell surface that are recognized by immune cells, such as major histocompatibility complex (MHC) molecules. By reducing MHC expression, cancer cells become less visible to the immune system, evading detection, and subsequent attack (Kallingal et al., 2023). Additionally, cancer cells can secrete immunosuppressive factors that dampen the activity of immune cells, preventing an effective immune response. These factors can inhibit the activation and

function of cytotoxic T cells and natural killer cells, which are essential for recognizing and eliminating cancer cells. Furthermore, cancer cells may exploit the immune checkpoint pathways, such as PD-1/PD-L1, to inhibit immune cell activation and promote immune tolerance (Ai et al., 2020). By engaging these inhibitory pathways, cancer cells effectively evade immune destruction, allowing them to persist and proliferate unchecked.

Enabling Replicative Immortality. Over the years, researchers have identified several signaling pathways that contribute to enabling replicative immortality in cancer cells. Two key components of this hallmark is the Hippo and Wnt signaling pathways.

The Hippo signaling pathway, which controls cell proliferation, apoptosis, and stem cell self-renewal, regulates organ size (Fu et al., 2022). This pathway ties into cancer development when it is not regulated correctly (Fu et al., 2022). Its mediators are Yes-associated protein 1 (YAP) and WW-domain-containing transcription regulator 1 (TAZ).

This pathway is 'off' when YAP and TAZ are not in their phosphorylated form (Kwon et al., 2013). If they are not phosphorylated, they will not translocate to the nucleus. It is only in the nucleus where YAP and TAZ can interact with other transcription factors. This interaction is important in regulating important cell proliferation and apoptosis genes.

The Hippo signaling pathway is involved in the development of various types of cancers, including liver, breast, lung, and pancreatic cancers. Targeting the Hippo signaling pathway has become an attractive therapeutic strategy for the treatment of cancer.

Like the Hippo signaling pathway, the Wnt signaling pathway can give cancer cells access to hallmark abilities, namely, replicative immortality. The main purpose of this pathway is to regulate stem cell differentiation during development (Azbazdar et al., 2021). Cancers show signs of transcriptional regulators accumulating in the nucleus. This is due to Wnt signaling (Koni et al., 2020).

β -catenin is a key downstream effector in the Wnt signaling pathway, and is linked to early embryonic development and tumorigenesis (Hayat et al., 2022). β -catenin translocate to the nucleus and binds to LEF1 and TCF, which provide docking sites for β -catenin (Koelman et al., 2022). This binding promotes the transcription of target genes once the Wnt signaling is activated.

Several studies have shown that the Wnt signaling pathway is dysregulated in various types of cancers, including colorectal, breast, and liver cancers. Targeting the Wnt signaling pathway has become an attractive therapeutic strategy for the treatment of cancer.

Tumor Promoting Inflammation To explain this hallmark simply, it occurs when tumors mimic the normal inflammatory environment (Greten & Grivennikov, 2019). Inflammation is a double-edged sword in the healing process. Normally, it is used to recruit the right factors, enzymes and regulators to damaged areas, but tumors can use this part of the healing process deceitfully to encourage tumorigenesis and ultimately progression to cancer (Kallingal et al., 2023). By 2000, there was evidence that the tumor-linked inflammatory response has contradictory effect of increasing tumorigenesis and progression, which helps early neoplasia gain hallmark capabilities (DeNardo & Ruffell, 2019; Grivennikov et al., 2010). In fact, inflammation is indicated in several hallmarks of cancer.

Furthermore, inflammation seems to be an important indication of earliest stages of neoplastic progression and is even able to provide the environment needed for developing neoplasia into cancers (Franceschi et al., 2018; Hanahan & Weinberg, 2011; Y. Li et al., 2017). Inflammatory cells are known to release reactive oxygen species (ROS), which are able to damage cells, accelerating their genetic development toward states that increase the chance of malignancy (Grivennikov et al., 2010). Therefore, inflammation is often seen as one of the most enabling characteristics for the acquisition of hallmark capabilities.

Activating Invasion and Metastasis. Invasion and metastasis are mechanisms of cancerous cell survival that are integral in the tumor cell's ability to escape from its primary site and disseminate into distant organs. It is a sequential, multistep process of discrete steps coined the invasion metastasis cascade (Fidler, 2003; Talmadge & Fidler, 2010). As cell-biological changes start with local invasion, the process proceeds with a succession of steps. The steps continue with cancer cell intravasation into blood and lymphatic vessels in surrounding areas. Next, cancer cells transverse through the lymphatic and hematogenous systems, which leads to metastasis of cancer cells often referred to as micro-metastasis (Hanahan & Weinberg, 2011). A transmembrane protein, such as e-cadherin, assists cells in adhesion to other cells and to the extracellular matrix (EC) in the metastatic process (Hanahan & Weinberg, 2011).

Inducing Angiogenesis. To sustain themselves, cancer cells use angiogenesis or the formation of new blood vessels. Tumors still need nutrients and oxygen to survive. The tumor-associated neo-vasculature, generated by the activity of angiogenesis gives the tumor micro-environment these needs. As a tumor progresses an 'angiogenic switch' is almost always activated. This causes normally inactive vasculature to repeatedly sprout new vessels that helps continue the expansion of neoplastic growths (Hanahan & Weinberg, 2011).

Genome Instability and Mutation. Subclones of cells are given a selection advantage by certain mutant genotypes, enabling their expansion and eventual domination in a specific tissue environment. As a result, it is possible to conceptualize multistep tumor evolution as a series of clonal expansions, each of which is initiated by the accidental discovery of an enabling mutant genotype.

Rates of spontaneous mutation are typically quite low throughout each cell generation due to the exceptional capacity of genome maintenance systems to identify and correct DNA flaws. Cancer cells frequently increase the rates of mutation as they amass the collection of mutant genes required to orchestrate carcinogenesis. This mutation is attained either by heightened susceptibility to mutagenic

agents, by a malfunction in one or more parts of the genomic maintenance machinery, or by a combination of the two. This accumulation is accelerated by failures in the surveillance systems that normally regulate the genome. This forces the cell into senescence or apoptosis (Jackson & Bartek, 2009; Kastan, 2008).

Resisting Cell Death. Apoptosis is a natural phase of the cell cycle that protects our bodies from the development of cancer. Understanding the signaling pathway that governs the apoptosis process has shed light on the ways in which various physiological stimuli or anticancer medications cause apoptosis. By removing the TP53 tumor suppressor function, the tumor cell develops a variety of methods to avoid or, at best, limit apoptosis (Papaliagkas et al., 2007). The apoptosis-inducing complex's severely damaged system is removed when the suppressor is eliminated. Other strategies may potentially be used by tumors to prevent apoptosis (Shukla et al., 2017; Yue et al., 2015).

Deregulating Cellular Energetics. It is difficult to precisely pinpoint the underlying processes of invasion and metastasis. However, it is evident that cancer cells usually undergo fluctuations in their shape, attachment to other cells, and in extracellular matrix (ECM) (Frantz et al., 2010; Rozario & DeSimone, 2010).

One of the most well-studied alterations include cancer cells losing E-cadherin, which is critical in cell-to-cell adhesion. E-cadherin assists in the formation of epithelial cell sheets and the maintenance of cell quiescence within these sheets by creating adherens junctions with neighboring epithelial cells. The widespread downregulation of E-cadherin in human carcinomas provides significant support for its involvement as a critical suppressor of this characteristic capability (Berx & Roy, 2009).

Sustaining Proliferative Signaling. Proliferative signaling is an extremely important hallmark trait of cancer. In normal tissue proliferative signaling controls, the production and release of growth-promoting signals conduct the entry and progression of the cell growth and division cycle. Cancer cells deregulate

these signals to proliferate infinitely. By deregulating these signals, cancer cells become masters of their own fate. The enabling signals are mainly mediated by growth factors that bind cell surface receptors that typically contain intracellular tyrosine kinase domains (Hanahan & Weinberg, 2011).

On the other hand, there is more research and a better understanding of mitogenic signaling in regards to cancer cells (Lemmon & Schlessinger, 2010). Cancer cells can develop the ability to sustain proliferative signals in a variety of ways such as generating their own growth factors. In response cancer cells express homologous receptors so the damage can be repaired. In addition, cancer cells may convey signals to encourage normal cells inside the tumor-associated stroma, which respond by providing numerous growth factors to the cancer cells (Bhowmick et al., 2004). Increased amounts of receptor proteins on the cancer cell surface can also disrupt receptor signaling.

2.02 New Approaches to Cancer Treatment

Cancer treatment has undergone significant advances in recent years, with novel therapies and treatment strategies being developed to improve patient outcomes. Precision medicine, immunotherapy, targeted therapy, and combination therapy are some of the latest approaches in cancer treatment.

Targeted therapies are designed to selectively target cancer cells while minimizing damage to healthy cells. The PI3K/Akt/mTOR (PAM) pathway is a crucial regulator of cell growth, survival, and proliferation (Miricescu et al., 2020). Endocrine-resistant breast cancers show increased activation of the PAM pathway, leading to a growing interest in targeting this pathway in cancer treatment (Miricescu et al., 2020; Zhu et al., 2022). PI3K is made up of two subunits, p85, and p110 (Jiménez et al., 2002). Upon receptor tyrosine kinase (RTK) stimulation, phosphorylated tyrosine residues to p85 subunits, which then recruit and activate p110 subunits via Ras proteins (Liu et al., 2009). This process leads to the conversion of phosphatidylinositol-4,5-biphosphate (PIP2) to phosphatidylinositol-3,4,5-triphosphate

(PIP3). After that a serine/threonine kinase is phosphorylated which then activates mTORC1 and mTORC2. The main function of this activation is cell anabolic growth from increased protein synthesis (Choo et al., 2010). Breast cancer cells may continue to proliferate, even in the presence of endocrine therapy, due to activating mutations in PI3K and/or aberrant signaling in the absence of growth factors.

Immunotherapy, which includes immune checkpoint inhibitors and CAR T-cell treatment, harnesses the immune system of the patient to combat cancer. Immune checkpoints play an important role in immune response regulation, immunological tolerance maintenance, and tissue damage prevention. However, increased expression of checkpoints during tumor formation and activation might contribute to immune evasion by limiting immune cell activity. Fortunately, immune checkpoint inhibitors can block immunosuppressive signals and restore or enhance the body's antitumor immune response (Sasidharan Nair & Elkord, 2018; Y. Zhang & Zheng, 2020). The primary immune checkpoints are cytotoxic T lymphocyte antigen 4 (CTLA-4), programmed cell death protein 1 (PD-1), and programmed cell death ligand 1 (PD-L1) (Ai et al., 2020; Chang et al., 2017). CTLA-4 is found on activated CD8+ and CD4+ T cells and competes with the costimulatory receptor CD28 to bind to ligands B7-1 and B7-2 on antigen-presenting cells (APCs) (H. Zhang et al., 2021). This competition results in the downstream negative regulation of immune responses, leading to T-cell suppression, and inhibiting the immune response to tumor cells. PD-1, like CTLA-4, is also expressed on T cells and binds to PD-L1 on tumor cells, APCs, and T cells, leading to the suppression of T cell responses and inhibiting adequate immune responses to tumor cells. Combination therapy, which involves the use of two or more therapies, has shown promise in overcoming treatment resistance and improving outcomes. Precision medicine uses genomic information to identify specific mutations that drive cancer growth, allowing for personalized treatment plans tailored to each patient's unique tumor characteristics.

2.03 The PARP Family

Poly (ADP-ribose) polymerase (PARP) is a family of enzymes that catalyzes the transfer of Poly (ADP-ribose) (PAR) onto proteins from NAD⁺. This important family of enzymes was first discovered over 50 years ago (Kraus, 2015). The PARP family contributes to many functions in the body (figure 4). Because of such a broad function, PARP1 is essential to many functions of the body including inflammation, cell death, DNA repair, transcription regulation, and chromatin modification. PARP enzymes have diverse sizes and structures, leading to a wide range of functions (table 1). They vary in size from 36.38 kDa to 202.8 kDa, and their catalytic activity produces either PAR or MAR modifications (Jubin et al., 2016).

Now, there are around 17 members in the PARP family identified (Demény & Virág, 2021). Based on the ribosylation type, PARPs can be categorized as mono- (ADP ribose) (MAR) or poly- (ADP ribose) (PAR). PARP1-2/4/5a/5b produce PAR modifications, and PARP3/4/6-12/14-16 produce MAR modifications (Demény & Virág, 2021; Jubin et al., 2016). This indicates differences in biological functions between the PARP family. The family can also be categorized by function. The structures and size of the PARP family vary vastly, and this causes many different and distinct functions. For example, the nicotinamide binding pocket (H-Y-E) is found in PARP1-3. This pocket is considered important for the addition of PAR chains except for PARP3 who transfers MARs.

The proteins PARP1-3 have been found to play a role in repairing single-strand breaks in DNA, and PARP inhibitors (PARPi) are being developed as a newer way to treat cancer. These inhibitors target tumors that have a defect in the double-strand break repair pathway, which is caused by dysfunction of proteins like BRCA1/2 due to gene mutation or promoter methylation. PARPi bind to the NAD⁺ binding domain of PARP1/2 and inhibits their activity, which helps trap them on DNA and target the tumors.

PARP inhibitors that are currently approved for clinical use target PARP1-3 as well as PARP4. However, the effects of inhibiting PARP4 on tumor cells are unclear. Recently, a study has reported the development of a new inhibitor, AEP07, designed to target PARP4 (Kirby et al., 2021). AEP07 was found to be 12 times more selective for PARP4 than other PARP family members and may serve as the basis for further research on specific PARP4 inhibitors for therapeutic use. PARP6, which also produces MAR modifications, is not currently classified within any subfamily due to its unique structure. Recent studies have revealed the involvement of PARP6 in important cellular functions. In one study, it was found that inhibiting the PARP6 enzyme led to the formation of Multi-Polar Spindle (MPS) and centrosome deficiencies while inhibiting other PARPs did not have the same effect (Z. Wang et al., 2018). This suggests that PARP6 plays a distinctive role in controlling MPS induction. Another study showed that PARP6 acts as a negative regulator of cell proliferation and its expression leads to cell accumulation in S-phase, likely due to its association in MPS induction and centrosome homeostasis (Tuncel et al., 2012). PARP6 expression levels are lower in colorectal cancer compared to non-cancerous tissue, possibly due to hypermethylation of the PARP6 promoter region. Additionally, PARP6 expression is negatively correlated with survivin expression, which is an inhibitor of apoptosis and is often associated with cancer (Sun et al., 2018). This suggests that PARP6 may act as a tumor suppressor. However, another study found that PARP6 is a positive regulator of survivin in gastric cancer, indicating that its regulatory role may vary in different tissue types.

PARP7 is a member of the CCCH-Zn finger PARP sub-family and adds MAR modifications (Figure 2; Table 1) to its substrates. The Zinc finger of PARP7 exhibits an elevated binding affinity for RNA, indicating its possible role in transcription regulation (Palavalli Parsons et al., 2021; Rasmussen et al., 2021). Reduction of PARP7 causes an increase in cells in mitosis phase but not reduced viability. This could mean that mitosis progresses slower in the absence of PARP7 (S. Vyas et al., 2013; S. (Sejal K. Vyas, 2014). Additionally, PARP7 has been found to regulate innate immunity, transcription factor activity, and

stress responses (Palavalli Parsons et al., 2021; Rasmussen et al., 2021; Richard et al., 2022). Other studies suggest PARP7 acts as a suppressor of aryl hydrocarbon receptor (AHR) as well as being a positive regulator of Liver X Receptors (LXRs), type I interferons (IFN-Is), and hypoxia-inducible factor 1 (HIF-1a), indicating its potential role in innate immunity.

PARP8 can create MAR modifications, and it does not currently belong to any structural subgroup (Hottiger et al., 2010). During most of the cell cycle, PARP8 is mostly located on the nuclear envelope, but during mitosis, it moves to centrosomes and spindle poles. Exhaustion of PARP8 is associated with defects in mitotic and nuclear morphology, and a reduction in cell viability, however why this is currently unknown (Challa et al., 2021; S. Vyas et al., 2013; S. (Sejal K. Vyas, 2014). The biological pathways in which PARP8 are involved are also a mystery. While structural modeling and experimental analysis have shown that PARP8 has MARYlation activity, its substrates are yet to be identified (Challa et al., 2021; Hottiger et al., 2010; S. (Sejal K. Vyas, 2014). The cellular function of PARP8 has not been demonstrated, and the potential anticancer activity or clinical development of PARP8 inhibitors has not been investigated.

One of the characteristics that stand out the most about PARP9 is that initially researchers assumed that it was inactive (Yang et al., 2017). This theory came from the fact that PARP9 cannot phosphorylate itself like many of the other PARPs in the family. However, it contains features common to some PARPs like macrodomains. These domains can also bind ADPr and PAR (Xing et al., 2021). PARP9 has also been linked to chemoresistance in prostate cancer (Camicia et al., 2013; Bachmann et al., 2014), and its levels are elevated in breast cancer. Its most unique role, however, is in the recognition of RNA viruses. PARP9 also plays a role in breast cancer cell migration because its depletion leads to inhibition of the migration (Tang et al., 2018). Further research is needed to see how PARP9 is connected to metastasis of breast cancer cells. As of right now, PARP9 inhibitors have not yet been identified or studied.

While PARP10 does not belong to any structural sub class, it is a MAR transferase (table 1). The substrates of PARP10 remain unclear, but over 70 potential substrates have been identified. (Yu et al., 2005). None of these are proven to be genuine substrates *in vivo*. In addition to its role in MAR transfer, PARP10 promotes cellular transformation by alleviating replication stress, and its depletion inhibits tumor growth in a mouse xenograft model. A new PARP10 inhibitor, A82-(CONHMe)-B354, has been developed, and various other proposed PARP10 inhibitors need further studies to determine their efficacy against tumor cells.

Like the two before, PARP11 has not been assigned to a structural subclass. It localizes in nuclear pores with nucleoporin153 (NUP153). Its main function is in the maintenance and regulation of the nuclear envelope's stability. is involved in the maintenance and regeneration of nuclear envelope stability during spermatogenesis(T. Guo et al., 2019). PARP11 activity is essential for spermatid formation in mice, and the silencing of PARP11 results in deformed sperm heads and infertility. ITK7 is a potent and highly selective inhibitor of PARP11 activity, resulting in the disassociation of PARP11 from the nuclear envelope.

PARP12 is a part of the Zinc Finger CCCH Domain-Containing Protein sub-family and produces MAR modifications on target proteins (table 1). It is localized in the Golgi and is expressed in the cytoplasm during interphase. PARP12 plays a role in cellular stress response through a PARP1-dependent pathway and translocate from the Golgi to stress granules after oxidative stress (Welsby et al., 2014). PARP12 may also have a tumor suppresser function, and minimal expression levels are associated with tumorigenesis.

PARP13 is another PARP that does not follow the grain of the others. It does not produce any MAR or PAR modifications, yet it is theorized that it can produce MAR modifications based solely on its structure (Hottiger et al., 2010). PARP13 belongs to the zinc-finger CCCH domain-containing protein

subfamily and localizes throughout the cell during interphase and to punctate structures in the cytoplasm during mitosis (Buch-Larsen et al., 2020; Challa et al., 2021; S. (Sejal K. Vyas, 2014). Depletion of PARP13 strongly impacts cell viability, although the reason for this remains unknown (S. Vyas et al., 2013). PARP13 plays a role in anti-viral pathways, such as recruiting cellular RNA degradation machinery like poly(A)-specific ribonuclease (PARN) that detaches the poly A tail of viral mRNA (S. Vyas et al., 2013). No PARP13 inhibitors have been reported, and the effect of its depletion on tumor cell growth is yet to be explored.

In comparison, PARP14 produces MAR modifications on target proteins (Qin et al., 2019). PARP14 is linked to a range of disease states, such as cancer, atherosclerosis, and inflammation due to allergens (Qin et al., 2019). As a Macro-domain-containing PARP that regulates the actin cytoskeleton. Depletion of PARP14 results in damage to the actin cytoskeleton and general defects in cell viability. In a study of PARP14, it was shown that its depletion leads to the elongated processes extending from the cell body in around 60% of siRNA transfected cells (Torretta et al., 2023; S. (Sejal K. Vyas, 2014). It is believed that this is because of the cells' inability to retract and unwind actin filaments during cell movement. This indicates that PARP14 plays a crucial role in retaining cytoskeletal structure and cell motility. PARP14 also acts as a regulator of B-cell survival factors. It can inhibit caspase-dependent apoptotic pathways (Cho et al., 2011). It is suggested that PARP14 is an effector of JNK2, which is an important part in the activation of the pro-apoptotic pathway (Barbarulo et al., 2013). Targeting PARP14 to treat cancer has been supported by the discovery of an inhibitor of PARP14, RBN012759, which leads to an inflammatory response in tumors (Torretta et al., 2023). RBN012759 could be a strong candidate for lead optimization because it shows strong inhibition of PARP14 at low concentrations.

PARP15 is a member of the macro-PARP subfamily that produces MAR modifications and is catalytically active. However, due to its low protein expression levels in cells, its localization and depletion effects remain unknown. Two single nucleotide polymorphisms (SNPs) of PARP15 have been

linked to reduced survival rates in patients with acute myeloid leukemia, but further studies are required to determine if PARP15 plays a role in tumorigenesis and if it could be an appropriate target for cancer therapy. Currently, no selective inhibitors of PARP15 have been reported.

As the last and smallest PARP described in this section, PARP16 possess a unique tail anchor that makes it stand out from the rest in the PARP family. This tail can attach to membranous structures, and is also classified as a MART. It localizes to the endoplasmic reticulum (ER) membrane and is involved in the maintenance and formation of the ER membrane. PARP16 positively regulates ER stress sensors during the unfolded protein response and inhibition of its activity has been found to reduce senescence-associated phenotypes. As a result, PARP16 is speculated to be an efficient cancer target, with some studies showing enhanced apoptosis when treated with PARP16 inhibitors in combination with other agents. Furthermore, PARP16 has been identified as an effective new anticancer drug target when inhibited together with PARP1. Chemical proteomics have identified PARP16 as a novel secondary target of Talazoparib, which might contribute to the potency of Talazoparib as a selective cancer therapeutic.

2.04 PARPs in Hallmark Cancer Traits

Research has proven the multifaceted ways PARPs contribute to the hallmarks of cancer. This is outlined in the review paper by Demény (Demény & Virág, 2021). This paper takes the essential hallmarks of cancer and describes how the PARP family is interlinked with not only DNA repair and genetics. We can see just how pivotal in cancer development PARPs are. PARP1 is not only connected with proliferation regulatory cycles, but also in the suppressor mechanisms. PARP-1 and proliferation have a close relationship in the DNA replication process.

This is demonstrated by the disruption of replication forks in PARPi-treated cancer cells. PARP-1 interacts with the multiprotein DNA replication complex (MRC). PARP1 may also play a role in the assembly of the active MRC (Simbulan-Rosenthal et al., 1998). PARP3 and tankyrase-1 are also

connected with proliferation regulatory cycles. Along with PARP1 these enzymes regulate the function of the centrosome (Augustin et al., 2003; Kanai et al., 2000; Smith & De Lange, 1999).

PARP1's role in resisting cell death is one of the most known connections in the hallmarks of cancer. However, PARP1 is not the only PARP linked to this hallmark. As DNA damage sensor proteins, PARP1 and PARP2 contribute to DNA repair and, as such, act as a survival mechanism for cells in DNA damage situations. The use of PARPi in BRCA-deficient ovarian or breast carcinomas takes advantage of this synthetic lethal effect of PARylation inhibition and in BRCA mutant tumors (Farmer et al., 2005).

In regards to enabling replicative immortality, PARP1 is detected irregularly in normal telomeres but in telomeres affected by DNA damage PARP1 accumulates causing erosion (Gomez et al., 2006). PARP-1 is included within the typical repair system of intra-telomeric single- and double-strand breaks (SSBs and DSBs) (Fernández-Marcelo et al., 2015).

PARPs effect on the genetic stability goes without saying. PARP-1, PARP-2, and PARP-3 have DNA-binding capabilities. These PARPs localize to DNA lesions and this association increases their basal catalytic activity (Alemasova & Lavrik, 2019).

PARPs have overwhelming and versatile effects on metabolism. The effect of PARPs on tumor metabolism occurs through transcriptional mechanisms, direct PAR/MARylation of metabolic proteins, cleaved PAR chains, or indirectly through changes in NAD⁺ and ATP levels. PARPs directly regulate enzymes or regulate key metabolic regulatory factors. PARP-10 physically interacts with MARylates and recruits GAPDH to cytosolic membrane-free granules (Demény & Virág, 2021). PARP-10-dependent MARylation inhibits glycogen synthase kinase 3 β (GSK3 β), which promotes glycolytic and anabolic pathways (Yu et al., 2005). Interaction between c-Jun N-terminal kinase 1 (JNK1) and PARP14 inhibits pyruvate kinase muscle type 2 (PKM2) activation of JNK1 and nuclear translocation of PKM2, where PKM2 would increase glycolysis gene expression via HIF1 α and MYC (Barbarulo et al., 2013). PARP-1

antagonizes PI3K/Akt pathway activity. The PI3K/Akt pathway increases glycolytic flux through glucose transporters (GLUT), HK and PFK2 and promotes nucleotide, protein and lipid biosynthesis and autophagy in cancer.

Table 1: Features of the PARP Family

Name	Other Names	Molecular Weight (Da)	Amino Acid length	Catalytic triad sequence	Type of ribosylation	DNA dependent activation	Inhibitors available- FDA approval status
PARP1	PARP, ARTD1	113,084	1,014	H-Y-E	PAR	Yes	Yes- Approved for prostate cancer, breast cancer, ovarian cancer, and gynecological cancer
PARP2	ARTD2	66,206	583	H-Y-E	PAR	Yes	Yes- Approved for prostate cancer, breast cancer, ovarian cancer, and gynecological cancer
PARP3	ARTD3	60,089	533	H-Y-E	MAR	Yes	Yes- Approved for ovarian Cancer
PARP4	ARTD4, vPARP	37,288	327	H-Y-E	MAR (PAR when localized to vault particles)	No	Yes- Not FDA approved
PARP5a	TNKS1, ARTD5	142,039	1,327	H-Y-E	PAR	Postulated	Yes- Not FDA approved
PARP5b	TNKS2, ARTD6	126,918	1,166	H-Y-E	PAR	Postulated	Yes- Not FDA approved
PARP6	ARTD17	71,115	630	H-Y-I	MAR	Undetermined	Yes- Not FDA approved
PARP7	tPARP, ARTD14	76,227	657	H-Y-I	MAR	Undetermined	Yes- Not FDA approved
PARP8	ARTD16	95,871	854	H-Y-I	MAR	Undetermined	No
PARP9	BAL1, ARTD9	96,343	854	Q-Y-T	MAR	Undetermined	No
PARP10	ARTD10	109,998	1,025	H-Y-I	MAR	No	Yes- Not FDA approved
PARP11	ARTD11	39,597	338	H-Y-I	MAR	Undetermined	Yes- Not FDA approved
PARP12	ARTD12	79,064	701	H-Y-I	MAR	Undetermined	Yes- (Nonselective)- Not approved for PARP12
PARP13	ZAP, ARTD13	101,431	902	Y-Y-V	Catalytically inactive	Undetermined	No
PARP14	BAL2, ARTD8	202,800	1,801	H-Y-L	MAR	Undetermined	Yes- Not FDA approved
PARP15	BAL3, ARTD4	74,576	678	H-Y-L	MAR	Undetermined	Yes (nonselective)- Not FDA approved for PARP15
PARP16	ARTD15	36,383	332	H-Y-Y	MAR	Undetermined	Yes (nonselective)- Not FDA approved for PARP16

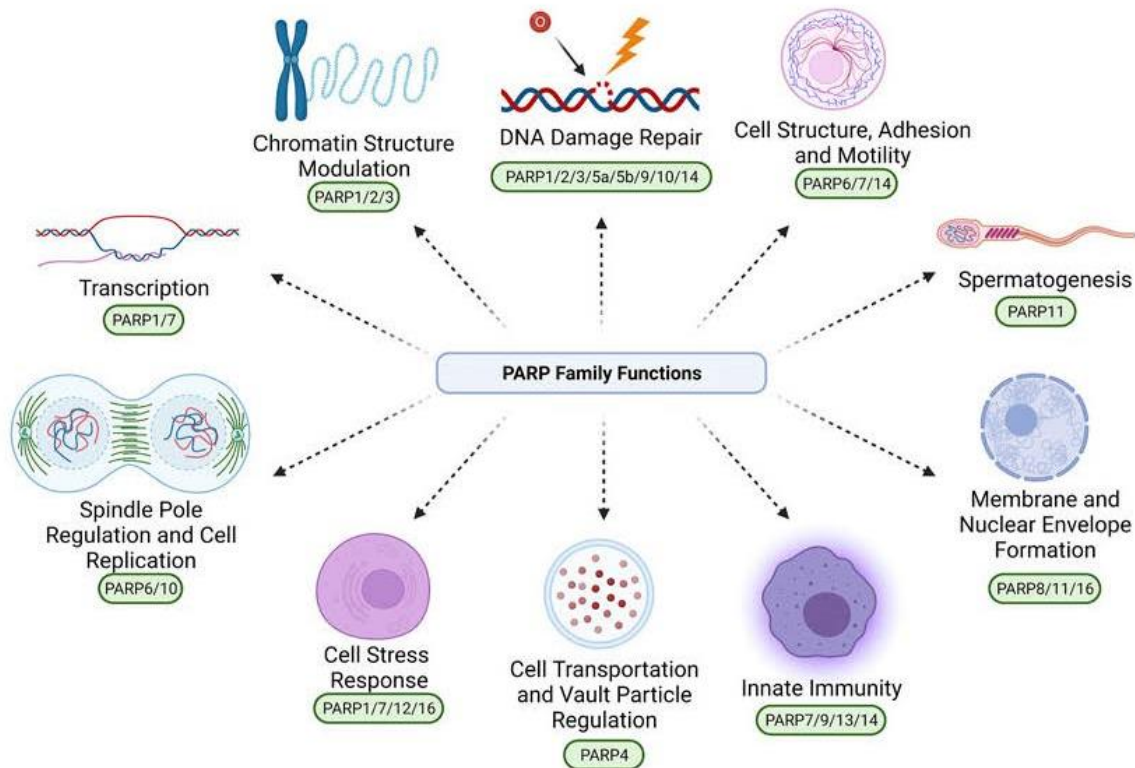


Figure 4: PARP Family Functions Reprinted from, “Beyond PARP1: The Potential of Other Members of the Poly (ADP-Ribose) Polymerase Family in DNA Repair and Cancer Therapeutics,” by Iain Richard et. al. 2022, retrieved from <https://www.frontiersin.org/articles/10.3389/fcell.2021.801200/full>

2.05 PARP1 Structure

Poly(ADP-ribose) polymerase 1 (PARP1) is a highly abundant protein that is associated with chromatin relaxation, and is an essential early responder to genomic stress in eukaryotes (Gibson & Kraus, 2012; Kumar et al., 2021). PARP-1 is made up of three main domains: the N-terminal DNA binding domain (DBD), the middle auto-modification domain (A), and the C-terminal catalytic domain (C). The DNA-binding domain has three Zinc fingers, ZI, ZII, and ZIII, however only ZI and ZII can interact with

DNA. The third ZIII is responsible for interactions between PARP-1 and other proteins. During the DNA damage response, PARP-1 forms an active complex around broken DNA, with ZI, ZIII, W, and Cat domains playing important roles (Aberle et al., 2020). The auto-modification domain, A, is the primary target of PARP1 activity and becomes modified by pADPr upon activation, causing PARP-1 to lose its ability to interact with DNA. Instead, it acts as a "shuttle" for proteins of chromatin. The N-terminal DBD and C-terminal ZIII-A-W-Cat domains are responsible for PARP-1's interaction with chromatin, and the presence of these domains is necessary for PARP-1-dependent chromatin condensation in vitro. Without the DBD, PARP1 cannot bind to or be activated by DNA. The binding of PARP1 to histones is regulated by its C-terminal subdomains.

When DNA damage occurs, particularly single-strand breaks (SSBs), which are the most common type of damage, PARP1 becomes strongly activated. It catalyzes the addition of poly(ADP-ribose) (PAR) to nearby proteins, including itself, and thereby signals for the assembly of downstream DNA repair factors (Jackson & Bartek, 2009; Kastan, 2008). Inhibiting PARP enzymes has emerged as an important approach to cancer therapy. This is because when you combine the effects of PARP inhibition and defective homologous recombination (HR), BRCA-deficient tumor cells are selectively killed, while healthy cells remain generally untouched (5, 6). This is an example of "synthetic lethality" because it results from the collective effects of losing two complementary repair mechanisms at once.

Similar effects have been shown when PARP inhibition is combined with additional tumor-associated repair deficiencies. The harmful effects of PARP inhibition in tumor cells are thought to be caused by inhibitor-bound PARP being stranded on DNA lesions, preventing replication and repair. However, the molecular mechanisms driving this trapping have remained a mystery. Previous research has shown that PARP-1 is a protein that responds early to genomic stress in eukaryotes, specifically single-strand breaks (SSBs)(Kumar et al., 2021). PARP-1 attaches to SSBs via its F1 and F2 zinc finger domains, bending and twisting the DNA and rendering it inaccessible to intact double-stranded DNA.

The DNA-dependent activity switch in PARP-1 is controlled by this interface. Previously, it was thought that the activation signal was sent to the active site via DNA-dependent distortions of the HD domain structure, but recent research has revealed that dynamics play an important role. The WGR and F3 domains are maintained together in the right configuration by DNA binding, allowing them to jointly produce the appropriate "landing pad" for the HD. The free energy required to alter the internal dynamics of the HD is provided through the interaction of HD with WGR and F3. In the absence of binding to DNA damage, mutants in the HD subdomain have a higher rate of PAR production than wild-type PARP-1, and these effects can be investigated in the isolated CAT domain. Adding inhibitors to the isolated CAT domain could reveal information on the importance of HD dynamics in trapping. PAR, a polymer composed of ADP-ribose units produced from NAD⁺, is highly resisted by DNA, allowing PARP to be released from DNA damage sites.

2.06 The multifunctionality of PARP1

PARP1, or poly (ADP-ribose) polymerase 1, is a multifunctional protein involved in various cellular processes, including DNA damage repair, chromatin remodeling, transcriptional regulation, and cell death. As an enzyme, PARP 1 plays a crucial role in the repair of single-stranded DNA breaks through base excision repair (BER) pathway. In this pathway, PARP 1 detects the damaged site and catalyzes the formation of poly ADP-ribose (PAR) chains, which recruit and activate the DNA repair machinery to fix the break. Apart from DNA repair, PARP 1 also regulates gene expression by modifying the chromatin structure through PARylation of histones and transcription factors. Moreover, PARP 1 can facilitate cell death by activating apoptosis-inducing factor (AIF) and promoting mitochondrial dysfunction. Dysregulation of PARP 1 activity has been associated with various diseases, including cancer, neurodegeneration, and inflammation. Therefore, targeting PARP 1 has emerged as a potential therapeutic strategy for these diseases, particularly in cancer treatment.

One of the most widely studied functions of PARP1 is its role in DNA repair. PARP1 has a crucial role in the repair of single-strand breaks (SSBs). These breaks usually occur from oxidative stress through the base excision repair/SSB repair (BER/SSBR) pathway. Historically, only PARP1 and 2 were thought to become active by DNA damage resulting to studies mainly focusing on targeting these two enzymes, but in current literature PARP3 has also been implicated in DNA DSB repair (Boehler et al., 2011).

The constitutive activation of the NF- κ B pathway, which is frequently observed in various human cancers, is primarily caused by its dysregulation. While this pathway is crucial for the acute immune response to eliminate cancerous cells, chronic inflammation induced by NF- κ B can promote immune evasion, angiogenesis, cancer survival, and metastasis (Kumar et al., 2021). PARP1 is a multifunctional protein that regulates the activation of the NF- κ B pathway through various mechanisms. For instance, PARP1 is acetylated by P300/CBP after inflammatory stimulation, leading to enhanced interaction of p50 with P300 and PARP1 and consequently activating NF- κ B. Additionally, PARP1 participates in the activation of the NF- κ B pathway by forming a complex with ATM, PIAS γ , and IKK γ after DNA damage detection. In this complex, PAR chains produced by PARP1 assist PIAS γ in SUMOylating IKK γ (Alemasova & Lavrik, 2019).

PARP1 is involved in several processes, including chromatin compaction and de-condensation (Kumar et al., 2021). PARP-1 can become enzymatically active by connecting with nicked DNA or attaching to a phosphorylated H2Av-histone-containing nucleosome, specifically histone H4. PARP-1 changes itself and other adjacent nuclear proteins when activated by generating pADPr strands using NAD as a substrate. PARP-1 alters histones as well as DNA repair enzymes. PARP-1 activity causes histones to move away from the DNA molecule and towards pADPr, resulting in chromatin loosening and transcription activation. This procedure also allows for DNA repair and replication. It also affects epigenetic marks by altering histone proteins and other chromatin remodeling enzymes via PARylation. It also increases transcription by improving promoter accessibility via histone and nucleosome

replacement, as well as allowing the substitution of negative transcriptional cofactors with positive ones (Kumar et al., 2021). Recently research has linked PARP1 in post-transcriptional gene expression regulation, including “rRNA biosynthesis, ribosome biogenesis, RNA-binding protein (RBP) regulation, and mRNA regulation” (Rudolph et al., 2021).

A new classification of PARP1-mediated cell death has been structured for better understanding of the execution of cellular death. There are two groups based on caspase involvement: caspase-independent (type I) and caspase-dependent (type II) (Kumar et al., 2021). Caspase-independent cell death can be further divided into three groups: PARthanatos, necrosis, and autophagy. PARthanatos is the only subgroup in caspase-dependent cell death, namely apoptosis. Hyperactivation of PARP1 leads to the release of PAR from PARP1 resulting in parthanatos. In necrosis, overexpression of PARP1 results in the hyperactivation of mitochondria mainly due to ROS and other stressors on the mitochondria, which damage the DNA and plasma membrane. In autophagy, cells subjected to stress and starvation through nutrient or growth factor deprivation result in the activation of PARP1, which mediates the PARylation of Forkhead box class O 3a (FOXO3a) (Kumar et al., 2021). Recently, it was discovered that PARP1 also acts as an RBP, binding to the cis-acting elements found in the 3' and 5' untranslated regions of mRNAs, leading to mRNA decay, and playing a key role in alternative splicing.

Researchers found that exposing cells to UVB irradiation led to an increase in lipophagy, which was dependent on PARP1 and provided a source of triglycerides (Aberle et al., 2020). Inhibition or deletion of PARP1 has been shown to impact the membrane lipid composition in skin cells and erythrocytes, as well as the levels of polyunsaturated fatty acid metabolites that have inflammatory properties in skin cells (Kumar et al., 2021).

Several studies have associated PARP1 with cholesterol regulation (Szántó et al. 2021). When PARP1 is inhibited, it decreases the overall levels of cholesterol in the serum. This results in an improved HDL/LDL ratio, leading to positive outcomes in conditions such as high-fat feeding, high-cholesterol feeding, and diabetes (Kumar et al., 2021).

PARP1 activation leads to the PARylation and subsequent inactivation of peroxisome proliferator-activated receptor (PPAR α) transcription factor, resulting in hepatic lipid accumulation by suppressing lipid oxidation (Choi et al., 2017). Conversely, inhibition of PARP1 reduces endoplasmic reticulum stress, which downregulates de novo lipid biosynthesis (Mukhopadhyay et al., 2017) and upregulates cell processes such as lipid uptake and lipolysis (Choi et al., 2017).

PARP1 has also been ensnared in the development of pathological lipid accumulation in non-alcoholic fatty liver disease (NAFLD) and alcoholic fatty liver disease (AFLD) (Mukhopadhyay et al., 2017). When considering the roles and mechanisms PARP1 has in the body, one should consider its overlapping functions, the type of cell, tissue, or organ that it is acting in, and its interactions with other proteins, factors, and enzymes. PARP1 takes part in a contradictory role in cell death and cell viability. On one hand, at normal expression levels in a healthy and normal cell, PARP1 functions as a regulator of transcription enzymes, inflammatory cytokines, etc. Keeping the cell functional. On the other hand, in a diseased cell, PARP1 can have an almost extreme approach. As mentioned before, some cancers hijack this enzymes function to escape cell death from damaged DNA, but also there are some cases, like in neurodegeneration, where the overexpression of PARP1 is detrimental to the cell.

2.07 PARP1 and Neurodegenerative Diseases

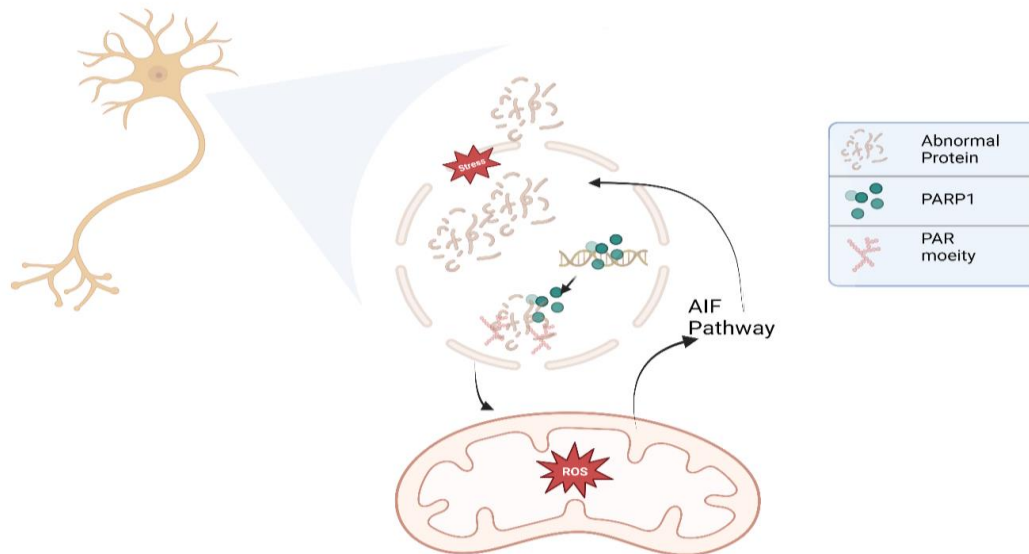


Figure 5: Molecular Mechanism of PARP1 in neurodegenerative diseases. PARP1 modulates the accumulation of abnormal proteins, causing the activation of the Apoptosis-Inducing Pathway (AIF).

Neurodegeneration refers to the loss of function in nerve cells, which can occur in both cardiac and neurological diseases. Alzheimer's disease and Parkinson's disease are the most common neurodegenerative diseases. PARP1's involvement in cell death and DNA damage repair has led to its study in these diseases. The process of neurodegeneration typically involves the accumulation of abnormal proteins, oxidative damage, activation of PARP1, depletion of NAD⁺ and oxidative phosphorylation, and ultimately, the activation of an apoptotic pathway that leads to cell death (figure 5). This PARP1-induced cell death pathway is known as PARthanatos and is caused by excessive oxidative damage to DNA. While PARP1 is a significant factor in this process, other enzymes and proteins can also activate apoptosis pathways. In neurodegenerative diseases like Alzheimer's, changes occur in enzymes involved in oxidative phosphorylation of A β and amyloid precursor protein, oxidative damage, and mitochondria. Similarly, in Parkinson's disease, mutations in mitochondrial proteins and mitochondrial DNA mutations have been identified in multiple studies (Abeti & Duchon, 2012; Arruri et al., 2021; Barati

et al., 2022). Mitochondrial respiratory chain enzymes and mitochondrial programmed cell death proteins undergo changes in ALS patients. Apoptosis-inducing factor (AIF) is a protein that is released from the mitochondria during apoptosis, leading to DNA cleavage and cell death. While it is not yet proven whether PARP1 activates the translocation of AIF, it is reasonable to assume that the overexpression of PARP1 and the activation of the AIF pathway are connected.

2.08 PARPi Mechanism

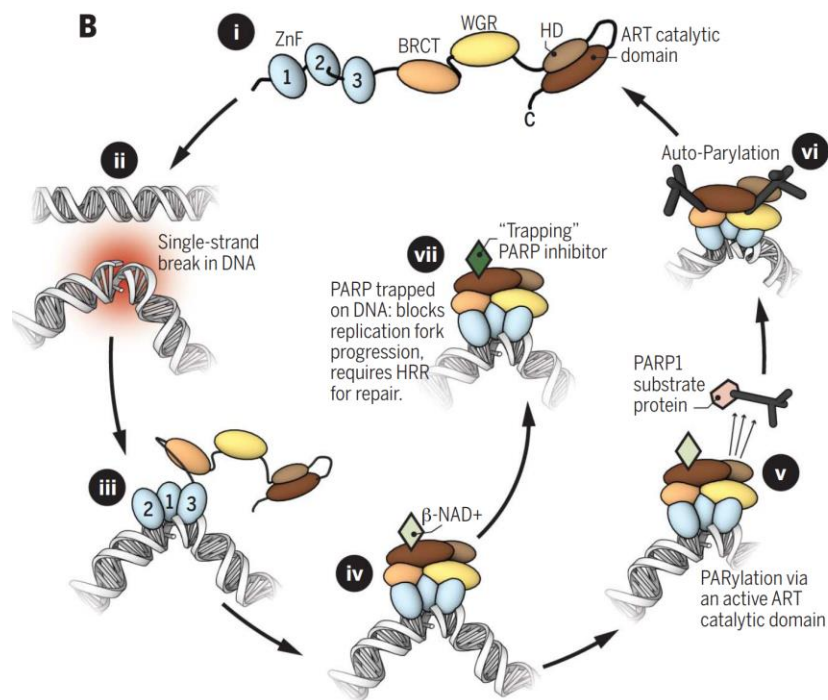


Figure 6: PARPi Trapping Mechanism

Reprinted from, "PARP inhibitors: Synthetic lethality in the clinic", by Christopher Lord et. al. 2017

retrieved from <https://pubmed.ncbi.nlm.nih.gov/28302823/>

One of the most dynamics focused on treatments is the use of PARP inhibitors (PARPi). PARPi are right now approved for the administration of an assortment of tumor types and represent a class of cancer treatment that essentially represses the catalytic activity of PARP1 and PARP2 (H. Li et al., 2020).

These are active in base excision repair of single-strand breaks (SSBs) in DNA. Starting with an aggregation of SSBs, the inhibitor traps the PARP-DNA complex on to the SSBs. This causes the disruption of the DNA replication fork and the formation of DSBs (figure 6).

PARP inhibition isn't successful in healthy cells since they can utilize the useful HR repair mechanism to repair DSBs, but it is exceptionally successful in cells that harbor HR deficiencies (HRDs), including the cells of certain types of breast and ovarian cancers with mutations in BRCA1 and BRCA2. This manufactured lethality is the concurrent loss of function of major molecules leading to cell death. It is important to note that an insufficiency of one molecule does not solely lead to cell death (Lord & Ashworth, 2017). It has been shown in the clinical setting that PARPi can still be a successful treatment regardless of BRCA1/2, HRD status, or other DDR quality changes, proposing that a more extensive populace of patients may benefit from PARPi therapy.

Although PARPi have been a better prognosis for progression-free survival (PFS), a few cancers may unavoidably create resistance to them. As with most therapies, there are several theories and mechanisms to explain these phenomena. Potential mechanisms of resistance to PARPi incorporate restoration of HR capacity, stabilization of replication forks, reduced trapping of PARP1, P-glycoprotein-mediated mediate efflux, modifications in cell cycle control, microRNA expression designs, and other dysregulated signaling pathways (H. Li et al., 2020). Continuous research is underway to improve understanding of how PARPi might help direct broader clinical use, optimize response, assess novel combinations with other therapies, and ultimately identify and overcome resistance in the tumor environment.

2.09 Overview of FDA-Approved PARP Inhibitors

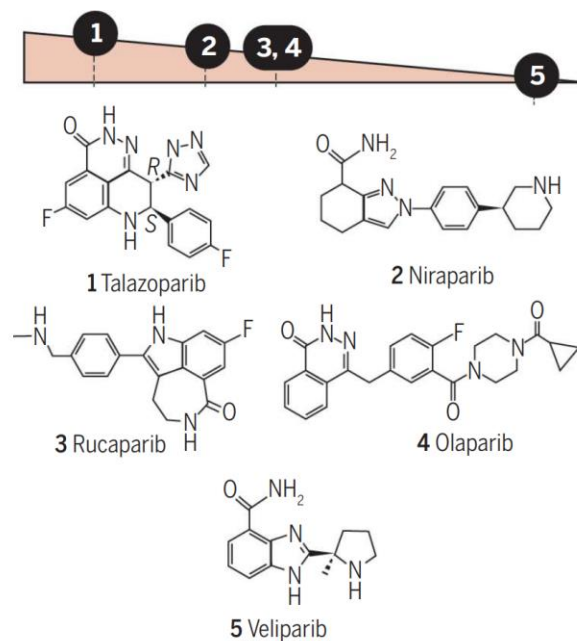


Figure 7: Potency and Structure of PARP Inhibitors Reprinted from, “PARP inhibitors: Synthetic lethality in the clinic”, by Christopher Lord et. al. 2017 retrieved from

<https://pubmed.ncbi.nlm.nih.gov/28302823/>

PARPi are a relatively new class of drug. The first to be FDA approved was Olaparib (Lynparza, AstraZeneca) in 2014. Since then, three other inhibitors have been approved for treatment of cancer such as Rucaparib (2016; Rubraca, Clovis Oncology, Inc.), Niraparib (2017; Zejula, Tesaro, Inc., and Talazoparib (2018; Talzenna, Pfizer) for treatment of ovarian cancer, breast cancer, prostate cancer, pancreatic cancer, and unspecified solid tumors. Talazoparib is the most potent inhibitor, and veliparib is the least potent (figure 7)(S. Vyas et al., 2013). Examining the expression level of PARP1 in different tumors is important to evaluate the potential therapeutic effects and side effects of PARP1 inhibitors in each cancer subtype. Of course, of these carcinomas, breast cancer has garnered the most attention. Also, many of these trials use combination therapy with monoclonal antibodies or kinase inhibitors.

PARP inhibitors (PARPi) are analogues of nicotinamide, the by-product of NAD cleavage. Researchers used nicotinamide as the basis for PARPi because nicotinamide is an inhibitor of PARP. In 1980, 3-aminobenzamide was reported as a competitive inhibitor of PARPs. Since then, there has been many advancements in PARP inhibitors as therapeutics. Including identifying isoquinolinone derivatives as inhibitors in 1990 ovarian cancer. Rucaparib is approved by regulatory agencies such as the US FDA and the European Medicines Agency (EMA) for the treatment of advanced ovarian, fallopian tube, or primary peritoneal cancer that has recurred after treatment with platinum-based chemotherapy. It is available in oral form and is used in patients who have a specific genetic mutation called a deleterious BRCA mutation or have undergone genetic testing and have homologous recombination deficiency (HRD). In 2017, Niraparib was approved for ovarian cancer regardless of BRCA status, and for the maintenance treatment of adults with recurrent epithelial ovarian, fallopian tube or primary peritoneal cancer who have had a complete or partial response to platinum-based chemotherapy (Hurvitz et al., 2020). The most recent monotherapy approval was in 2018 for Talazoparib. It was approved for treatment of BRCA mutated breast cancer and metastatic breast cancer, specifically for the treatment of adult patients with germline BRCA-mutated, HER2-negative locally advanced or metastatic breast cancer (*Talazoparib*, n.d.). It is available in oral form and is used in patients who have a specific genetic mutation called a deleterious BRCA mutation. PARPi have emerged as a promising class of antineoplastic inhibitors because of its exploitation of synthetic lethality and how they potentiate the cytotoxic effect of chemotherapy and radiation.

2.10 PARPi Resistance

BRCA1/2-deficient tumor cells are more susceptible to the synthetic lethality of PARP inhibitors (PARPi) because of the DNA repair deficiency. Currently, ovarian cancer and breast cancer indications have been approved for a few PARPi targeting poly (ADP-ribose) polymerase (PARP). However, PARPi resistance is commonplace in medical settings. More than 40% of patients with BRCA1/2 deficiency do

not react to PARPi. Additionally, with continued oral PARPi therapy, many patients develop PARPi resistance. In order to achieve synthetic lethality, homologous recombination repair deficient (HRD) is a necessary requirement (H. Li et al., 2020). As a result, HRR (homologous recombination repair and restoration) emerges as the main cause of PARPi resistance. According to a recent publication, PARPi resistance in BRCA1/2-deficient cells and patients was also influenced by DNA replication fork protection. Additional variables that contribute to PARPi resistance include reversion mutations, epigenetic modification, the restoration of ADP-ribosylation (PARylation), and pharmacological changes.

2.11 Promising Novel PARPi

There are many PARPi in development, a few promising PARPi are summarized in table 2. Venadaparib was evaluated using in vitro/ex vivo systems and animal models (Lee et al., 2023). The conclusion of this research is that Venadaparib improved efficacy and safety compared to FDA approved PARPi (Lee et al., 2023). Further research will be needed in the clinical phase to see Venadaparib's efficacy.

YHP-836 had great inhibitory activity for PARP1 and PARP2 enzymes (Du et al., 2022). Furthermore, it allosterically regulates PARP1 and PARP2 via DNA trapping. The inhibitor also displayed cytotoxicity in tumor cell lines with BRCA (Du et al., 2022).

DDPF-20 was studied with human lung cancer cells and displayed inhibitory activity against proliferation, induced G2/M cycle arrest, and activated apoptosis (T. Wang et al., 2022). Recent research confirmed that DDPF-20 induced DDBs. Interestingly, DDPF-20 inhibited tube formation and inhibited CAM neovascularization, revealing the anti-angiogenic ability of DDPF-20. Mechanistic studies have shown that DDPF-20 inhibits the PI3K/Akt/VEGF signaling pathway. (T. Wang et al., 2022).

2.12 PARP1 Assay Method

Picking the right assay methods for PARP1 activity detection revolves around its ribosylation with NAD⁺. Such methods include colorimetric, chemiluminescent, ELISA, and enzymatic assays. The rational, methods, and set up have similarities and differences.

PARP1 colorimetric assays are designed to measure PARP1 activity via its function in catalyzing the NAD-dependent addition of PAR onto histones. This is directly related to PARP1's chromatin modification function. The plates are coated with histone mixture, and the reaction components include PARP1, NAD, and Biotin NAD so that the ribosylation reaction can occur. Streptavidin-HRP is added and HRP substrate is used for detection, giving off a blue color. The absorbance is directly related to PARP1 activity. In chemiluminescent assay an ELISA ECL substrate is used instead of HRP substrate to produce chemiluminescence that can be measured using a chemiluminescence reader. The rationale of the chemiluminescence assay is the same as the colorimetric assay (*PARP1 Chemiluminescent Assay Kit*, n.d.). The development of "non-native NAD⁺ analogs as a substrate may yield different kinetics than unmodified NAD⁺, A lack of flexibility in protein/peptide substrates, and multiple wash steps" are seen as potential disadvantages of this assay (*PARP1 Chemiluminescent Assay Kit*, n.d.). Even with these disadvantages in mind, this method is still a flexible and reliable assay for quantifying PARP1 activity (*PARP1 Chemiluminescent Assay Kit*, n.d.).

2.13 Clinical Trials

Table 2: Overview of Clinical Trials using PARP inhibitors.

PARPi	Cancer	Study Design	Polpulation	Target	Reference
5F02	Prostate cancer	<i>In vitro</i> and <i>in vivo</i>	PC-3 xenograft	Non-NAD-like PARP-1 inhibitor	(Karpova et al., 2019)
Simmiparib	Breast cancer	<i>In vitro</i> and <i>in vivo</i>	Xenografts, CDX and PDX	PARP-1, PARP-2	(Yuan et al., 2017)
DDHCB	Breast cancer	<i>In vitro</i> and <i>in vivo</i>	HCC-1937 cell line xenografts	PARP-1	(L. Wang et al., 2020)
BTH-8	Breast cancer	<i>In vivo</i> and <i>in vitro</i> , using BRCA-deficient cancer cells	HCC-1937 cell line xenograft	PARP-1	(C. Guo et al., 2020)
YHP-836	Ovarian cancer	<i>In vitro</i> and <i>in vivo</i>	MDA-MD-436 cell line xenograft	PARP-1, PARP-2	(Du et al., 2022)
ZC-22		<i>In vitro</i> and <i>in vivo</i>	MDA-MD-231 cell line xenograft	PARP and CDK4/6	(Tian et al., 2022)
Mefuparib hydrochloride (MPH)		<i>In vitro</i> and <i>in vivo</i>	MDA-MB-436 cell line xenograft	PARP-1, PARP-2	(He et al., 2016)
1,2,4-triazoles		<i>In silico</i> and <i>in vitro</i>	MCF-7 cell line	PARP-1	(Boraei et al., 2019)
Mortaparib		<i>In vitro</i> and <i>in vivo</i>	SKOV3 ovarian cancer cells xenograft	PARP-1 and mortalin	(Putri et al., 2019)
ZC-22		<i>In vitro</i> and <i>in vivo</i>	OVCAR5 Ovarian cancer cells xenograft	PARP and CDK4/6	(Ghafouri-Fard et al., 2022; Tian et al., 2022)

PARP1 has also been identified in the cytoplasm of cancer cells. Clinical data implicates that nuclear PARP1 expression is usually upregulated in most breast tumors, while the overexpression of nuclear–cytoplasmic PARP1 was present only in a small percentage of breast tumors (Domagala et al.,

2011). Moreover, nuclear, and nuclear–cytoplasmic PARP1 expression levels found to be of clinical relevance for cancer prognosis and overall survival in lymph node-negative early breast carcinoma. When comparing, non-small cell lung carcinoma (NSCLC) and small cell lung cancer (SCLC), PARP1 protein level were higher in small cell lung cancer (SCLC). This leads to an overall higher sensitivity of SCLC to PARP1 inhibitors. OlympiA was a Phase III clinical trial that evaluated the use of the PARP inhibitor Olaparib in patients with early-stage, HER2-negative breast cancer who had a high risk of recurrence (Geyer et al., 2022). The trial showed that Olaparib significantly reduced the risk of disease recurrence or death compared to placebo. PRIMA was a Phase III clinical trial that evaluated the use of the PARP inhibitor niraparib as a maintenance therapy in patients with newly diagnosed advanced ovarian cancer who had responded to platinum-based chemotherapy (Banerjee et al., 2020). The trial showed that niraparib significantly prolonged progression-free survival compared to placebo. PROfound was a Phase III clinical trial that evaluated the use of the PARP inhibitor Olaparib in patients with metastatic castration-resistant prostate cancer who had mutations in genes involved in DNA repair (De Bono et al., 2017). The trial showed that Olaparib significantly improved radiographic progression-free survival compared to the standard of care. EMBRACA was a Phase III clinical trial that evaluated the use of the PARP inhibitor Talazoparib in patients with locally advanced or metastatic breast cancer who had a germline BRCA mutation (Hurvitz et al., 2020). The trial showed that Talazoparib significantly improved progression-free survival compared to chemotherapy.

PARP1-assisted DNA repair in cancers is complicated. On one hand, tumor cells continuously harbor DNA repair defects to preserve the DNA lesions that can cultivate carcinogenesis. Also, damaging DNA of cancer cells is continuously used as the treatment mechanism of a few anticancer agents. PARP1 inhibitors can further stifle the DNA repair process and drive cancer cell death, hence inhibiting cancers freely, or as anticancer assistant agents. Conversely, DNA lesion in cells actuated by excessive reactive oxygen species (ROS) is one of the major components of carcinogenesis. In microenvironment

homeostasis of cellular, this could be deflected by PARP1-BER pathway. In any case, oxidative clustered DNA lesions (OCDLs), which occur over the top DNA injuries happened as often as possible in tumors, may aggravate the microenvironment homeostasis and lead to more extreme DNA damage. Maintained activation of PARP1 and deficient DNA repair will lead to advanced mutagenesis, metastasis, and energy-depleted corruption of tumors. In this condition, PARP1 inhibitors may suppress mutagenesis and metastasis, as well as turn necrosis to apoptosis aiming to maintain a strategic distance from inflammation-mediated cytotoxicity.

2.14 Screening Libraries

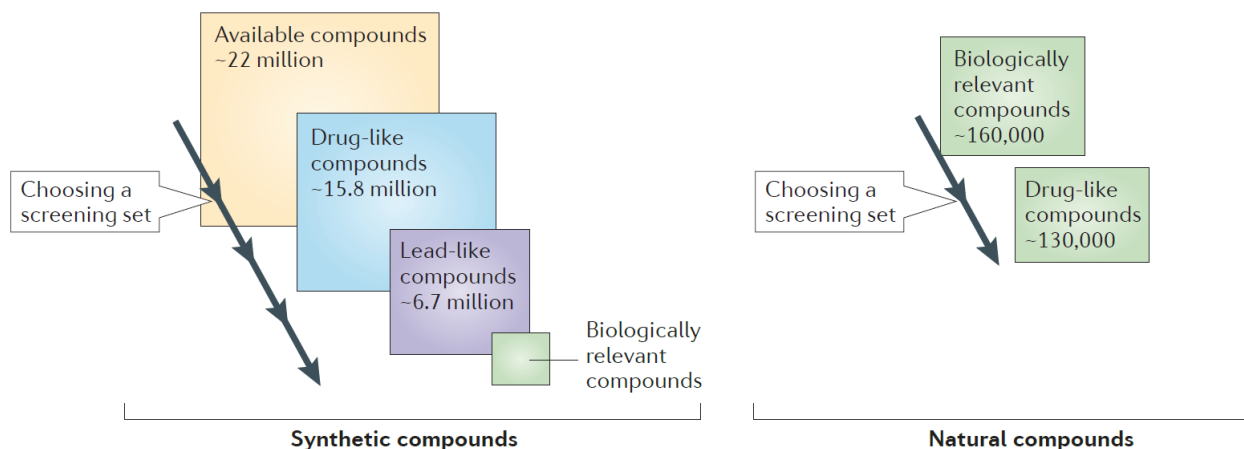


Figure 8: Differences between synthetic and natural screening sets

Reprinted from, “The re-emergence of natural products for drug discovery in the genomics era,” by Alan Harvey et. al. 2015 retrieved from <https://www.nature.com/articles/nrd4510>

Choosing a library to screen from is just as important as choosing a target. Screening libraries either consist of synthetic compounds or natural compounds. The major difference is the size of the screening sets and the amount of filtering needed to get a screening set that is biologically relevant (figure 8). Screening sets of natural compounds usually consists of a smaller set, but less initial filtering is needed for biologically relevant compounds and drug-like compounds. On the other hand screening sets of synthetic compounds like from the ZINC database has millions of compounds that require more filtering steps.

2.15 Criteria of Drug Target Identification and Validation

Regarding structure-based drug design, optimal macromolecule target is highly associated with human disease and binds a small molecule resulting in a desired function. A good target needs to be efficacious, safe, meet clinical and commercial needs and “druggable” (Blagg & Workman, 2014; Hughes

et al., 2011). A “druggable” target is accessible to the accepted drug molecule, that can range from a small molecule or larger biologicals. Binding to the target must elicit a biological response that can be measured in vitro and in vivo. Drugs come up short in clinical phases for two fundamental reasons; the primary is that they are unable to get the same results as the preclinical phase and the second is that they are not efficacious (Hughes et al., 2011).

2.16 Lipinski’s Rule of Five

The rule of five (Ro5) has been an integral part of drug design since the late 90s (Lipinski et al., 1997; Walters, 2012). Because of the extremely high failure rate of novel drugs, identifying a lead drugs pharmacokinetics, pharmacodynamics, and the extent of its pharmacological effects at its target is very important. In 1997, Lipinski and colleagues developed Rule of 5 criteria (Walters, 2012). These rules were developed as a useful guideline for the structural and physicochemical properties manipulating the bioavailability of orally administered active compounds. These criteria include “a molecular weight greater than 500 Da; greater than 5 hydrogen bond donors; greater than 10 hydrogen bond acceptors, and a partition coefficient (Log P) greater than 5” (figure 9 - 12)(Lipinski et al., 1997). However, this is not the end-all-be-all of drug design. For instance, the average molecular mass and the threshold for hydrogen-bond acceptors, has greatly increased since the Rule of Five was identified.

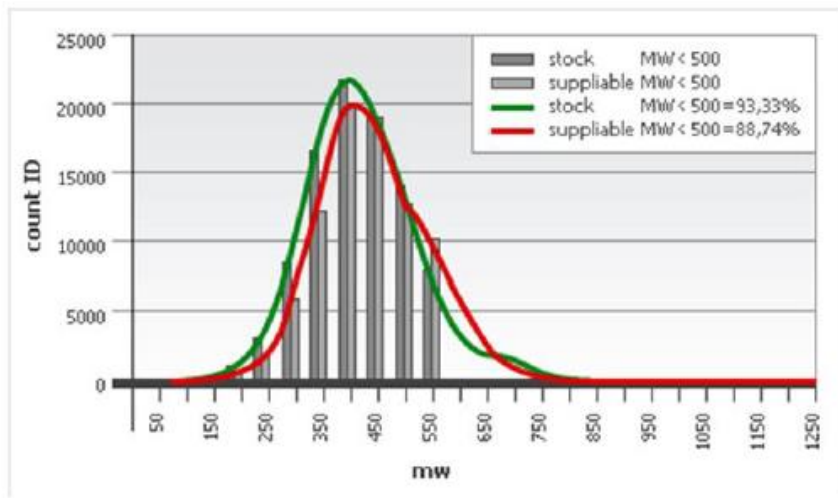


Figure 9: The Lipinski Rule of 5, Molecular Weight

Reprinted from, “Experimental and Computational approaches to estimate solubility and permeability in drug discovery and development settings,” by Christopher Lipinski et. al. 1997, retrieved from

[https://doi.org/10.1016/S0169-409X\(96\)00423-1](https://doi.org/10.1016/S0169-409X(96)00423-1)

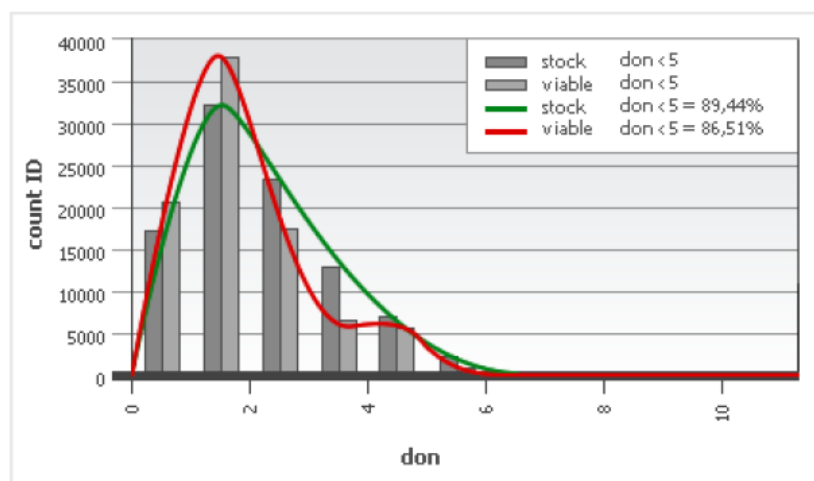


Figure 10: The Lipinski Rule of 5, Hydrogen bonds

Reprinted from, “Experimental and Computational approaches to estimate solubility and permeability in drug discovery and development settings,” by Christopher Lipinski et. al. 1997, retrieved from

[https://doi.org/10.1016/S0169-409X\(96\)00423-1](https://doi.org/10.1016/S0169-409X(96)00423-1)

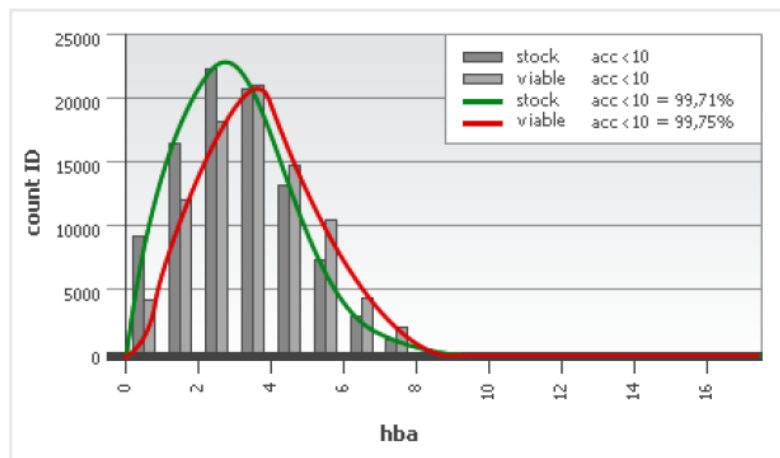


Figure 11: The Lipinski Rule of 5, Hydrogen Bond Acceptors

Reprinted from, “Experimental and Computational approaches to estimate solubility and permeability in drug discovery and development settings,” by Christopher Lipinski et. al. 1997, retrieved from

[https://doi.org/10.1016/S0169-409X\(96\)00423-1](https://doi.org/10.1016/S0169-409X(96)00423-1)

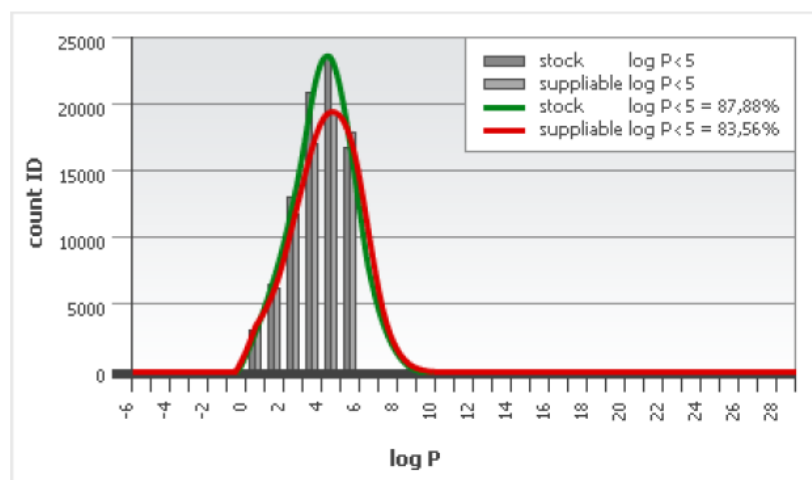


Figure 12: The Lipinski Rule of 5, LogP

Reprinted from, “Experimental and Computational approaches to estimate solubility and permeability in drug discovery and development settings,” by Christopher Lipinski et. al. 1997, retrieved from

[https://doi.org/10.1016/S0169-409X\(96\)00423-1](https://doi.org/10.1016/S0169-409X(96)00423-1)

2.17 Virtual High Throughput Screening

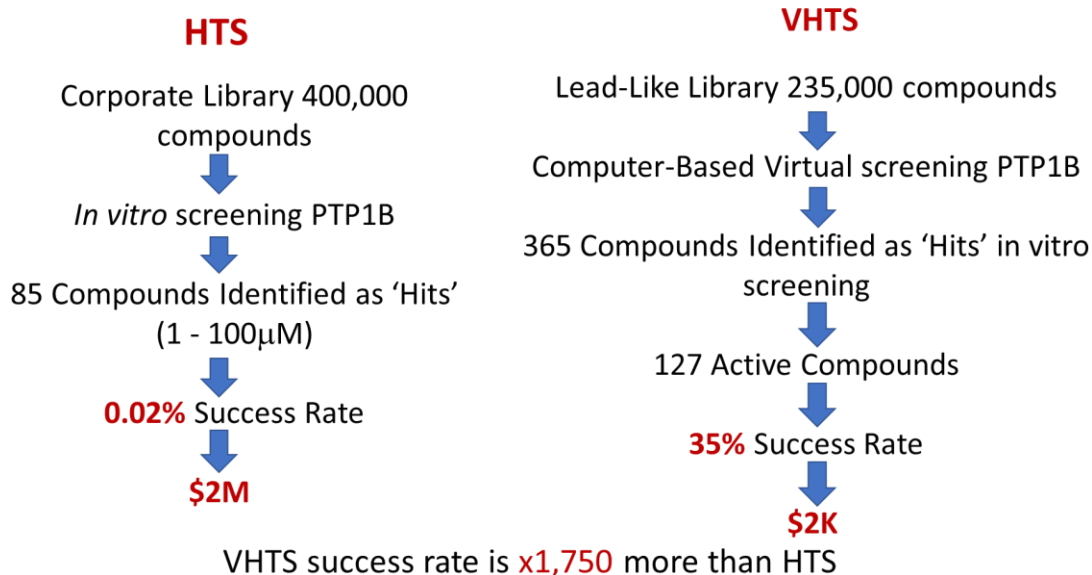


Figure 13: High throughput screening vs. Virtual High throughput screening

Reprinted from, "Molecular docking and high-throughput screening for novel inhibitors of protein tyrosine phosphatase-1B" by Thompson Doman et. al. 2002, retrieved from

<https://pubs.acs.org/doi/full/10.1021/jm010548w>

High throughput screening (HTS) is a method used in drug discovery and other scientific fields to rapidly test large numbers of compounds or molecules for their biological activity, with the aim of identifying potential drug candidates or targets. The process involves the use of automated and robotic systems to perform many tests simultaneously, allowing researchers to quickly analyze the effects of thousands or even millions of compounds on a specific biological target (Doman et al., 2002).

The HTS process begins with the identification of a target, such as a protein or enzyme that is involved in a disease or cellular process. Next, large libraries of compounds are tested for their ability to interact with the target in a desired way. These libraries can contain a wide range of molecules, including natural products, synthetic compounds, or compounds derived from combinatorial chemistry techniques.

The screening process itself typically involves several steps, which are performed in parallel by robotic systems. First, the compounds are dispensed into individual wells of a microplate, which is a small plastic tray containing multiple wells. Next, the target molecule is added to each well, and the plate is incubated under specific conditions to allow the compounds to interact with the target. The effect of each compound on the target is then measured using a variety of assays, such as enzyme activity assays, receptor binding assays, or cell-based assays (Entzeroth et al., 2009).

The data generated from the screening process is then analyzed using statistical methods and machine learning algorithms to identify the most promising compounds. These compounds can be further tested and optimized for their efficacy, safety, and other properties, in a process known as lead optimization.

HTS has revolutionized drug discovery by enabling the rapid identification of potential drug candidates and targets, thereby accelerating the drug development process. However, the process is not without its limitations, including the cost and complexity of building and maintaining the necessary robotic systems, and the challenge of designing assays that accurately reflect the biological activity of the target molecule in vivo (Ferreira et al., 2015). When comparing HTS to VTS for the development of an inhibitor of PTP1B, VTS had a 35% success rate while the HTS method had a 0.02% success rate (figure 13).

2.18 Drug Design and its methods

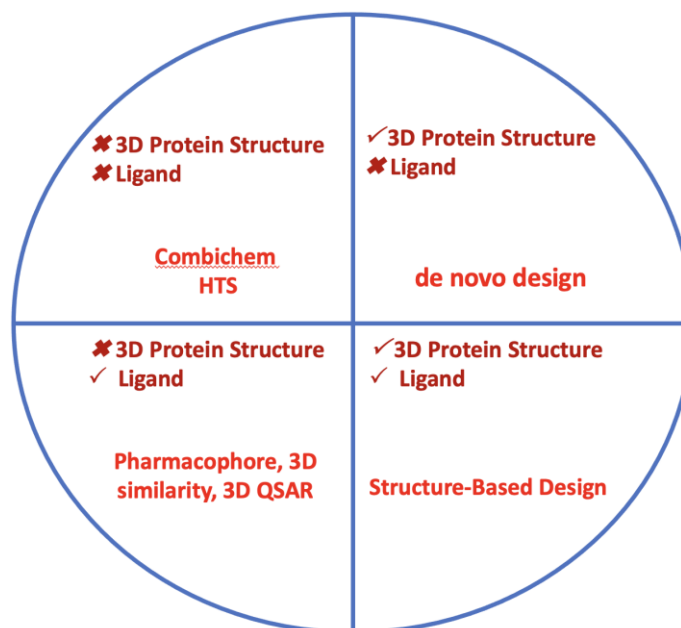


Figure 14: The four major classifications of drug design methods.

Drug design is a complex process that involves multiple stages, starting from the identification of a target molecule to the development of a drug that can interact with the target molecule and produce a therapeutic effect. There are several methods of drug design, structure-based drug design, ligand-based drug design, pharmacophore drug design, combinatorial chemistry, and fragment-based drug design (figure 14).

Structure-based drug design method involves the use of computer simulations and experimental techniques such as X-ray crystallography and nuclear magnetic resonance (NMR) to determine the structure of the target molecule (figure 15) (Baig et al., 2016). This information is then used to design molecules that can interact with the target molecule in a specific way, either by mimicking its shape or by binding to specific sites on the molecule.

Ligand-based drug design method, the structure of a known ligand that binds to the target molecule is used as a starting point for designing new molecules (Gupta et al., 2021). The structure of the ligand is modified to improve its binding affinity and selectivity for the target molecule.

A pharmacophore-based drug design method involves the identification of a set of chemical features or pharmacophores that are important for the activity of a known ligand or drug (Sakthivel & Habeeb, 2018). The pharmacophore is then used as a template for designing new molecules that can interact with the target molecule in a similar way.

Combinatorial chemistry method involves the synthesis of large libraries of compounds that can be screened for activity against the target molecule. The libraries are created by combining different chemical building blocks in a systematic way, and the resulting compounds are tested for activity in high-throughput screening assays.

Fragment-based drug design involves the identification of small fragments of molecules that can bind to the target molecule. The fragments are then linked together to form larger molecules that can interact with the target molecule in a more specific way.

Overall, the choice of method depends on the nature of the target molecule and the resources available for drug design. Often, a combination of methods may be used to increase the chances of success in drug discovery.

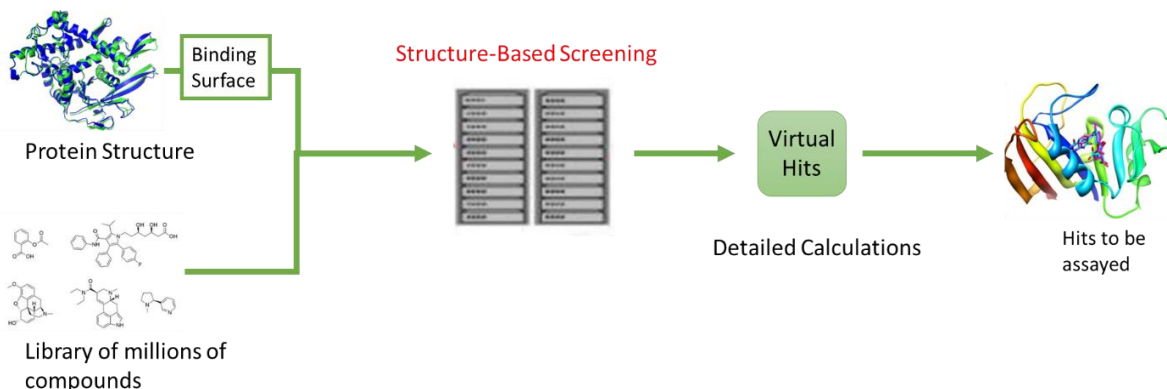


Figure 15: Structure- based high throughput screening begins with the conformational structure information of the ligand and protein then continues with docking studies, virtual Hit generation, and concludes with in vivo or in vitro assay.

2.19 Methods of Virtual High Throughput Screening

There are several methods of drug design, *in silico* screening methods are broadly classified as structure- or ligand-based methods. If the three-dimensional (3D) structure or model of a macromolecular target is known, structure-based approach is used. This approach is also referred to as high-throughput docking (HTD) which consists of: identifying the plausible binding sites where the small molecules may interact with the target (binding site identification/target druggability prediction); virtual chemical library selection; positioning of the selected compounds into the binding site(s) of the target (this process is called docking); and the scoring of each compound, which represents the probability of binding to the target (scoring and ranking) (Arimont et al., 2017). Thus, HTD may be considered as the *in-silico* equivalent of HTS, as, in principle, attempts to computationally reproduce ligand-receptor binding. This project will be using the structure-based virtual high throughput screening design for drug discovery. This is because the 3D protein structure of PARP1 exists and there

are already known ligands that inhibit PARP. Virtual high throughput screening is the sensible alternative to traditional high throughput screening (HTS).

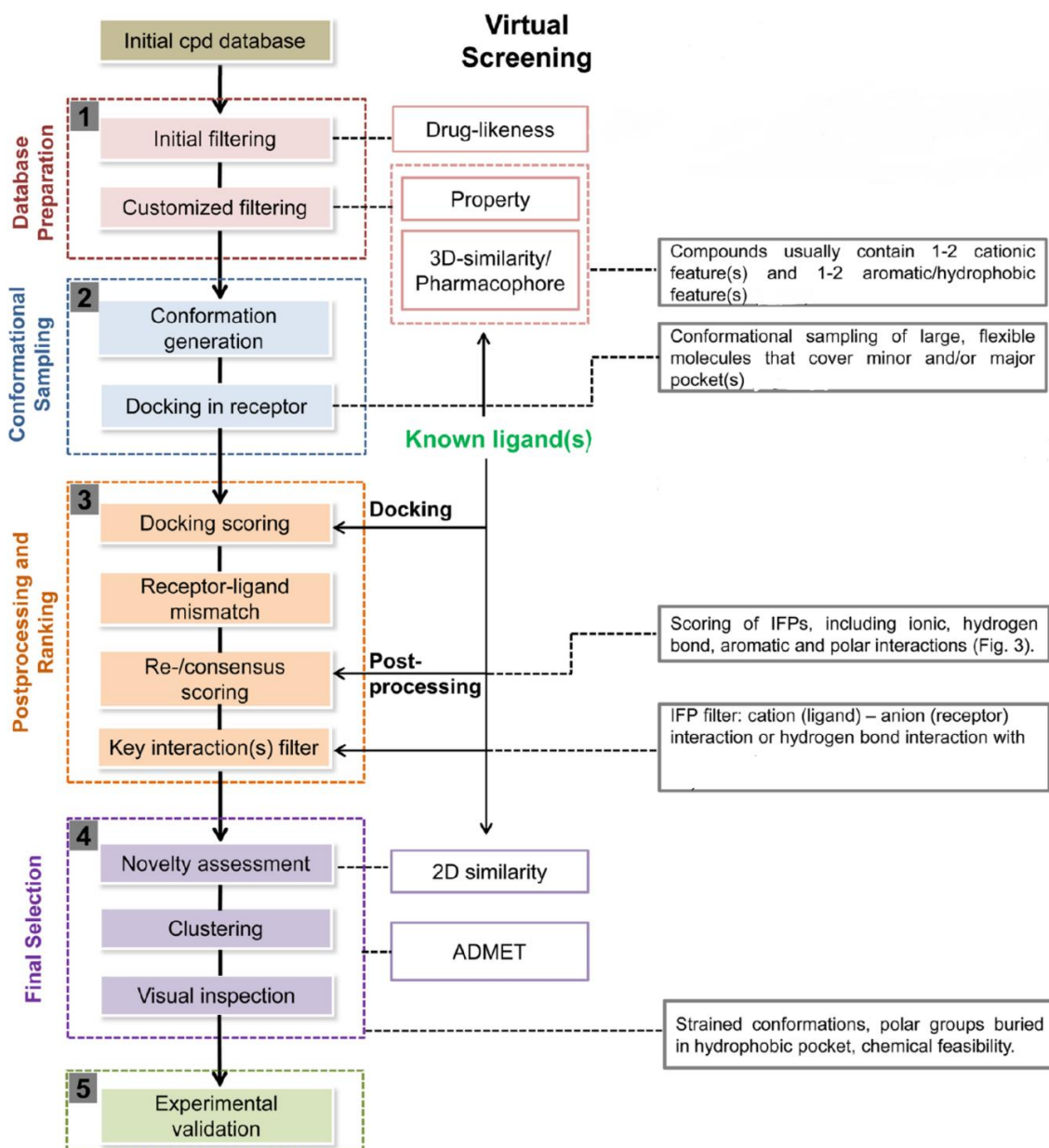


Figure 16: Methods of Virtual Screening

Reprinted from, "Structural Analysis of Chemokine Receptor-Ligand Interactions," by Marta Arimont et.

al. 2017, retrieved from <https://pubs.acs.org/doi/full/10.1021/acs.jmedchem.6b01309>

Not only is virtual HTS labor efficient, but it is also cost effective and saves time. A main difference between experimental and virtual screening is the cost and time involved. Months are required to design an assay, set up the HTS experiment, run it and analyze results, despite recent advances in miniaturization and robotics. On the contrary, this time is much shorter in VS, although the post-screening/analysis stage could take more time than usually acknowledged. An important edge of HTD compared to HTS and non-receptor-based VS methods is the ability to provide a tentative 3D representation (binding mode) of the ligand: receptor complex (Arimont et al., 2017). In cases where these binding modes can explain the SAR data, results from HTD may then be used for the lead optimization stage. On the other side, a main advantage of HTS is that, in principle, it provides an actual measurement of the compound's activity, compared to VS methods, which only furnish a prioritized list of compounds for further experimental testing.

There are five major steps to virtual HTS (Figure 16). The first step is database preparation. This is where the initial filtering takes place. Properties such as drug-likeness and 3D-similarity are considered. Does the ligand follow Lipinski's rule of five? Is the structure of the ligand like known inhibitors? The next step is conformational sampling. Since compounds can exist in many different conformations due to bond lengths or the rotation of flexible bonds, we must make sure the ligands are in the right conformation. After conformation generation, the ligands are ready for docking in the receptor, and we can move on to the third step, postprocessing ranking. Ligands are ranked based on docking score, receptor-ligand mismatch, hydrogen bonding and polarity. A docking score considers the calculated noncovalent three-dimensional (3D) interactions between a ligand and a protein. Quantitatively, docking scores with more negative binding energy values are considered good. This means that the docking score is based on free energy of binding of a ligand to a receptor. The next step is the final selection phase. The novelty of the ligands are considered and its ADMET properties. Also, a visual inspection of the ligands are done to see if there are any unfavorable properties such as a strained

conformation, The polar groups buried in hydrophobic pockets, and if the ligands are chemically feasible. The Final step in this process is experimental validation of the ligands that made it through the filtering. The ligand's inhibition can be validated through molecular dynamics, *in vitro* studies, and *in vivo* studies.

2.20 Molecular Dynamics

Classical molecular dynamics (MD) is a useful tool that can incorporate Newtonian physics to identify structural properties of the drug-target complex. This computer-based algorithm can confirm and explain the molecular interaction and even the motion of the atoms responsible for the interaction (Warshel, 2002). It is amazing how years of lab work can be circumnavigated by using MD to yield the same or sometimes even more concise results. MD usually measures free energy, kinetics measures, and other macroscopic amounts, which can be compared with lab-based observations and used to draw conclusions of the overall interactions of ligands and their target molecules (Karplus & McCammon, 2002).

Studies by Karplus and McCammon (Karplus & McCammon, 2002) and by Warshel (Warshel, 2002) outline the important role classical MD simulations play in studying biological systems. Over the years, researchers have increasingly realized that MD can also overcome important limitations of structure-based drug design. Ligand docking calculations cannot fully show all the major conformational changes proteins undergo when ligands bind to it.

CHAPTER 3

DESIGN OF STUDY

3.01 Central Hypothesis and Aims

PARP inhibitors are a relatively new drug classification with only four having the status of FDA-approved. The purpose of this project is to identify PARP1 inhibitors by *in silico* high throughput screening. The project aims and objectives are the following:

1. To discover novel hit molecules using *in silico* high-throughput screening of 4,591,276 lead-like molecules from ZINC database for PARP1 inhibitory activity.
2. To analyze structure-based virtual screening hit molecules by post processing analysis and ranking for PARP1 inhibitory activity.
3. To investigate the top 5 hit molecules using molecular dynamics.
4. Test virtual high throughput screening top hit molecules for their PARP1 inhibitory activity.

3.02 Materials, Compounds, and chemicals

- DMSO (Sigma-Aldrich, St. Louis, MO)
- DTT (Promego, Madison, WI)
- PBS (VWR, Randor, PA)
- Tween-20 (VWR, Randor, PA)
- Sulfuric Acid (Sigma-Aldrich, St. Louis, MO)
- PARP1 Colorimetric Assay Kit (BPS Bioscience #80580, San Deigo, CA)
- 25 PARP1 inhibitor hits (Enamine, Monmouth Junction, NJ)
- Virtual Hits Compounds: Compounds were purchased from Enamine using the following catalog numbers and SMILES.

Z19572914: Cc4cc(C)n3nc(C(=O)OCC(=O)c1c[nH]c2cccc12)nc3n4

Z28077285: Cc1ccc2c(c1)CCCN2C(=O)CCc4nc3cccc3c(=O)[nH]4

Z110096110: CC4Oc3ccc(NC(=O)Cc1c[nH]c2cccc12)cc3NC4=O

Z74715974: Cn2c(c1cccc1)cnc2SCc4nc3cccc3c(=O)[nH]4

Z225653548: O=C(c1n[nH]c(=O)c2cccc12)N5CCc4[nH]c3cccc3c4C5

Z30644325: O=C(Cc1n[nH]c(=O)c2cccc12)Nc4ccc(N3CCCC3)cc4

Z32391921: O=C(Cc1c[nH]c2cccc12)N4CCN(c3cccc3O)CC4

Z124826588: CN(CC(=O)c1c[nH]c2cccc12)Cc4nc3cccc3c(=O)[nH]4

Z167798216: Nc3nc(COC(=O)Cc1c[nH]c2cccc12)nc4cccc34

Z372757196z: O=C(NCCCN2CCc1cccc1C2)c3n[nH]c4cccc34

Z321249898: O=C(Nc3ccc(n2cnc1cccc12)cc3)c5cc(C4CC4)[nH]n5

Z148570968: O=C(OCc2cc(c1cccc1)on2)c3n[nH]c(=O)c4cccc34

Z729248128: O=c3[nH]c(CCN1CCCC1c2ccc[nH]2)nc4cccc34

Z421514920: O=C(NC2CCN(c1ncccn1)CC2)c4cc3cccc3c(=O)[nH]4

Z421625134: O=C(NC2CCN(c1cccc1)CC2)c4cc3cccc3c(=O)[nH]4

Z729231748: O=c3[nH]c(CCN2CCN(C1CCCC1)CC2)nc4cccc34

Z195904178: Cc4cccc(N3CCN(Cc2nc1ccsc1c(=O)[nH]2)CC3)c4

Z1118682269: Cc3cccc4[nH]cc(CC(=O)NC2CCN(c1ncccn1)CC2)c34

Z1037500644: O=C(CCNC(=O)c1[nH]nc2cccc12)Nc3nnc4cccc34

Z91830525: Cc2nc1cccc1nc2COC(=O)c3n[nH]c(=O)c4cccc34

Z1021215630z: CC(NC(=O)c1[nH]nc2cccc12)C(=O)Nc3nnc4cccc34

Z1359552843: Cn4c(CCCNc2nc1cccc1c(=O)[nH]2)nc3cccc34

Z224755122: O=c3[nH]c(CN2CCN(Cc1cccc1)CC2)nc4ccsc34

Z1695739736: O=C(NCCc2nc(c1cccc1)n[nH]2)c3n[nH]c4cccc34

Z990888126: O=c3[nH]c(NCCn2nc1CCCN1c2=O)nc4cccc34

Supplies

- Pipettes (2-20 µl, 20-200 µl, 200-1000 µl) (Rainin Instruments, LCC, Oakland, CA, USA)
- Pipette Tips (10 µl, 200 µl, 1000 µl) (Molecular BioProducts, San Diego, CA, USA)
- Microcentrifuge tubes (multicolored and clear, 1.5 mL) (VWR, West Chester, PA, USA)

Equipment, Apparatus, and Software

- Temperature controlled shaker (VWR, Randor, PA)
- BMG UV-Vis plate reader (BMG LABTECK, Cary, NC)
- Omega2 (Openeye Scientific, Sante Fe, New Mexico, USA)
- MakeReceptor (Openeye Scientific, Sante Fe, New Mexico, USA)
- FRED (Openeye Scientific, Sante Fe, NM, USA)
- Discovery Studio (Accelrys, Bovia Systems, Waltham, MA, USA)
- ZINC²⁰ Database (University of California, San Fransisco, CA)
- Protein Data Bank (RCSB PDB)

3.03 Methods

Protein-Ligand Interactions. To determine the crucial protein-ligand interactions active site amino acid residues and the types of interactions for PARP1 inhibitory activity, we used the Protein Data Bank (PDB) for x-ray crystal structure of good resolution for the PARP1-inhibitory complex. Other selection criteria include, the enzyme being from the human genome, no mutations, all parts of the inhibitor included, binding occurring at the catalytic domain. PARP1 inhibitor complex 5A00 was selected based on those criteria.

Lead-Like Library. The ZINC²⁰ database is a free database consisting of more than 35 million commercially available compounds available for purchase that was used for the study. The molecules in the database may be searched using several criteria options. Our criteria were as follows, lead-like molecules that did not possess chemically reactive functional groups, were not promiscuous inhibitors, or frequent hitters. The Zinc²⁰ database search resulted in 4.5 million lead-like molecules. The 4.5 million molecules were placed in 32 manageable subsets containing approximately 200,000 molecules each.

Receptor File generation. To prepare for docking to the receptor, a receptor file needs to be generated. PARP-1's crystal structure was taken from 5A00 in the protein data bank (PDB). We used MakeReceptor program from Openeye to generate receptor file. These receptor files have the protein's active site and the ligand.

3D Conformer Generation. To convert the 2D structure from the ZINC database to 3D structures we used conformer generation method via OMEGA2. The software converts the 2D structures to 3D and obtains the most stable conformation of the molecules.

Filters Applied for Virtual High Throughput Screening. For our initial filtering, we selected the molecules that follow Lipinski's rule of 5, drug likeness, chemical properties, and similarity. The result yielded 32 subsets containing 500 Hit molecules totaling 20,000 Hit molecules. Our study also performed SciFinder Analysis for each molecule. We searched the SciFinder to establish novelty of the molecules. Molecules that had not been reported for PARP inhibitory activity were selected. Following the scoring and SciFinder search, we selected molecules based on their commercial availability resulting in 25 molecules.

Molecular Dynamics Simulations. To comprehend the structural alterations and the relative stability of the target associated with ligands, MD simulations were run. The protein-ligand complexes were positioned in a cubic box and parameterized using the Amber-ff14SB. The TIP3P water models were used to solvate the box. Using the RESP approach, partial atomic charges for ligands were assigned using quantum chemical calculations at the M06-2X/6-311++G** level. The ions were added to the system to neutralize it. By employing the steepest descent approach, the protein-ligand complexes were reduced to a minimum. Additionally, to maintain the temperature and pressure at 300 K and 1 bar, respectively, the complete system was equilibrated under an NVT and NPT ensemble for 5 ns utilizing velocity-rescaling and Berendsen coupling. For all three dimensions, periodic boundary condition (PBC) was

utilized. With a threshold of 1.2 nm, the electrostatic interactions were calculated using the Particle Mesh Ewald (PME) method. All bonds involving hydrogen atoms were constrained using the LINCS method. The entire system was simulated during the production run for 100 ns, with a 2 fs integration time step. The Gromacs 2016.3 software was used to run MD simulations. Using the g_mmpbsa tool, the binding free energy between the receptors and ligands was determined. PyMOL is used to visualize the trajectories and structural conformations.

Molecular Dynamics (MD) simulations were performed using Gromacs 2020.4, an online software available for public use. The forcefield parameters were used amberff19SB-ILDN and General Amber Force Field (GAFF) for PARP1 protein and the ligands, respectively. The protein-ligand complexes were placed in a cubic box with the dimensions of $\sim 12.4 \times 12.4 \times 12.4$ nm³. The SPC/E water models were used and 15 Cl⁻ ions were added to neutralize the system. The atomic partial charges were calculated using Restrained Electrostatic potential (RESP) method. Initial geometries of the system is minimized using steepest descent algorithm. Further, the system is equilibrated with NVT and NPT for 2 ns at the temperature T=300k and pressure P= 1 bar. V-rescale thermostat and Parrinello-Rahman barostat were used for maintaining the temperature and pressure, respectively. Periodic boundary conditions were applied for all three dimensions. The long-range electrostatic interactions were calculated using Particle Mesh Ewald (PME) method with the cut-off distance is 1.2 nm. All H-atoms are constrained using the LINCS algorithm. The production run was performed for 100ns.

To determine the structural stability during the simulation, root mean square deviation (RMSD) is applied to the target complexes' backbone. By analyzing the RMSD along a structure's trajectory in relation to the reference structure, the conformational changes in the structure are identified. Because the C α of the target complexes represents the fluctuations in each residue during the simulation, root mean square fluctuation. RMSF is carried out for the C α atoms target proteins to determine the

remaining fluctuations. R_g is used to calculate the protein's compactness and folding rate for the target proteins' backbones. For PARP-1, RMSD, RMSF, and R_g were computed using the reference structure.

The MM/PBSA approach was employed to assess the binding free energy of protein-ligand complexes. In silico predictions of protein-ligand affinities have been successfully improved using the MM-PBSA technique to assess free binding energy. In an MM-PBSA analysis, the total potential of the system is affected negatively by electrostatic, van der Waals (vdW), and solvent-accessible surface area (SASA) interactions, while positively affected by polar solvation energy.

3.04 Stock Solution Preparation

1X PBS Preparation. One packet of PBS powder was added to 1L graduated cylinder, and then water was added to the 1000 mL line. The solution was mixed midway through adding water and after all water was added.

PBST Preparation. A 1000 mL stock solution of PBS-T was made with 100 mL 10X PBS, 1 mL of Tween-20, and 900 mL deionized water.

10 mM DTT preparation. A 10 mL 10 mM DTT solution was prepared by weighing 1.54 grams of DTT powder. Using a graduated cylinder, 10 mL of water was added.

1X Histone Mixture Preparation. Using the 5X histone mixture provided, we diluted 1 mL of the mixture with 5 mL of 1X PBS.

Master Mix Preparation. Using formula provided by the assay kit, the master mix proportions were calculated for a 96 well plate. It was prepared by adding 245 μ L of 10X PARP1 Bbuffer, 245 μ L of PARP substrate, 490 μ L of diluted DNA, 1225 μ L of water, and 245 μ L of 10 mM DTT solution.

Blank Control Preparations. All blanks were made with 5 μ L of diluent solution, 20 μ L of 1X PARP1 buffer with DTT, and 25 μ L of Master Mix for a final volume of 50 μ L. A total of 4 blanks were prepared.

Virtual Hits Preparation in DMSO. The virtual hits were obtained from Enamine, LCC of Cincinnati one through twenty-five respectively. 100 mM stock solutions of our hits were prepared in DMSO. Stock solutions were stored at -80°C until needed.

Serial Dilution of Virtual Hits. The dilutions were made with 1XPARP assay buffer containing DTT. Serial dilutions for each compound was done to obtain 50 μ M and 25, μ M.

Diluted Streptavidin-HRP Preparation. Diluted streptavidin-HRP was prepared using 1:50ratio with 1X PARP1 buffer with DTT.

3.05 PARP1 Colorimetric Assay

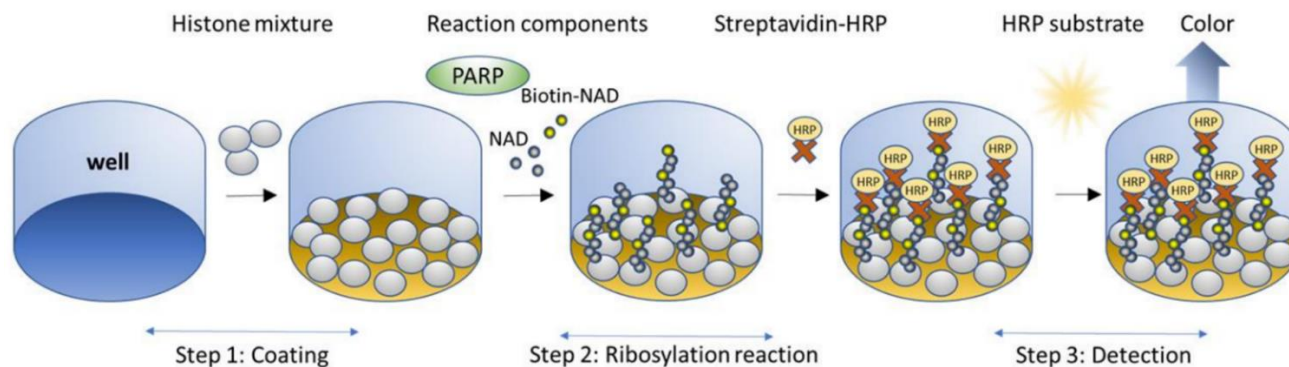


Figure 17: Schematic representation of PARP1 Colorimetric Assay

Reprinted from, "PARP1 Colorimetric Assay Kit," by BPS Bioscience, 2022, retrieved from

<https://bpsbioscience.com/parp1-colorimetric-assay-kit-80580>

Coating the plate with histone mixture. The assay was performed in triplicate, and protocol was followed throughout the experiment (figure 17). We diluted 5x histone mixture 1:5 with PBS to make 1x histone mixture, added 50 μl of histone mixture to each well and incubate at 4°C overnight. The next morning, we washed the plate three times using 200 μl of PBST buffer (1x PBS containing 0.05% Tween 20) per well. Wells were blocked using 200 μl of Blocking buffer 3 to every well. Incubated at room temperature for 90 minutes. We washed the plate three times with 200 μl /well of PBST buffer.

Ribosylation reaction. First, we prepared a fresh solution of 10 mM DTT in DI water, and dilute activated DNA 1:32 with PBS. Master mix was prepared as suggested by the protocol (Number of wells times wells x (2.5 μl of 10x PARP buffer + 2.5 μl of PARP Substrate Mixture 1 + 5 μl of diluted Activated DNA + 12.5 μl of water + 2.5 μl of 10 mM fresh DTT). 25 μl of Master Mix was added to every well.

Prepared 1x PARP buffer with DTT. Dilute 10x PARP assay buffer to 1x PARP assay buffer containing DTT by adding 1 volume of 10x PARP assay buffer + 1 volume of 10 mM DTT + 8 volumes of water. We added 5 μ l of Test Inhibitor to each well labeled as "Test Inhibitor" as seen in Figure ____.

For the "Positive Control" and "Blank," we added 5 μ l of the same diluent solution used to dilute the inhibitor, but without inhibitor (Diluent Solution).

Lastly, the PARP1 enzyme was thawed on ice and diluted the enzyme with 1x Buffer for a final concentration of 1 nM. Aliquot the remaining undiluted PARP1. Once the 20 μ l of diluted PARP1 enzyme is added to the appropriate wells, the reaction is initiated. To the wells designated as "Blank," we added 20 μ l of 1x PARP buffer with DTT. The plate was left to incubate at room temperature for one hour. After the one-hour mark, we washed the plate three times with 200 μ l PBST buffer and tap the plate onto clean paper towel as described above.

Detection. For detection, we diluted Streptavidin-HRP 1:50 in Blocking buffer 3, added 50 μ l of diluted Streptavidin-HRP to each well. We incubated the plate at room temperature for an additional 30 minutes. Wash three times with 200 μ l PBST buffer and added 100 μ l of the colorimetric HRP substrate to each well and incubate the plate at the room temperature until blue color is developed in the positive control well.

After the blue color is developed, we added 100 μ l of 2 M sulfuric acid to each well. Read the absorbance at 450 nm using BMF UV/Vis spectrophotometer microplate reader. The negative control-blank well was 0.05 absorbance at 450 nm.

CHAPTER 4

RESULTS AND DISCUSSION

4.01 Protein-Ligand Interaction

Human PARP1-Inhibitor bound crystallography structure with a good resolution was obtained from the Protein Data Bank (PDB). The binding interactions from the PDB were compared to the FDA approved inhibitors (Olaparib, Rucaparib, Niraparib, and Talazoparib) (figures 18 and 19). The crucial interactions for hydrogen bonding were with the residues Gly863, Ser904, and Arg878 (Figure 18-20). The inhibitor having an amide functional group is important for hydrogen bonding. Ionic interactions were found with residues Glu763 and Asp766. Tyr896, Tyr907, Tyr889, and Arg878 are important residues for Van der Waals interaction. There is also π - π stacking interaction between the benzene ring of Tyr907 and aromatic ring of the inhibitor. The marketed PARP1 inhibitors showed comparable results. Rucaparib and Niraparib had ionic interactions with Glu763 and Asp766 respectively. With this information, we conclude that crucial hydrogen bonding was with PARP1's Gly863, Ser904, and Arg878 residues, ionic interactions with Glu763 and Asp766 are important, as well as Van der Waals' interaction with Tyr896, Tyr907, Tyr889, and Arg878 (figure 21).

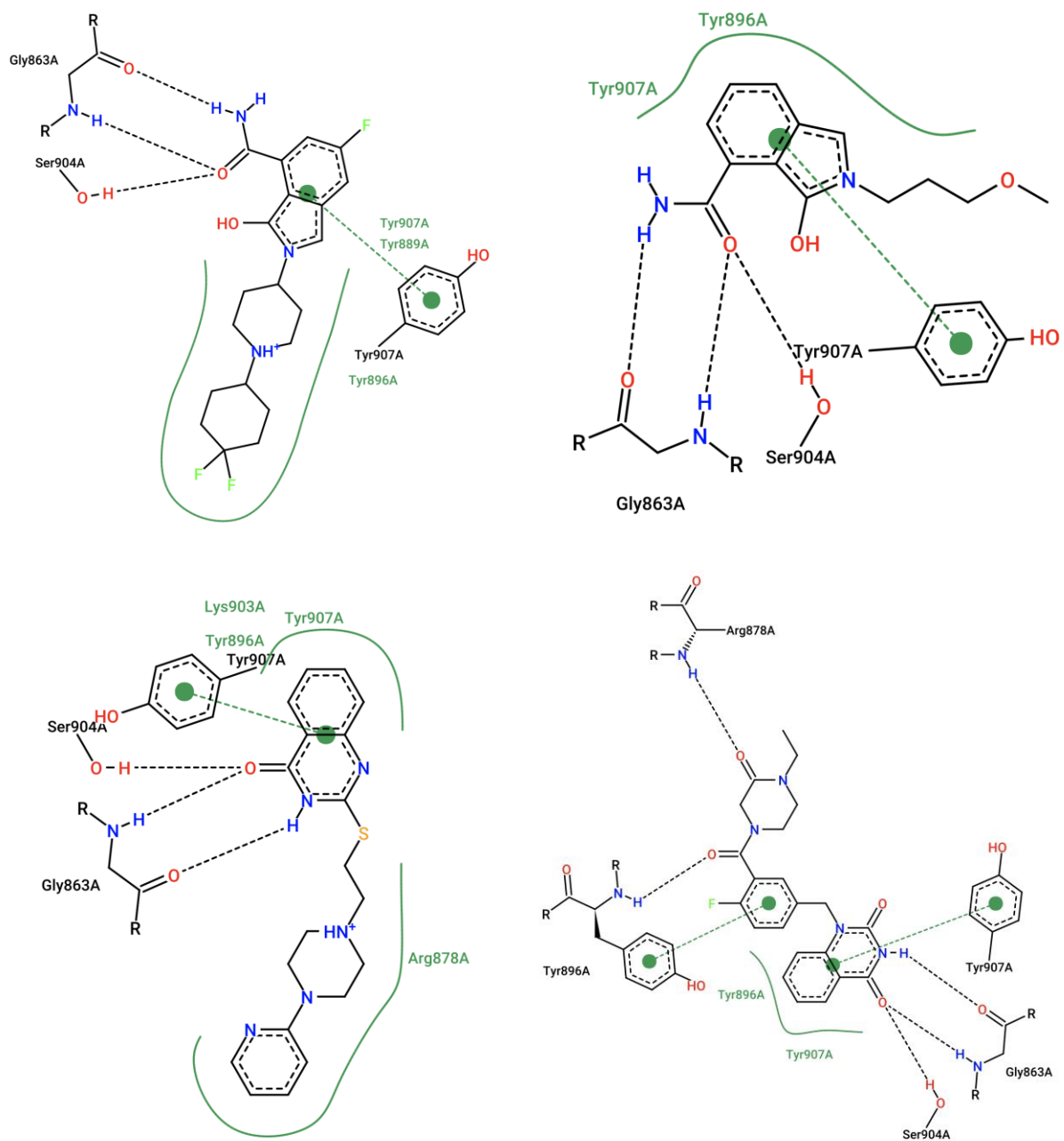


Figure 18: Protein Ligand Interactions

Interactions between PARP1 and compounds from the ZINC database. Dashes indicate bond formation with red elements being hydrogen bond acceptors, blue elements hydrogen bond donors, and green dots indicating π - π stacking formation, and green, solid lines indicating Van der Waals interactions, and minus symbol indication ionic interactions.

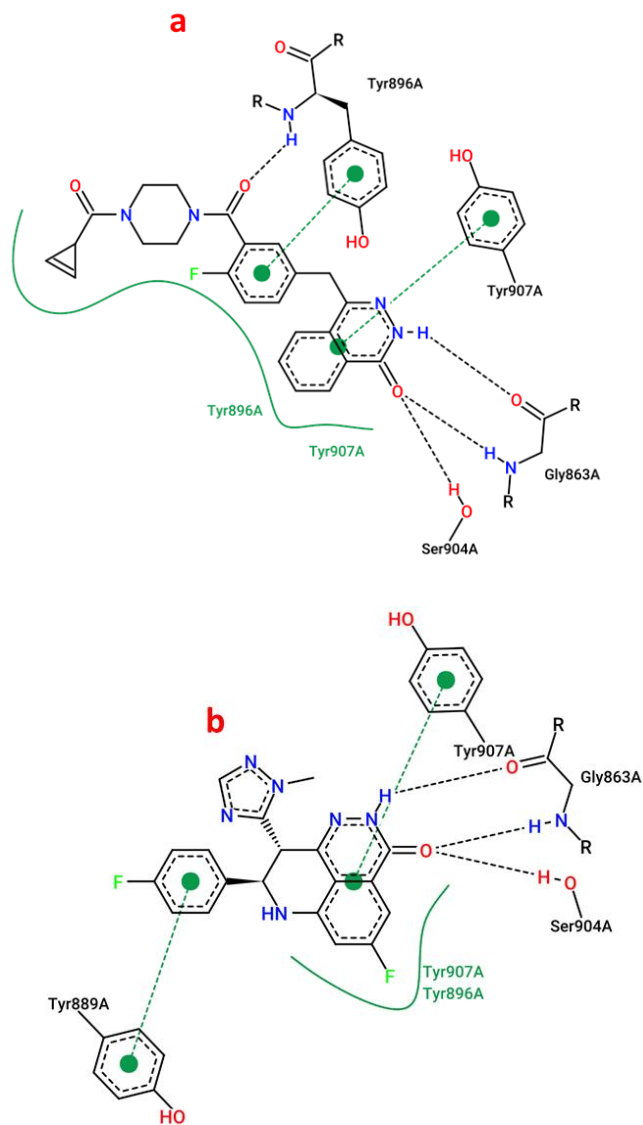


Figure 19: Crucial interactions between PARP1 and marketed drugs, (a) Olaparib (7AAD.pdb), (b) Talazoparib (7KK3.pdb). Dashes indicate bond formation with red elements being hydrogen bond acceptors, blue elements hydrogen bond donors, and green dots indicating π - π stacking formation, and green, solid lines indicating Van der Waals interactions, and minus symbol indicating ionic interactions.

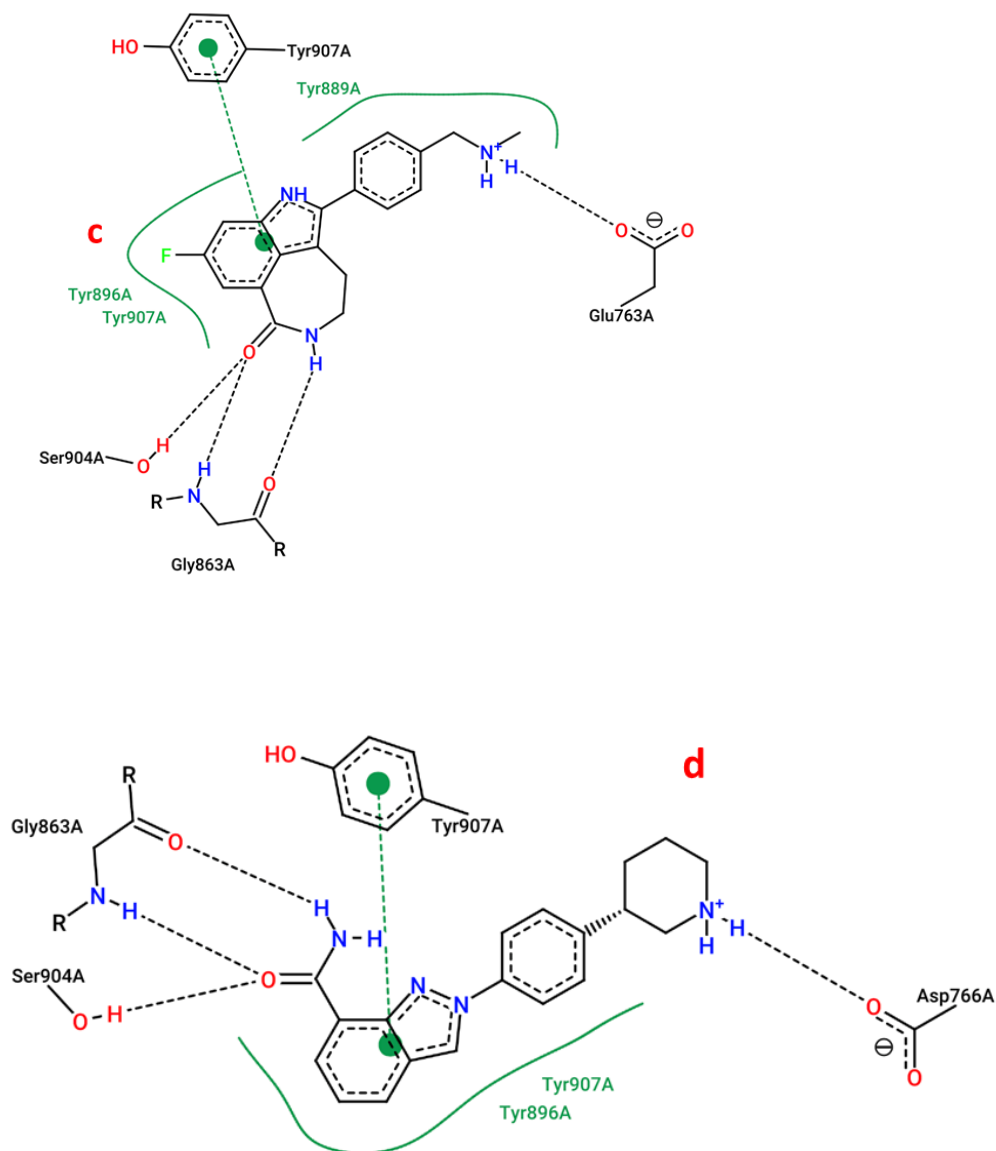


Figure 20: Crucial interactions between PARP1 and marketed drugs, (c) Rucaparib (6VKK.pdb) & (D) Niraparib (7KK5.pdb). Dashes indicate bond formation with red elements being hydrogen bond acceptors, blue elements hydrogen bond donors, and green dots indicating π - π stacking formation, and green, solid lines indicating Van der Waals interactions, and minus symbol indication ionic interactions.

Gly863
Ser904
Arg878

H-Bonding

Glu763
Asp766

Ionic interaction

Tyr896
Tyr907
Tyr889
Arg878

Van der waals interaction

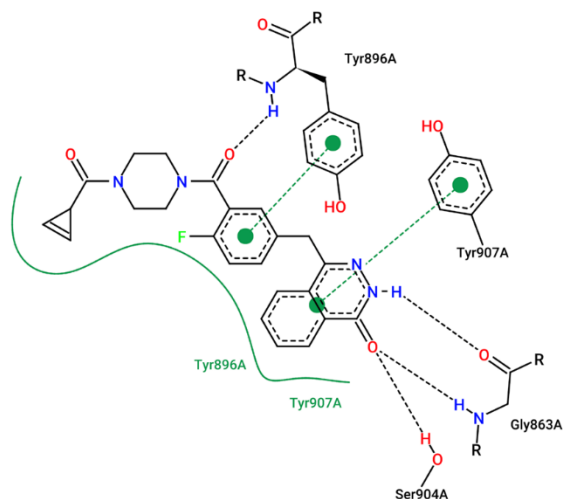


Figure 21: Summary of the crucial interactions. Dashes indicate bond formation with red elements being hydrogen bond acceptors, blue elements hydrogen bond donors, and green dots indicating π - π stacking formation, and green, solid lines indicating Van der Waals interactions, and minus symbol indication ionic interactions.

4.02 Receptor File Generation

The generated receptor files contain PARP1 active site and the ligand (figure 22). These results are used for the molecular docking process. In the docking process the favored orientation of the ligand is predicted, and its results contain the residue fingerprint, shape score, hydrogen bond score, protein desolvation score, ligand desolvation score, and these scores and up to the total score (figure 23). Also, the ligand's characteristics are summarized such as the molecular weight or XloP value.

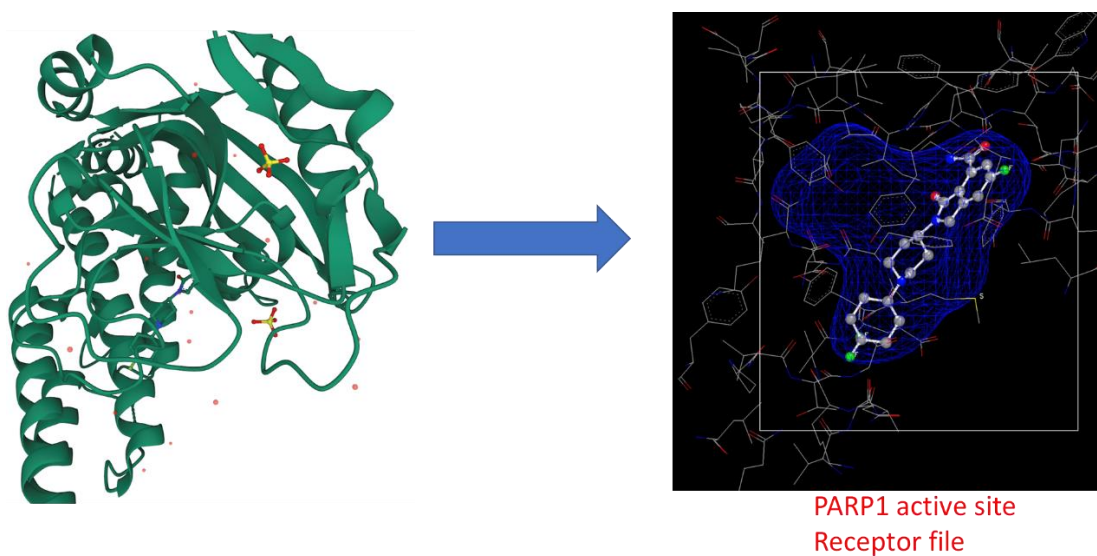
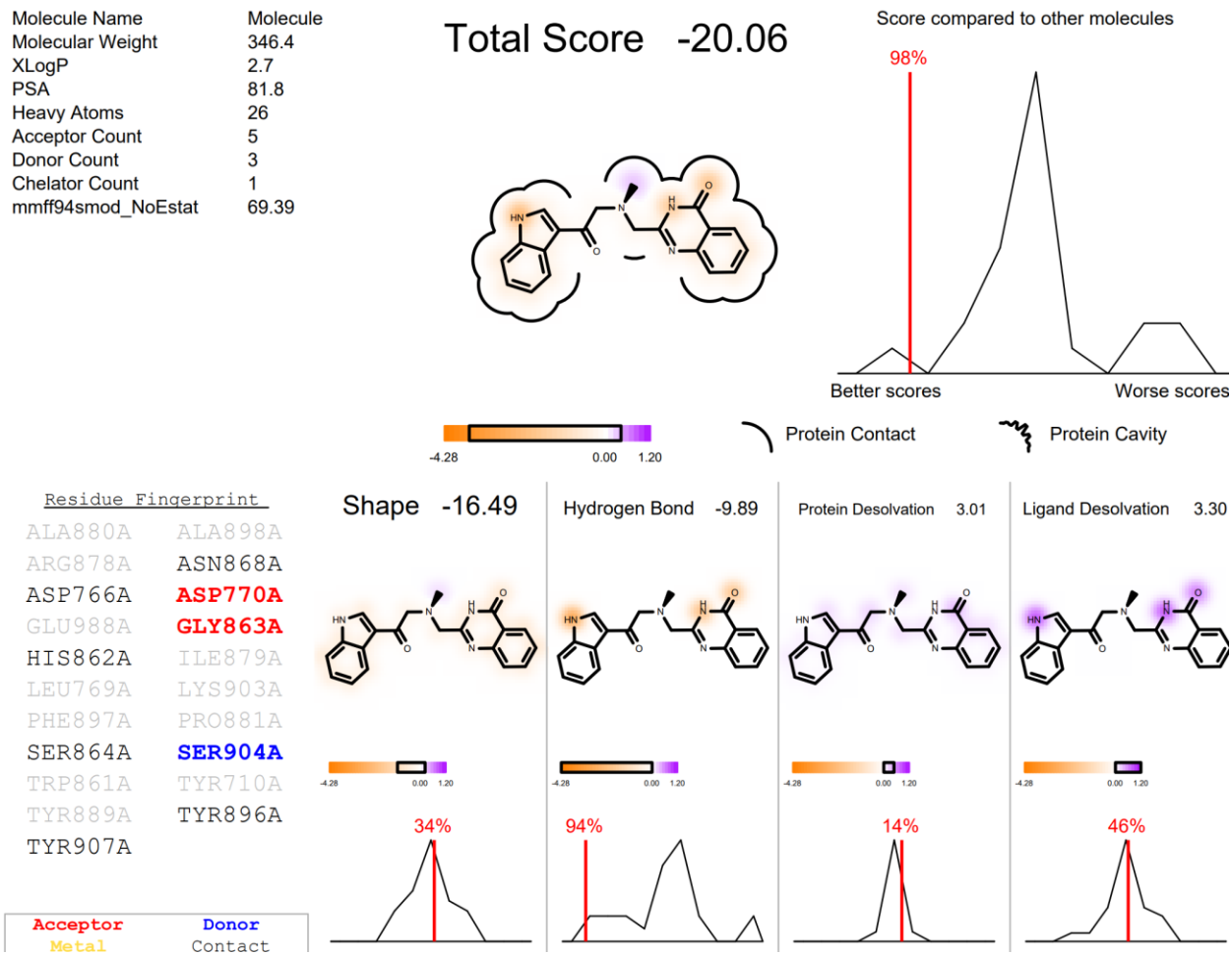


Figure 22: Receptor File Generation. Was generated using MakeReceptor PARP1 PDB 5A00

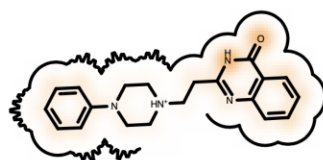
Figure 23: Results from FRED docking of 25 selected ZINC database compounds



Molecule Name ZINC54152523
 Molecular Weight 335.4
 XLogP 2.2
 PSA 53.4
 Heavy Atoms 25
 Acceptor Count 3
 Donor Count 3
 Chelator Count 1
 mmff94s_NoEstat 86.32

Total Score -18.78

Score compared to other molecules



Protein Contact

Protein Cavity

Residue Fingerprint

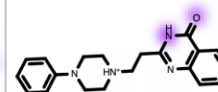
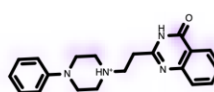
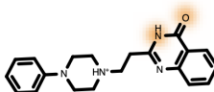
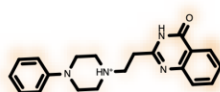
ALA880A	ALA898A	ARG865A
ARG878A	ASN868A	ASN987A
ASP766A	ASP770A	GLN759A
GLU763A	GLU988A	GLY863A
GLY888A	GLY894A	HIS862A
ILE872A	ILE879A	ILE895A
LEU769A	LEU877A	LYS903A
MET890A	PHE897A	PRO881A
SER864A	SER904A	THR887A
TRP861A	TYR710A	TYR889A
TYR896A	TYR907A	VAL762A

Shape -18.21

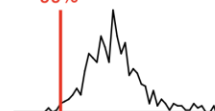
Hydrogen Bond -5.59

Protein Desolvation 2.92

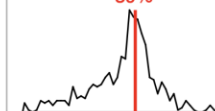
Ligand Desolvation 2.10



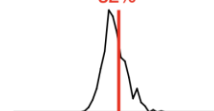
99%



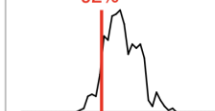
39%



32%



92%



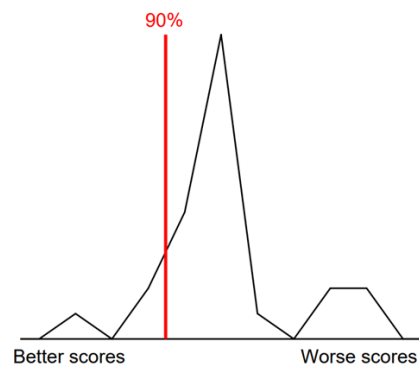
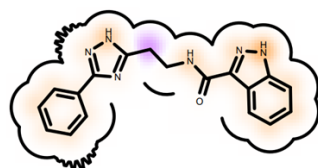
Acceptor
Metal

Donor
Contact

Molecule Name	Molecule
Molecular Weight	332.4
XLogP	3.0
PSA	99.3
Heavy Atoms	25
Acceptor Count	6
Donor Count	6
Chelator Count	3
mmff94smod_NoEstat	41.46

Total Score -18.30

Score compared to other molecules



Protein Contact

Protein Cavity

Residue Fingerprint

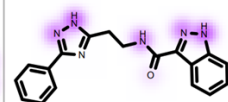
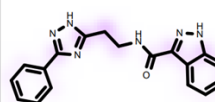
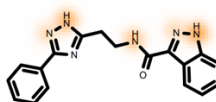
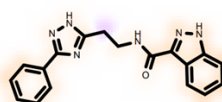
ALA880A	ALA898A
ARG878A	ASN868A
ASP766A	ASP770A
GLU988A	GLY863A
HIS862A	ILE879A
LEU769A	LYS903A
PHE897A	PRO881A
SER864A	SER904A
TRP861A	TYR710A
TYR889A	TYR896A
TYR907A	

Shape -16.78

Hydrogen Bond -10.10

Protein Desolvation 3.29

Ligand Desolvation 5.29

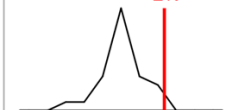
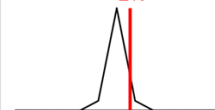
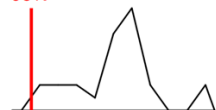
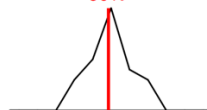


50%

98%

2%

2%

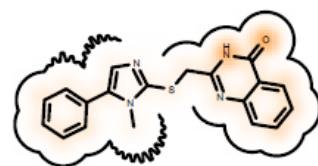


Acceptor Donor
Metal Contact

Molecule Name	Molecule
Molecular Weight	348.4
XLogP	3.4
PSA	63.6
Heavy Atoms	25
Acceptor Count	4
Donor Count	2
Chelator Count	2
mmff94smod_NoEstat	67.03

Total Score -18.08

Score compared to other molecules



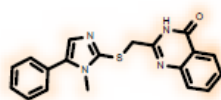
Protein Contact

Protein Cavity

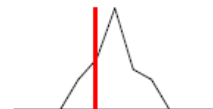
Residue Fingerprint

ALA880A	ALA898A
ARG878A	ASN868A
ASP766A	ASP770A
GLU988A	GLY863A
HIS862A	ILE879A
LEU769A	LYS903A
PHE897A	PRO881A
SER864A	SER904A
TRP861A	TYR710A
TYR889A	TYR896A
TYR907A	

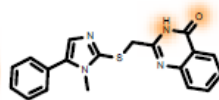
Shape -17.58



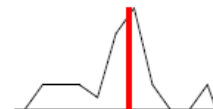
84%



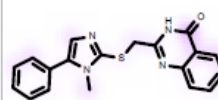
Hydrogen Bond -5.50



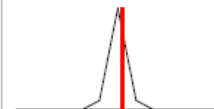
26%



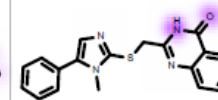
Protein Desolvation 2.89



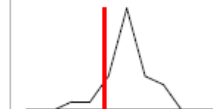
22%



Ligand Desolvation 2.11



86%

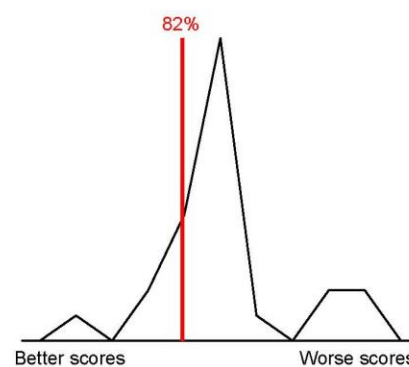
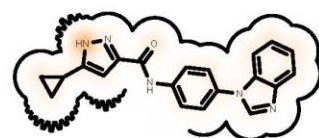


Acceptor	Donor
Metal	Contact

Molecule Name	Molecule
Molecular Weight	343.4
XLogP	3.2
PSA	75.6
Heavy Atoms	26
Acceptor Count	4
Donor Count	3
Chelator Count	2
mmff94smod_NoEstat	75.20

Total Score -17.89

Score compared to other molecules



Protein Contact

Protein Cavity

Residue Fingerprint

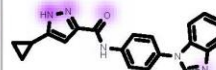
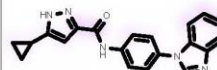
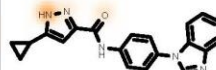
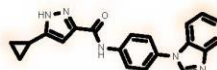
ALA880A	ALA898A
ARG878A	ASN868A
ASP766A	ASP770A
GLU988A	GLY863A
HIS862A	ILE879A
LEU769A	LYS903A
PHE897A	PRO881A
SER864A	SER904A
TRP861A	TYR710A
TYR889A	TYR896A
TYR907A	

Shape -16.72

Hydrogen Bond -6.84

Protein Desolvation 2.37

Ligand Desolvation 3.29

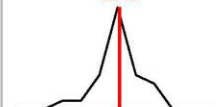
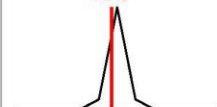
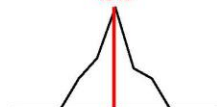


46%

74%

78%

50%

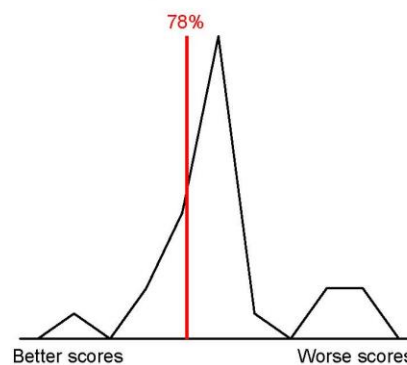
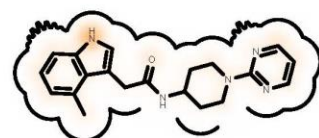


Acceptor Donor
Metal Contact

Molecule Name	Molecule
Molecular Weight	349.4
XLogP	2.2
PSA	73.9
Heavy Atoms	26
Acceptor Count	3
Donor Count	2
Chelator Count	2
mmff94smod_NoEstat	66.03

Total Score -17.72

Score compared to other molecules



Protein Contact

Protein Cavity

Residue Fingerprint

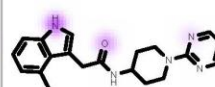
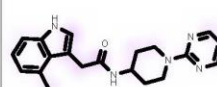
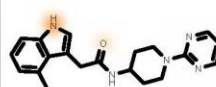
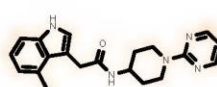
ALA880A	ALA898A
ARG878A	ASN868A
ASP766A	ASP770A
GLU988A	GLY863A
HIS862A	ILE879A
LEU769A	LYS903A
PHE897A	PRO881A
SER864A	SER904A
TRP861A	TYR710A
TYR889A	TYR896A
TYR907A	

Shape -17.00

Hydrogen Bond -5.69

Protein Desolvation 2.73

Ligand Desolvation 2.24



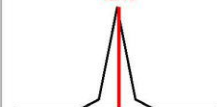
64%



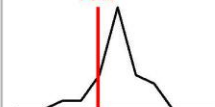
46%



42%



78%

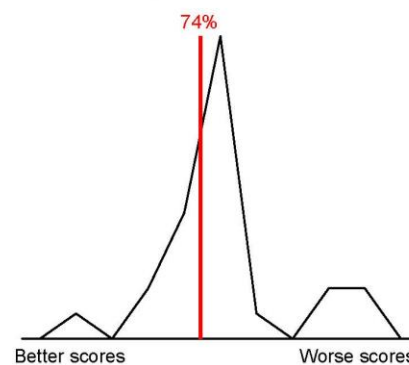
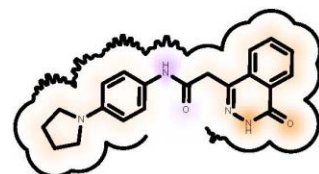


Acceptor	Donor
Metal	Contact

Molecule Name	Molecule
Molecular Weight	348.4
XLogP	2.6
PSA	78.1
Heavy Atoms	26
Acceptor Count	4
Donor Count	3
Chelator Count	1
mmff94smod_NoEstat	88.95

Total Score -17.43

Score compared to other molecules



Protein Contact

Protein Cavity

Residue Fingerprint

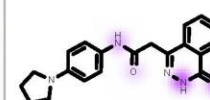
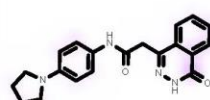
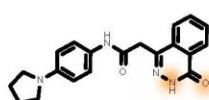
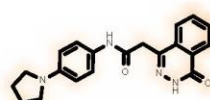
ALA880A	ALA898A
ARG878A	ASN868A
ASP766A	ASP770A
GLU988A	GLY863A
HIS862A	ILE879A
LEU769A	LYS903A
PHE897A	PRO881A
SER864A	SER904A
TRP861A	TYR710A
TYR889A	TYR896A
TYR907A	

Shape -17.16

Hydrogen Bond -5.61

Protein Desolvation 2.35

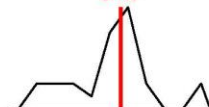
Ligand Desolvation 2.98



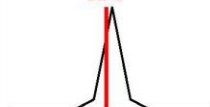
72%



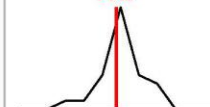
34%



82%



70%

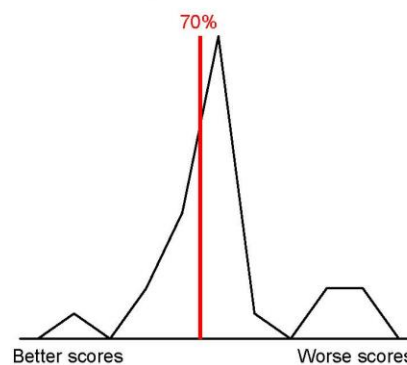
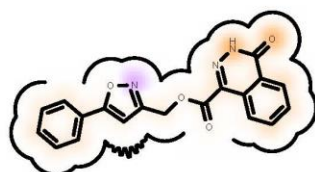


Acceptor	Donor
Metal	Contact

Molecule Name	Molecule
Molecular Weight	347.3
XLogP	2.6
PSA	98.1
Heavy Atoms	26
Acceptor Count	6
Donor Count	2
Chelator Count	2
mmff94smod_NoEstat	66.51

Total Score -17.40

Score compared to other molecules



Protein Contact

Protein Cavity

Residue Fingerprint

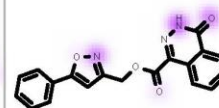
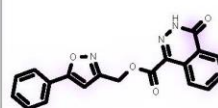
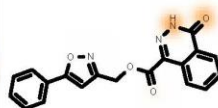
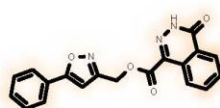
ALA880A	ALA898A
ARG878A	ASN868A
ASP766A	ASP770A
GLU988A	GLY863A
HIS862A	ILE879A
LEU769A	LYS903A
PHE897A	PRO881A
SER864A	SER904A
TRP861A	TYR710A
TYR889A	TYR896A
TYR907A	

Shape -17.33

Hydrogen Bond -5.87

Protein Desolvation 2.49

Ligand Desolvation 3.32

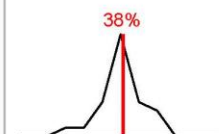
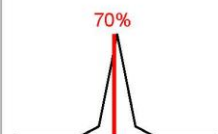
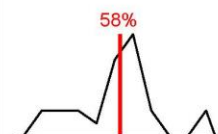
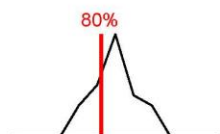


80%

58%

70%

38%

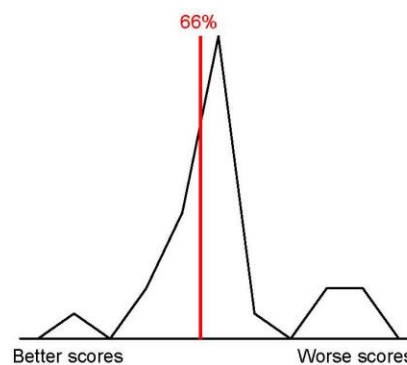
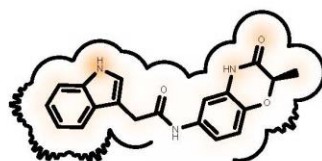


Acceptor Donor
Metal Contact

Molecule Name	Molecule
Molecular Weight	335.4
XLogP	2.1
PSA	83.2
Heavy Atoms	25
Acceptor Count	3
Donor Count	3
Chelator Count	0
mmff94smod_NoEstat	67.41

Total Score -17.39

Score compared to other molecules



Protein Contact

Protein Cavity

Residue Fingerprint

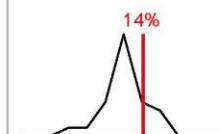
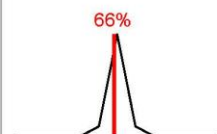
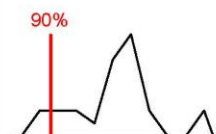
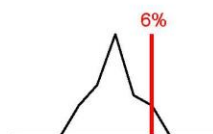
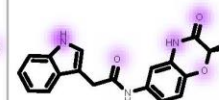
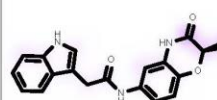
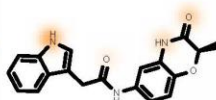
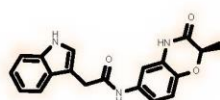
ALA880A	ALA898A
ARG878A	ASN868A
ASP766A	ASP770A
GLU988A	GLY863A
HIS862A	ILE879A
LEU769A	LYS903A
PHE897A	PRO881A
SER864A	SER904A
TRP861A	TYR710A
TYR889A	TYR896A
TYR907A	

Shape -14.88

Hydrogen Bond -9.15

Protein Desolvation 2.50

Ligand Desolvation 4.14

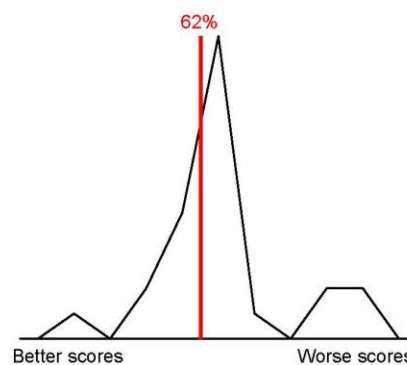
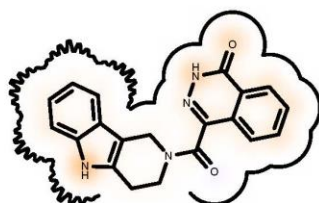


Acceptor	Donor
Metal	Contact

Molecule Name	Molecule
Molecular Weight	344.4
XLogP	1.9
PSA	81.8
Heavy Atoms	26
Acceptor Count	4
Donor Count	3
Chelator Count	1
mmff94smod_NoEstat	72.79

Total Score -17.38

Score compared to other molecules



Protein Contact

Protein Cavity

Residue Fingerprint

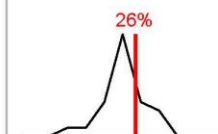
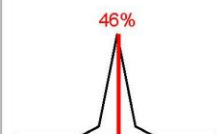
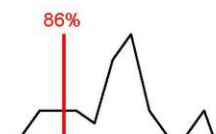
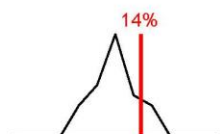
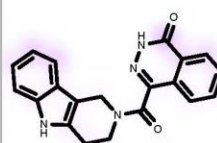
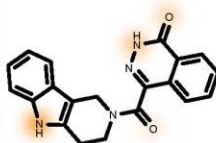
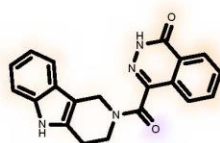
ALA880A	ALA898A
ARG878A	ASN868A
ASP766A	ASP770A
GLU988A	GLY863A
HIS862A	ILE879A
LEU769A	LYS903A
PHE897A	PRO881A
SER864A	SER904A
TRP861A	TYR710A
TYR889A	TYR896A
TYR907A	

Shape -15.41

Hydrogen Bond -8.52

Protein Desolvation 2.72

Ligand Desolvation 3.83

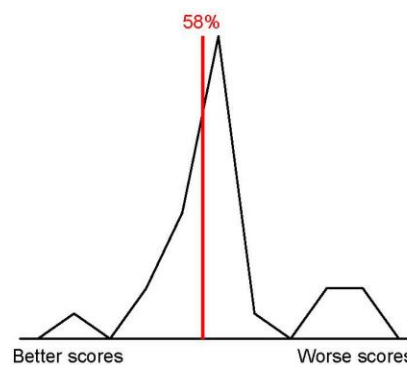
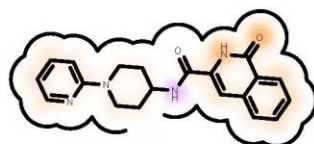


Acceptor Donor
Metal Contact

Molecule Name	Molecule
Molecular Weight	348.4
XLogP	1.9
PSA	78.1
Heavy Atoms	26
Acceptor Count	3
Donor Count	2
Chelator Count	1
mmff94smod_NoEstat	78.27

Total Score -17.33

Score compared to other molecules



Protein Contact

Protein Cavity

Residue Fingerprint

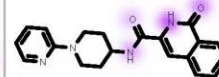
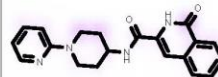
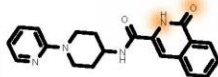
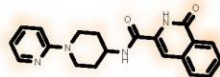
ALA880A	ALA898A
ARG878A	ASN868A
ASP766A	ASP770A
GLU988A	GLY863A
HIS862A	ILE879A
LEU769A	LYS903A
PHE897A	PRO881A
SER864A	SER904A
TRP861A	TYR710A
TYR889A	TYR896A
TYR907A	

Shape -18.15

Hydrogen Bond -5.30

Protein Desolvation 2.86

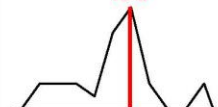
Ligand Desolvation 3.25



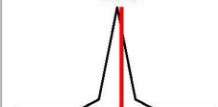
94%



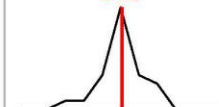
18%



26%



54%

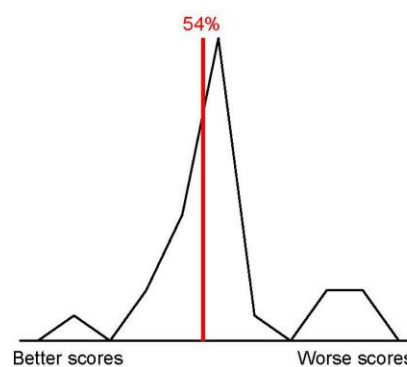
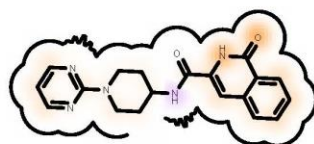


Acceptor Donor
Metal Contact

Molecule Name	Molecule
Molecular Weight	349.4
XLogP	1.1
PSA	91.0
Heavy Atoms	26
Acceptor Count	4
Donor Count	2
Chelator Count	2
mmff94smod_NoEstat	73.40

Total Score -17.32

Score compared to other molecules



Protein Contact

Protein Cavity

Residue Fingerprint

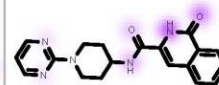
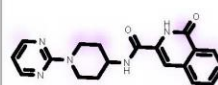
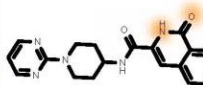
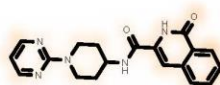
ALA880A	ALA898A
ARG878A	ASN868A
ASP766A	ASP770A
GLU988A	GLY863A
HIS862A	ILE879A
LEU769A	LYS903A
PHE897A	PRO881A
SER864A	SER904A
TRP861A	TYR710A
TYR889A	TYR896A
TYR907A	

Shape -18.04

Hydrogen Bond -5.56

Protein Desolvation 2.82

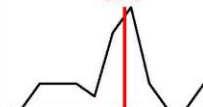
Ligand Desolvation 3.45



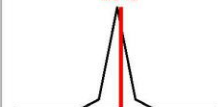
90%



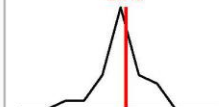
30%



38%



30%

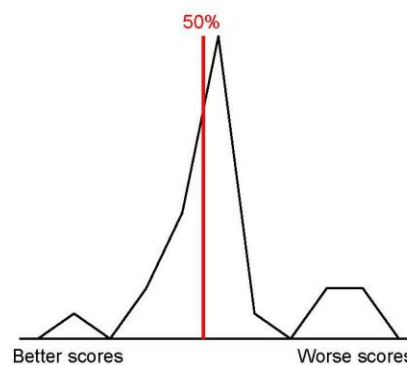
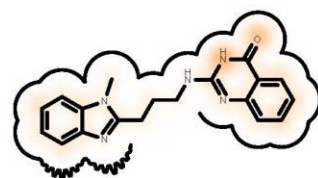


Acceptor	Donor
Metal	Contact

Molecule Name	Molecule
Molecular Weight	333.4
XLogP	2.8
PSA	75.6
Heavy Atoms	25
Acceptor Count	4
Donor Count	3
Chelator Count	2
mmff94smod_NoEstat	55.44

Total Score -17.32

Score compared to other molecules



Protein Contact

Protein Cavity

Residue Fingerprint

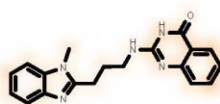
ALA880A	ALA898A
ARG878A	ASN868A
ASP766A	ASP770A
GLU988A	GLY863A
HIS862A	ILE879A
LEU769A	LYS903A
PHE897A	PRO881A
SER864A	SER904A
TRP861A	TYR710A
TYR889A	TYR896A
TYR907A	

Shape -17.11

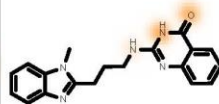
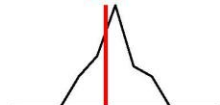
Hydrogen Bond -5.88

Protein Desolvation 2.66

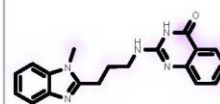
Ligand Desolvation 3.01



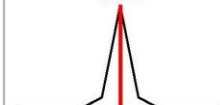
70%



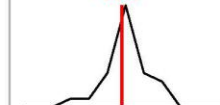
62%



54%



66%

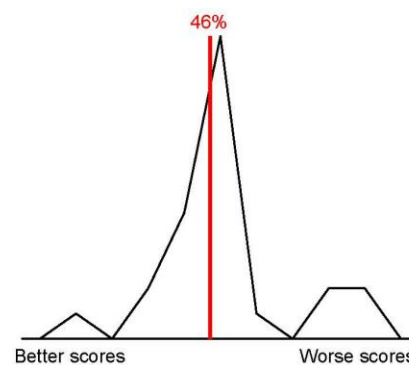
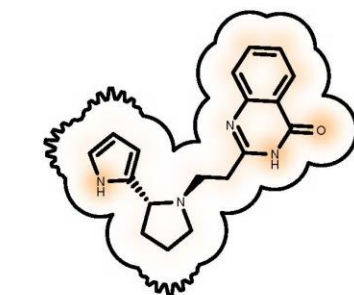


Acceptor	Donor
Metal	Contact

Molecule Name	Molecule
Molecular Weight	308.4
XLogP	2.1
PSA	64.8
Heavy Atoms	23
Acceptor Count	4
Donor Count	3
Chelator Count	1
mmff94smod_NoEstat	50.77

Total Score -17.20

Score compared to other molecules



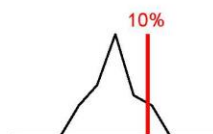
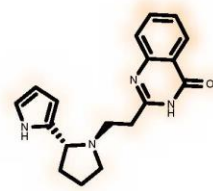
Protein Contact

Protein Cavity

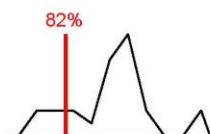
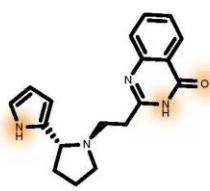
Residue Fingerprint

ALA880A	ALA898A
ARG878A	ASN868A
ASP766A	ASP770A
GLU988A	GLY863A
HIS862A	ILE879A
LEU769A	LYS903A
PHE897A	PRO881A
SER864A	SER904A
TRP861A	TYR710A
TYR889A	TYR896A
TYR907A	

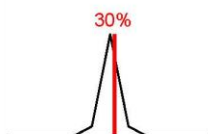
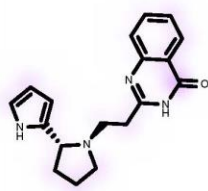
Shape -15.08



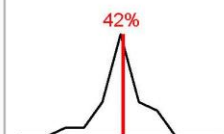
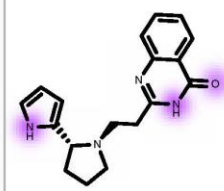
Hydrogen Bond -8.28



Protein Desolvation 2.85



Ligand Desolvation 3.31

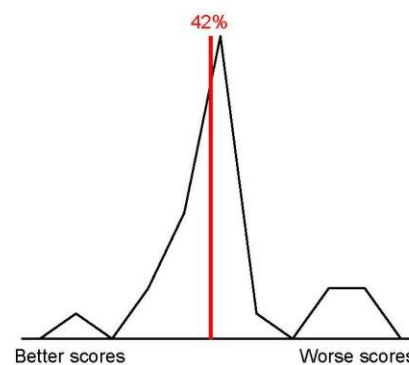
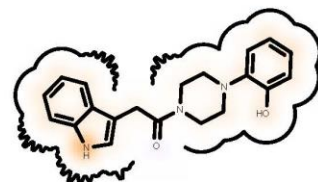


Acceptor Donor
Metal Contact

Molecule Name	Molecule
Molecular Weight	335.4
XLogP	1.8
PSA	59.6
Heavy Atoms	25
Acceptor Count	2
Donor Count	2
Chelator Count	1
mmff94smod_NoEstat	73.26

Total Score -17.19

Score compared to other molecules



Protein Contact

Protein Cavity

Residue Fingerprint

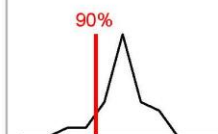
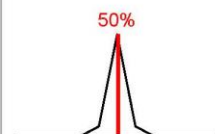
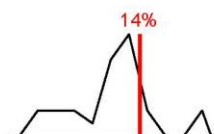
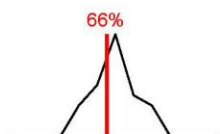
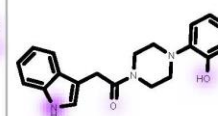
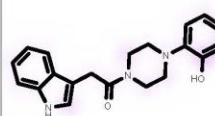
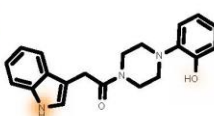
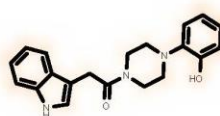
ALA880A	ALA898A
ARG878A	ASN868A
ASP766A	ASP770A
GLU988A	GLY863A
HIS862A	ILE879A
LEU769A	LYS903A
PHE897A	PRO881A
SER864A	SER904A
TRP861A	TYR710A
TYR889A	TYR896A
TYR907A	

Shape -17.06

Hydrogen Bond -4.71

Protein Desolvation 2.70

Ligand Desolvation 1.89



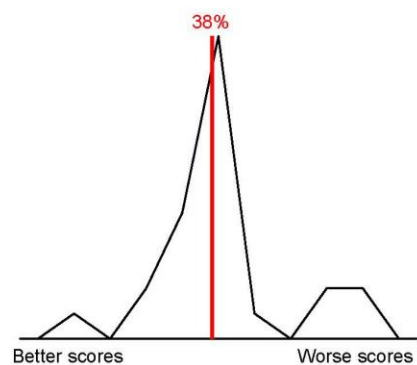
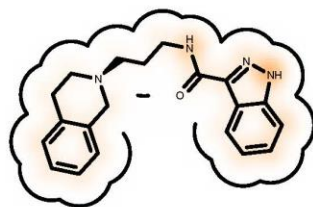
Acceptor
Metal

Donor
Contact

Molecule Name	Molecule
Molecular Weight	334.4
XLogP	2.9
PSA	61.0
Heavy Atoms	25
Acceptor Count	4
Donor Count	3
Chelator Count	1
mmff94smod_NoEstat	49.83

Total Score -17.10

Score compared to other molecules



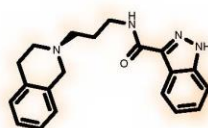
Protein Contact

Protein Cavity

Residue Fingerprint

ALA880A	ALA898A
ARG878A	ASN868A
ASP766A	ASP770A
GLU988A	GLY863A
HIS862A	ILE879A
LEU769A	LYS903A
PHE897A	PRO881A
SER864A	SER904A
TRP861A	TYR710A
TYR889A	TYR896A
TYR907A	

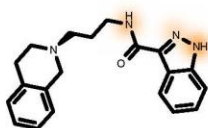
Shape -16.58



44%



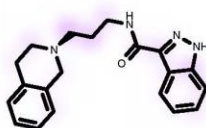
Hydrogen Bond -6.52



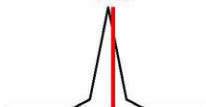
70%



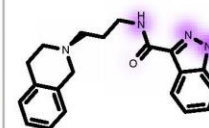
Protein Desolvation 2.89



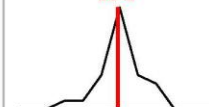
18%



Ligand Desolvation 3.11



58%

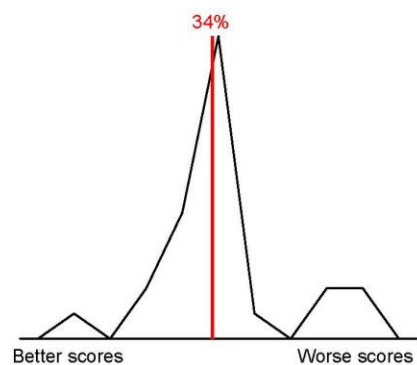
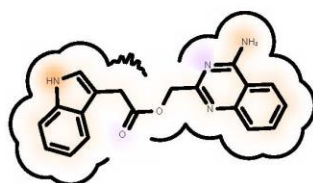


Acceptor	Donor
Metal	Contact

Molecule Name	Molecule
Molecular Weight	332.4
XLogP	2.6
PSA	93.9
Heavy Atoms	25
Acceptor Count	4
Donor Count	2
Chelator Count	2
mmff94smod_NoEstat	65.55

Total Score -17.10

Score compared to other molecules



Protein Contact

Protein Cavity

Residue Fingerprint

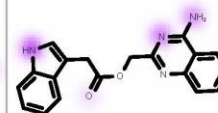
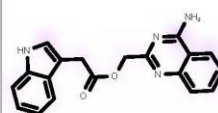
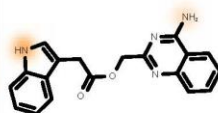
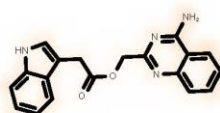
ALA880A	ALA898A
ARG878A	ASN868A
ASP766A	ASP770A
GLU988A	GLY863A
HIS862A	ILE879A
LEU769A	LYS903A
PHE897A	PRO881A
SER864A	SER904A
TRP861A	TYR710A
TYR889A	TYR896A
TYR907A	

Shape -16.55

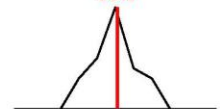
Hydrogen Bond -5.69

Protein Desolvation 2.11

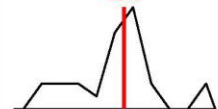
Ligand Desolvation 3.03



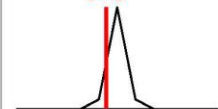
38%



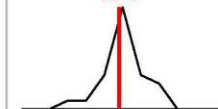
42%



94%



62%

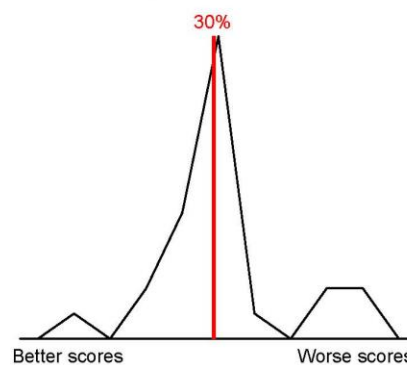
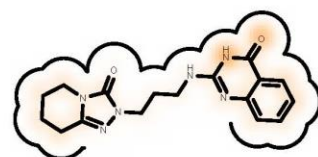


Acceptor Donor
Metal Contact

Molecule Name	Molecule
Molecular Weight	340.4
XLogP	1.1
PSA	97.6
Heavy Atoms	25
Acceptor Count	5
Donor Count	3
Chelator Count	2
mmff94smod_NoEstat	53.45

Total Score -17.06

Score compared to other molecules



Protein Contact

Protein Cavity

Residue Fingerprint

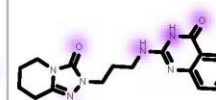
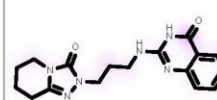
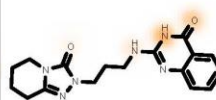
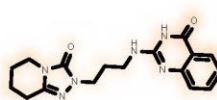
ALA880A	ALA898A
ARG878A	ASN868A
ASP766A	ASP770A
GLU988A	GLY863A
HIS862A	ILE879A
LEU769A	LYS903A
PHE897A	PRO881A
SER864A	SER904A
TRP861A	TYR710A
TYR889A	TYR896A
TYR907A	

Shape -17.30

Hydrogen Bond -5.84

Protein Desolvation 2.22

Ligand Desolvation 3.86

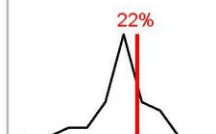
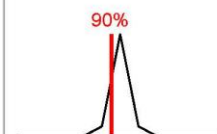
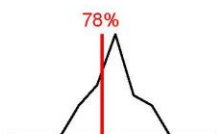


78%

54%

90%

22%

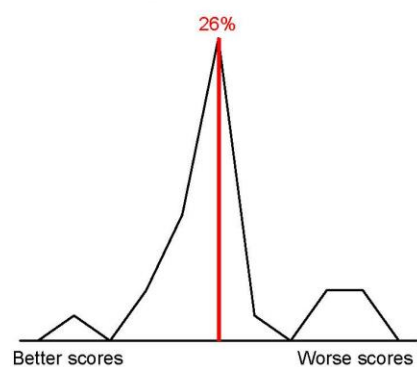
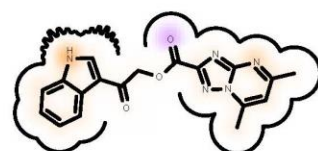


Acceptor	Donor
Metal	Contact

Molecule Name	Molecule
Molecular Weight	349.3
XLogP	2.1
PSA	102.2
Heavy Atoms	26
Acceptor Count	5
Donor Count	1
Chelator Count	3
mmff94smod_NoEstat	54.29

Total Score -16.94

Score compared to other molecules



Protein Contact

Protein Cavity

Residue Fingerprint

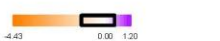
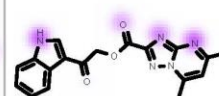
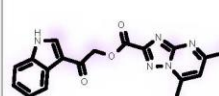
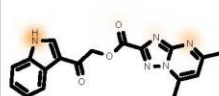
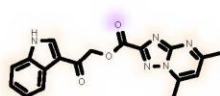
ALA880A	ALA898A
ARG878A	ASN868A
ASP766A	ASP770A
GLU988A	GLY863A
HIS862A	ILE879A
LEU769A	LYS903A
PHE897A	PRO881A
SER864A	SER904A
TRP861A	TYR710A
TYR889A	TYR896A
TYR907A	

Shape -15.80

Hydrogen Bond -7.93

Protein Desolvation 2.85

Ligand Desolvation 3.94

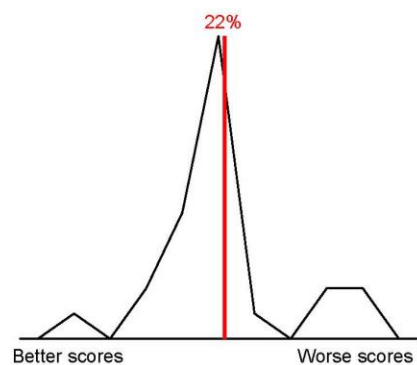
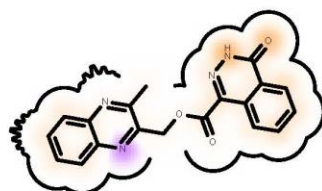


Acceptor	Donor
Metal	Contact

Molecule Name	Molecule
Molecular Weight	346.3
XLogP	2.2
PSA	97.8
Heavy Atoms	26
Acceptor Count	6
Donor Count	2
Chelator Count	3
mmff94smod_NoEstat	85.77

Total Score -16.80

Score compared to other molecules



Protein Contact

Protein Cavity

Residue Fingerprint

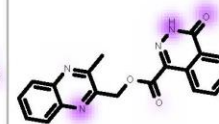
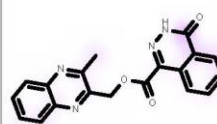
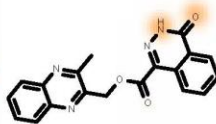
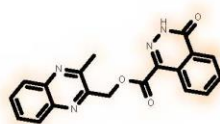
ALA880A	ALA898A
ARG878A	ASN868A
ASP766A	ASP770A
GLU988A	GLY863A
HIS862A	ILE879A
LEU769A	LYS903A
PHE897A	PRO881A
SER864A	SER904A
TRP861A	TYR710A
TYR889A	TYR896A
TYR907A	

Shape -16.85

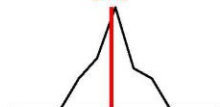
Hydrogen Bond -5.71

Protein Desolvation 2.44

Ligand Desolvation 3.33



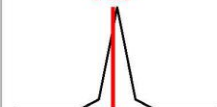
54%



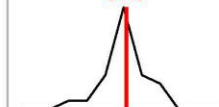
50%



74%



34%

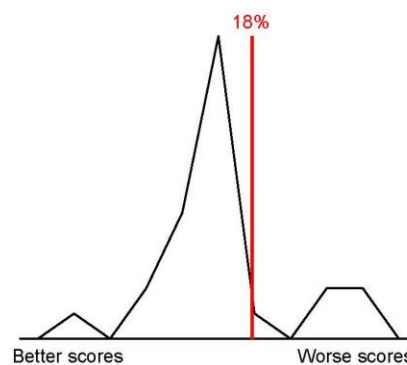
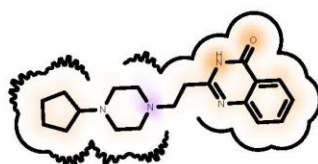


Acceptor	Donor
Metal	Contact

Molecule Name	Molecule
Molecular Weight	326.4
XLogP	2.1
PSA	52.2
Heavy Atoms	24
Acceptor Count	5
Donor Count	2
Chelator Count	1
mmff94smod_NoEstat	59.26

Total Score -16.11

Score compared to other molecules



Protein Contact

Protein Cavity

Residue Fingerprint

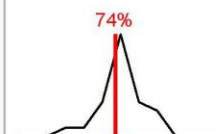
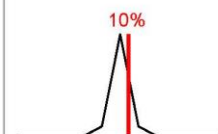
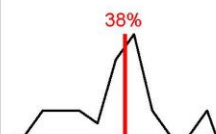
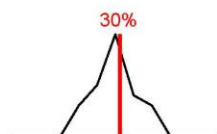
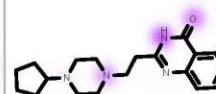
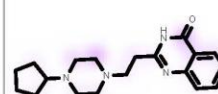
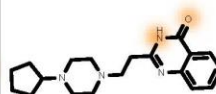
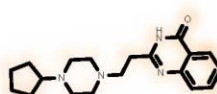
ALA880A	ALA898A
ARG878A	ASN868A
ASP766A	ASP770A
GLU988A	GLY863A
HIS862A	ILE879A
LEU769A	LYS903A
PHE897A	PRO881A
SER864A	SER904A
TRP861A	TYR710A
TYR889A	TYR896A
TYR907A	

Shape -16.42

Hydrogen Bond -5.68

Protein Desolvation 3.05

Ligand Desolvation 2.94

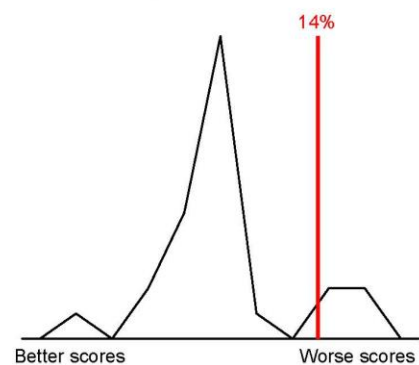


Acceptor Donor
Metal Contact

Molecule Name	Molecule
Molecular Weight	349.3
XLogP	1.3
PSA	117.1
Heavy Atoms	26
Acceptor Count	6
Donor Count	4
Chelator Count	3
mmff94smod_NoEstat	51.38

Total Score -14.54

Score compared to other molecules



Protein Contact

Protein Cavity

Residue Fingerprint

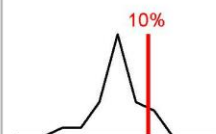
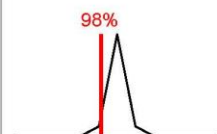
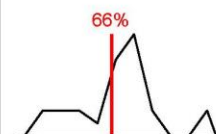
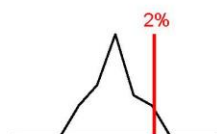
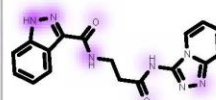
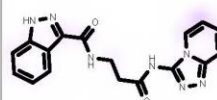
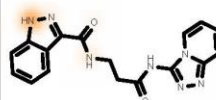
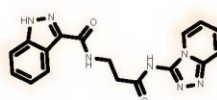
ALA880A	ALA898A
ARG878A	ASN868A
ASP766A	ASP770A
GLU988A	GLY863A
HIS862A	ILE879A
LEU769A	LYS903A
PHE897A	PRO881A
SER864A	SER904A
TRP861A	TYR710A
TYR889A	TYR896A
TYR907A	

Shape -14.75

Hydrogen Bond -6.33

Protein Desolvation 1.86

Ligand Desolvation 4.68

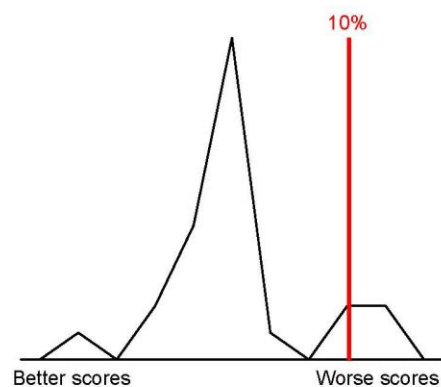


Acceptor	Donor
Metal	Contact

Molecule Name	Molecule
Molecular Weight	349.3
XLogP	1.4
PSA	117.1
Heavy Atoms	26
Acceptor Count	6
Donor Count	4
Chelator Count	3
mmff94smod_NoEstat	59.36

Total Score -14.23

Score compared to other molecules



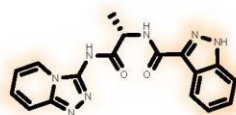
Protein Contact

Protein Cavity

Residue Fingerprint

ALA880A	ALA898A
ARG878A	ASN868A
ASP766A	ASP770A
GLU988A	GLY863A
HIS862A	ILE879A
LEU769A	LYS903A
PHE897A	PRO881A
SER864A	SER904A
TRP861A	TYR710A
TYR889A	TYR896A
TYR907A	

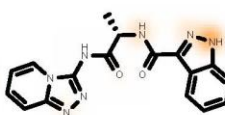
Shape -16.87



60%



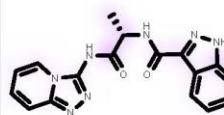
Hydrogen Bond -4.64



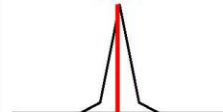
10%



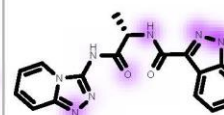
Protein Desolvation 2.56



58%



Ligand Desolvation 4.73



6%

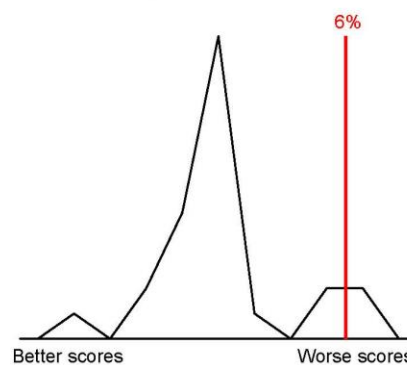
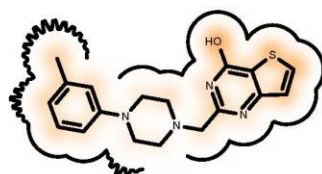


Acceptor	Donor
Metal	Contact

Molecule Name	Molecule
Molecular Weight	340.4
XLogP	2.3
PSA	52.5
Heavy Atoms	24
Acceptor Count	4
Donor Count	1
Chelator Count	3
mmff94smod_NoEstat	72.87

Total Score -13.81

Score compared to other molecules



Protein Contact

Protein Cavity

Residue Fingerprint

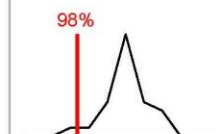
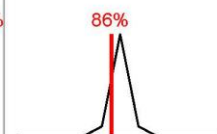
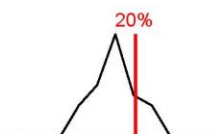
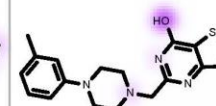
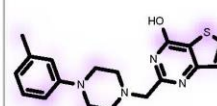
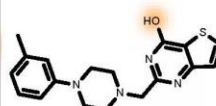
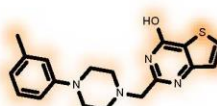
ALA880A	ALA898A
ARG878A	ASN868A
ASP766A	ASP770A
GLU988A	GLY863A
HIS862A	ILE879A
LEU769A	LYS903A
PHE897A	PRO881A
SER864A	SER904A
TRP861A	TYR710A
TYR889A	TYR896A
TYR907A	

Shape -15.67

Hydrogen Bond -1.20

Protein Desolvation 2.22

Ligand Desolvation 0.84

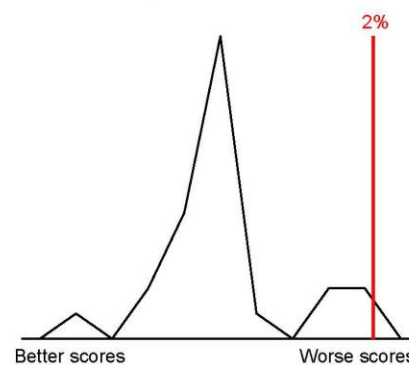
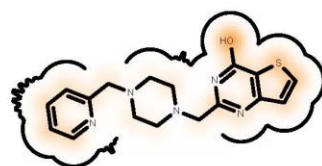


Acceptor Donor
Metal Contact

Molecule Name	Molecule
Molecular Weight	341.4
XLogP	0.8
PSA	65.4
Heavy Atoms	24
Acceptor Count	6
Donor Count	1
Chelator Count	4
mmff94smod_NoEstat	59.72

Total Score -13.18

Score compared to other molecules



Protein Contact

Protein Cavity

Residue Fingerprint

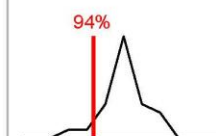
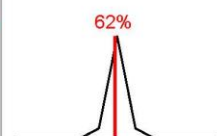
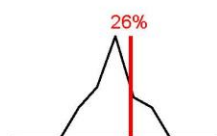
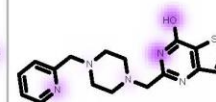
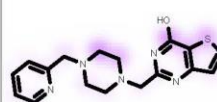
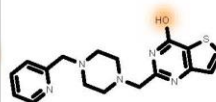
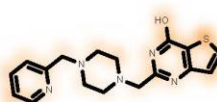
ALA880A	ALA898A
ARG878A	ASN868A
ASP766A	ASP770A
GLU988A	GLY863A
HIS862A	ILE879A
LEU769A	LYS903A
PHE897A	PRO881A
SER864A	SER904A
TRP861A	TYR710A
TYR889A	TYR896A
TYR907A	

Shape -15.90

Hydrogen Bond -1.54

Protein Desolvation 2.53

Ligand Desolvation 1.73



Acceptor	Donor
Metal	Contact

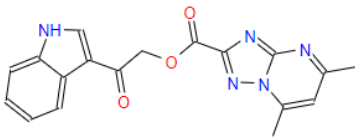
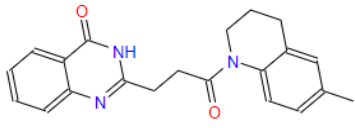
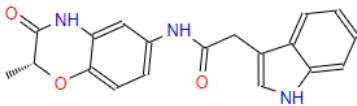
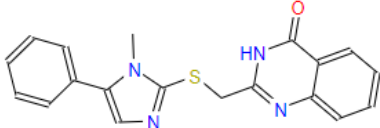
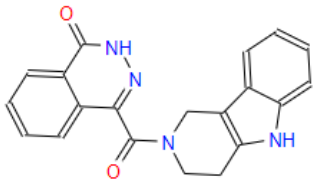
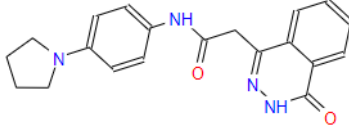
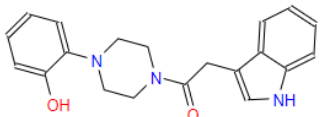
4.03 Hits Chemical Classification

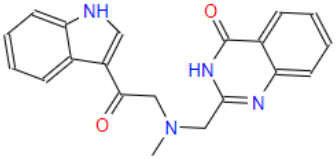
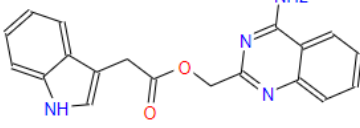
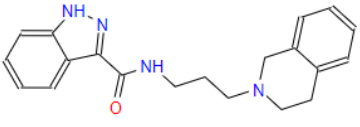
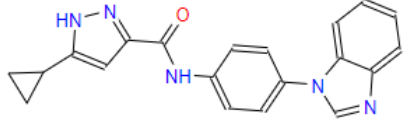
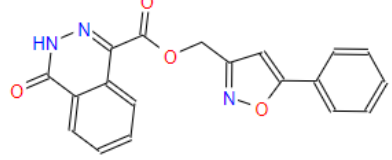
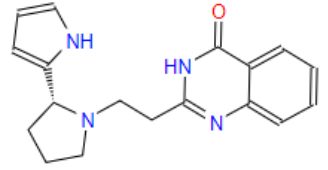
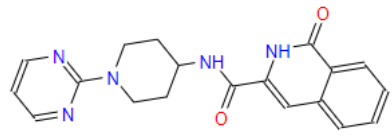
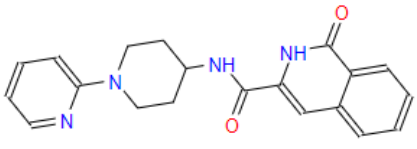
Hits were classified based on their functional groups. Out of the 25 hits, benzopyrimidine and indole were the most common functional groups with nine and five hits having these functional groups respectively (table 3 and 4). Benzopyrazole and phthalazine each had three hits, two isoquinolone analogs, four phthalazine, four benzopyrazole, one benzimidazole, and one thienopyridine. These functional groups are important for deciding the types of bonds formed with PARP1.

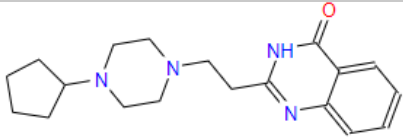
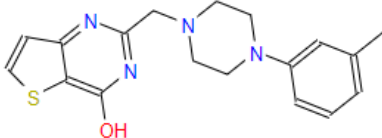
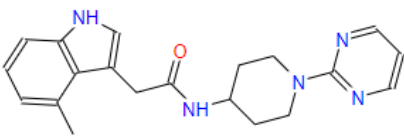
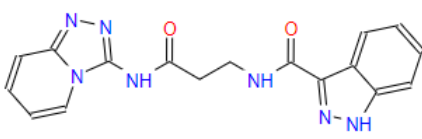
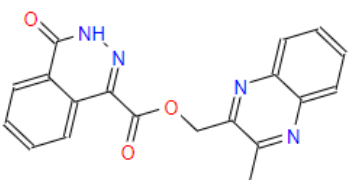
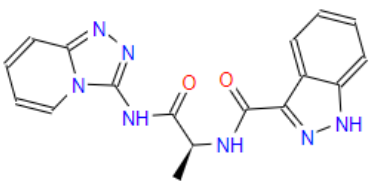
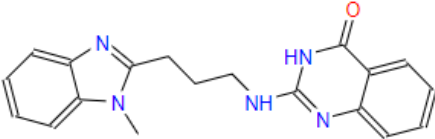
Table 3: Classification of hits based on heterocyclic ring.

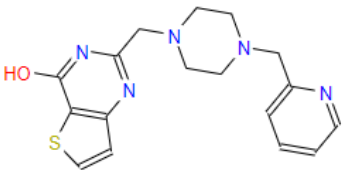
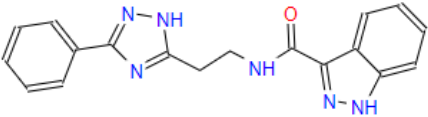
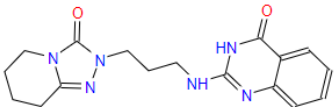
Chemical Structure	Number of Hits
Isoquinoline	2
Phthalazine	4
Benzopyrazole	4
Benzimidazole	1
Indole	5
Benzopyrimidine	9
Thienopyrimidine	1

Table 4: Chemical Structure and LogP of Top 25 Hits

Catalog Number	Structure	Hit	CLogP	Total Score
Z19572914		1	1.3	-16.94
Z28077285		2	2.53	-18.79
Z110096110		3	1.985	-17.39
Z74715974		4	2.961	-18.08
Z225653548		5	1.202	-17.38
Z30644325		6	0.991	-17.43
Z32391921		7	2.56	-17.19

Z124826588		8	1.877	-20.06
Z167798216		9	2.496	-17.10
Z372757196		10	3.689	-17.10
Z321249898		11	3.915	-17.89
Z148570968		12	2.029	-17.40
Z729248128		13	1.246	-17.20
Z421514920		14	0.059	-17.72
Z421625134		15	0.824	-17.33

Z729231748		16	0.88	-16.11
Z195904178		17	2.362	-13.81
Z1118682269		18	1.123	-17.72
Z1037500644		19	2.138	-14.54
Z91830525		20	1.541	-16.80
Z1021215630		21	2.162	-14.23
Z1359552843		22	2.65	-17.32

Z224755122		23	0.657	-13.18
Z1695739736		24	2.754	-18.30
Z990888126		25	1.64	-17.06

4.04 MD Simulations of Protein-ligand Complexes

After completing the conformer generation and docking, the top five scores from the virtual high throughput screening were analyzed using molecular dynamics (figure 24). These hits consists of 3 benzopyrimidines, an indole, and a benzimidazole (figure 25). The hits for the molecular docking Z124826588 (Hit 8), Z28077285 (Hit 2), Z1118682269 (Hit 18), Z1359552843 (Hit 22) Z729248128 (Hit 13).

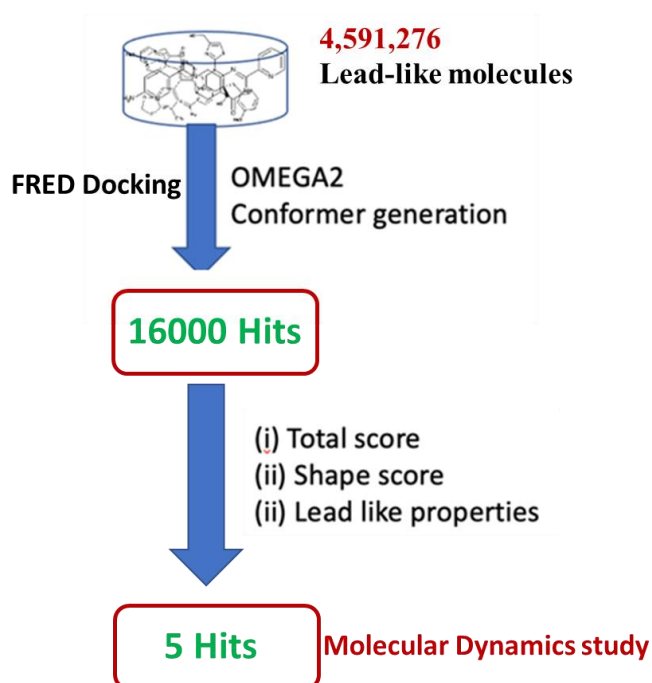


Figure 24: Schematic representation of molecular dynamics study

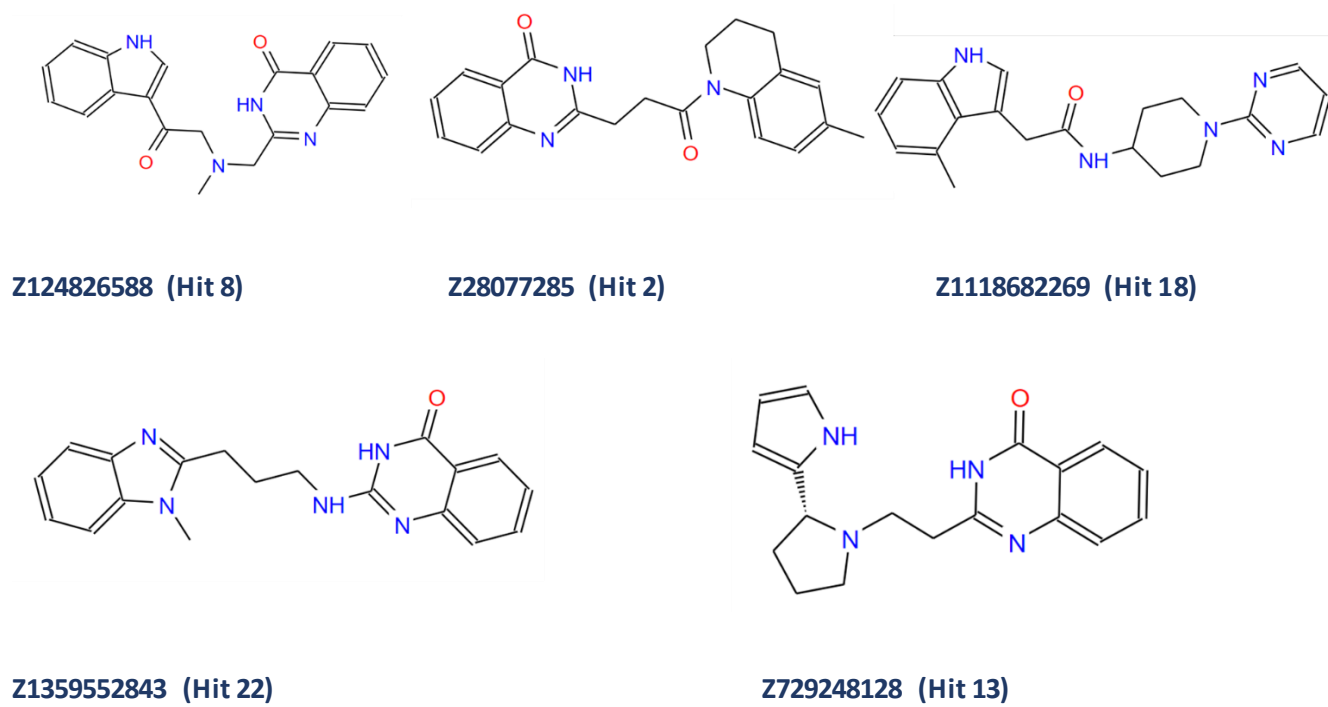


Figure 25: Chemical structures of five hits selected for molecular dynamics study

Root-Mean-Square Deviation (RMSD). The RMSD plot shows that, with average RMSD values between 1.7 and 1.9 nm, the complexes of PARP-1 with Hit 8 2, and 18 have been remarkably stable throughout the simulation (figure 26). Like the reference structure of PARP-1, the complexes of PARP-1 with Hit 22 and Hit 13 have similarly remained stable, with RMSD values of 0.2 nm. The RMSD data show that the binding of these two substances to PARP-1 is constant (figure 27).

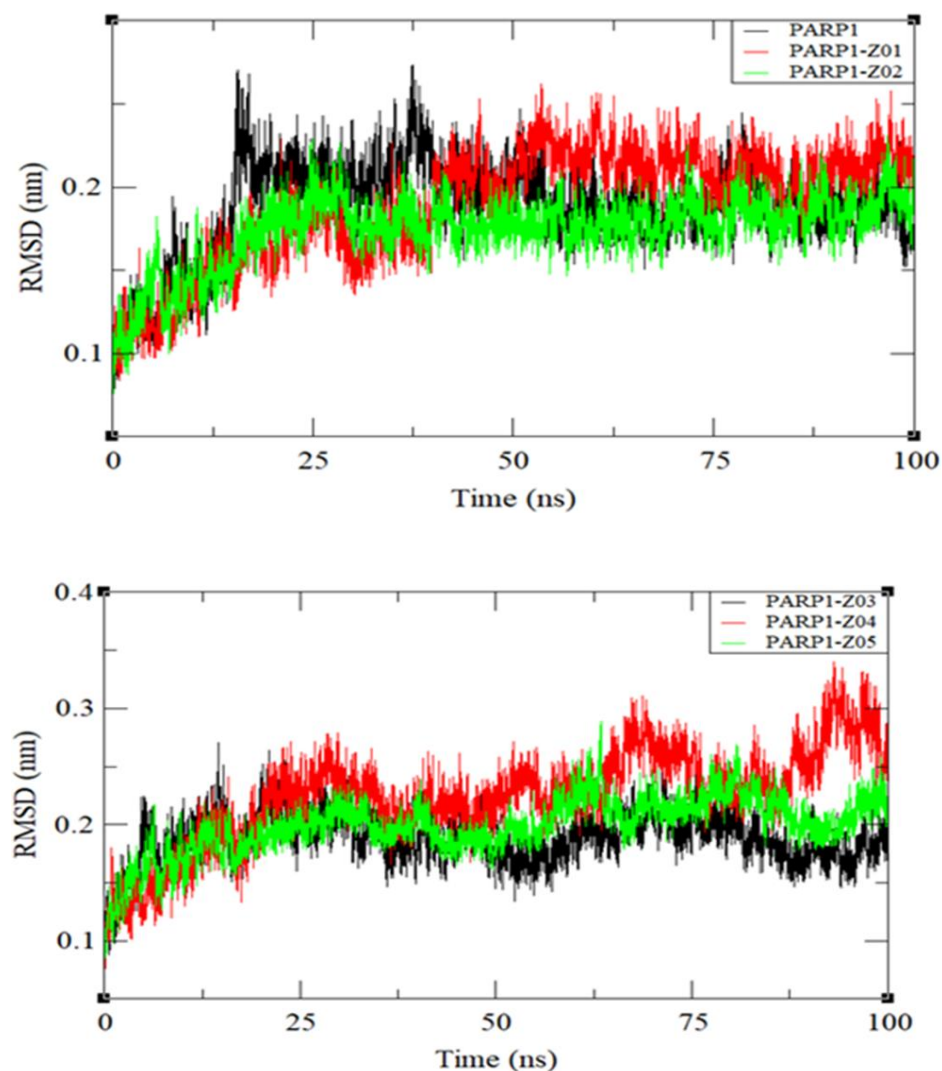


Figure 26: Results from RMSD analysis. PARP1-Z01 denotes hit 8, PARP1-Z02 is hit 2, PARP1-Z03 is hit 18, PARP1-Z04 is hit 22, PARP1-Z05 is Hit 13

Root-Mean-Square Fluctuation (RMSF). All the complexes of PARP-1 have average RMSF values that range from 0.10 to 0.13 nm. Since the RMSF values of the complexes do not significantly differ from one another, we draw the conclusion that they were all effectively stabilized throughout the MD simulation (figure 27).

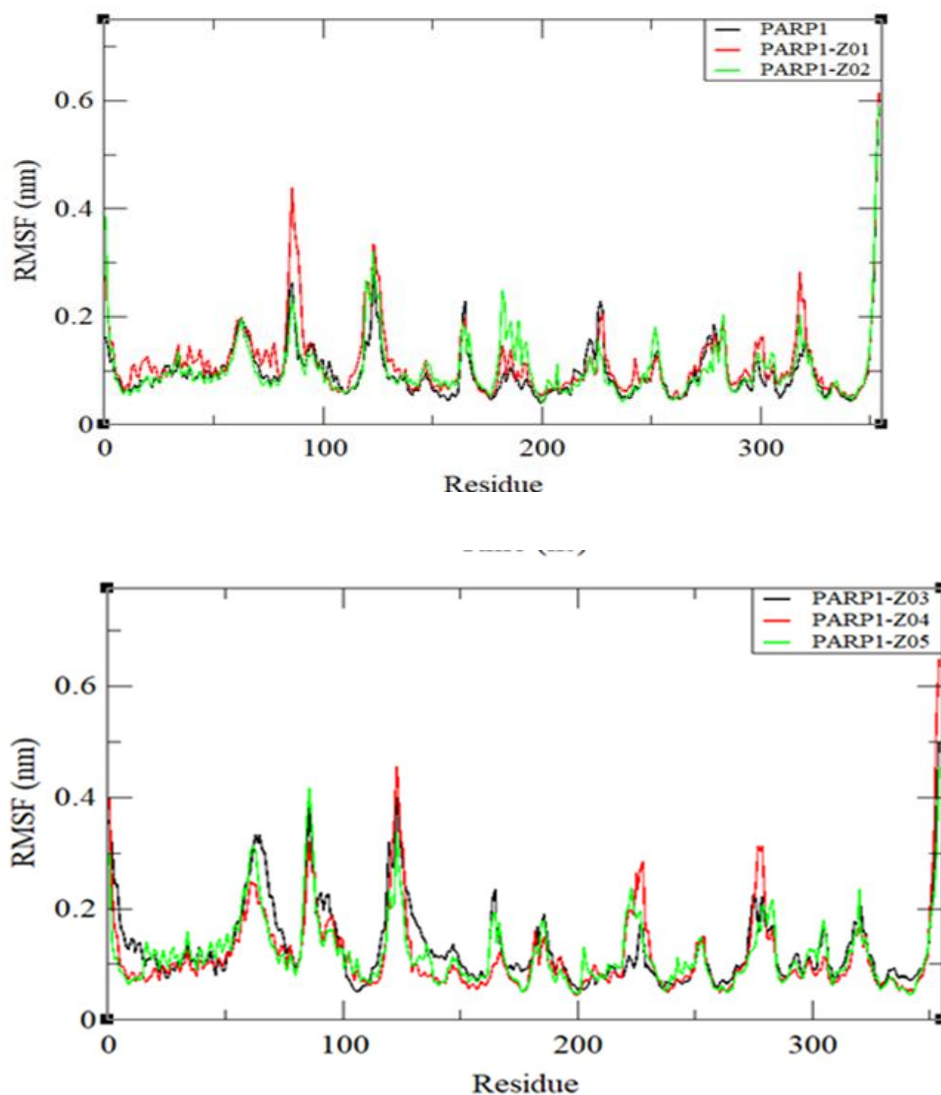


Figure 27: Results from RMSF analysis. Z01 is Hit 8, Z02 is hit 2, Z03 is hit 18, z04 is hit 22, and Z05 is hit 13.

Radius of Gyration (R_g). All systems were found to have R_g values that were coherent with the RMSF system. This reveals that over the entire 100 ns, the protein-ligand complexes were stable and compressed (figure 28).

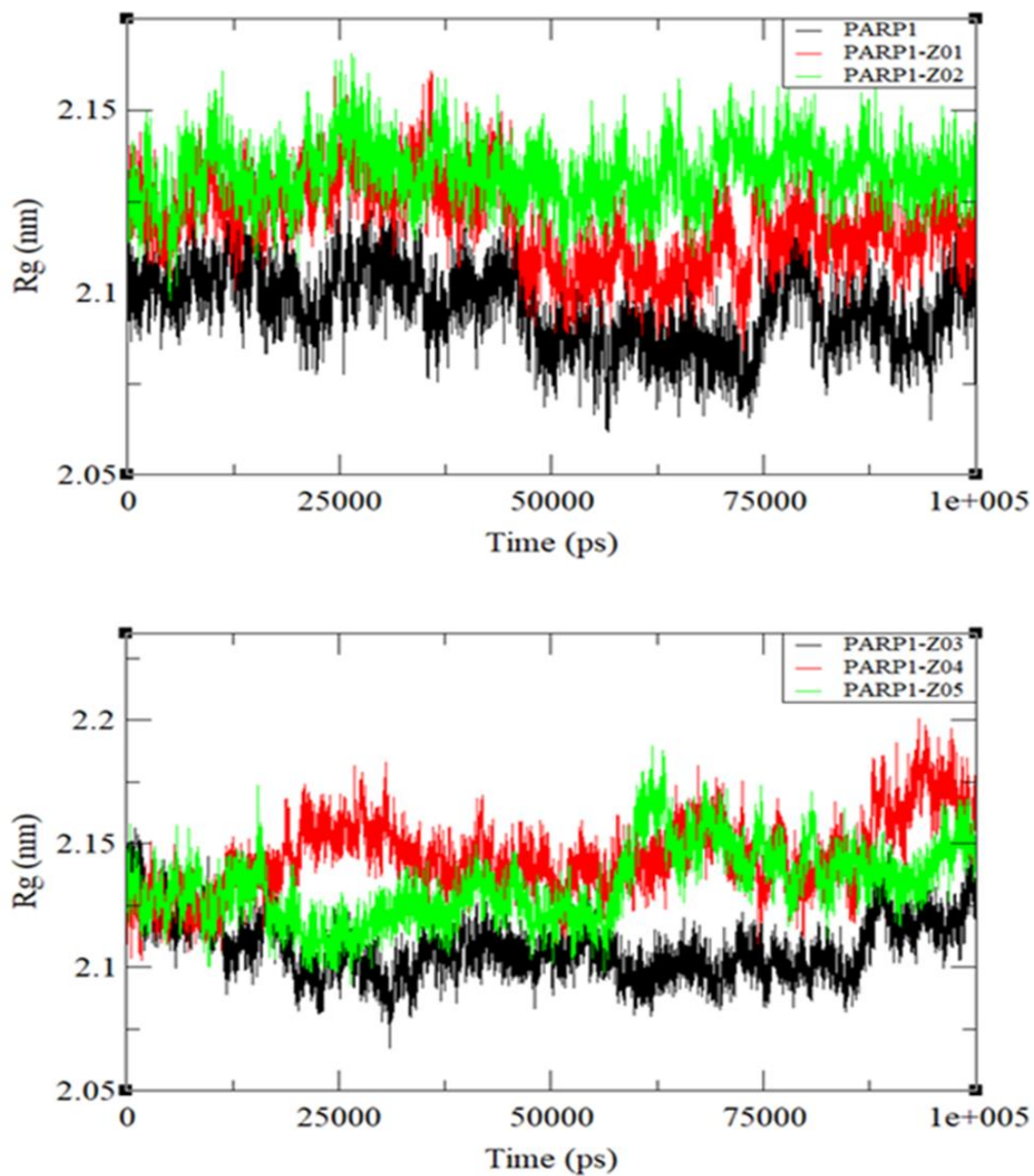


Figure 28: Results from the R_g analysis. Z01 is Hit 8, Z02 is hit 2, Z03 is hit 18, z04 is hit 22, and Z05 is hit 13.

Hydrogen Bonding Interactions. The H-bonding analysis of all the complexes shows that Z01 and Z03 have generated several H-bonded interactions with PARP-1, compared to the number of interactions formed by the other compounds, which is fewer in number (figure 29).

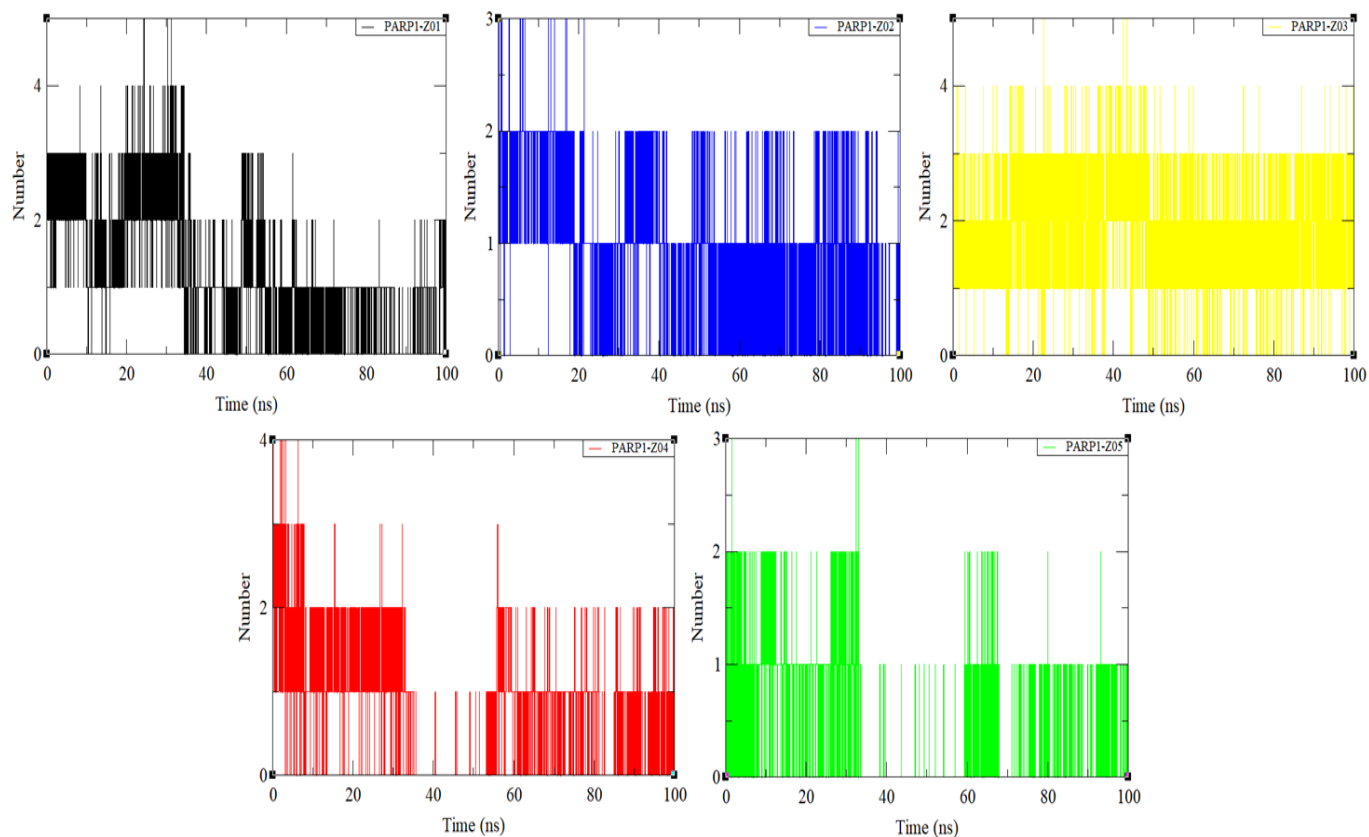


Figure 29: Results from H-bonding analysis. Black graph is Hit 8, the blue graph is hit 2, yellow graph is hit 18, red graph is hit 22, and green graph is hit 13.

MM/PBSA Calculations. Due to its strong vdW, electrostatic, and polar energies, Hit 22 possesses the highest binding affinity to PARP-1, measuring -19.6 kcal/mol. Hit 2 and 18 have a greater affinity for PARP-1 with an energy of -18.1 kcal/mol and Hit 13 has an energy of 17.8 kcal/mol due to the predominating vdW, electrostatic, and polar energies. Hit 8 has the lowest binding energy to PARP-1, which is -12.6 kcal/mol (Table 5).

Table 5: Summary of MM/PBSA Calculations

S.No	Protein-Ligand complexes	vdW	Electrostatic	Polar	SASA	Binding energy (kcal/mol)
1	Hit 8 (Z01)	-37.4	-5.3	34.2	-4.1	-12.6 +/- 4.6
2	Hit 2 (Z02)	-45.9	-8.1	40.5	-4.6	-18.1 +/- 5.4
3	Hit 18 (Z03)	-44.6	-7.6	38.6	-4.6	-18.1 +/- 3.4
4	Hit 22 (Z04)	-43.1	-7.7	35.4	-4.2	-19.6 +/- 4.4
5	Hit 13 (Z05)	-41.9	-6.1	34.1	-3.9	-17.8 +/- 4.5

4.05 PARP1 Colorimetric Assay

After the scoring of the lead-like compounds we selected 25 hits for the PARP1 colorimetric assay (figure 30). Out of the top 25 hits, four hits showed strong inhibitory activity against PARP1 (Table 4 and 5). Twelve of the inhibitors had moderate inhibition of PARP1. Of the four strong inhibitors, two (Hit 10 and 22) are benzopyrazole analogs. The benzopyrazole ring provides an amide group for hydrogen bonding and an aromatic ring for the π - π stacking interaction. Hit 22, which had good results in the molecular dynamics study, has ionic interactions with Asp770 (figure 31).

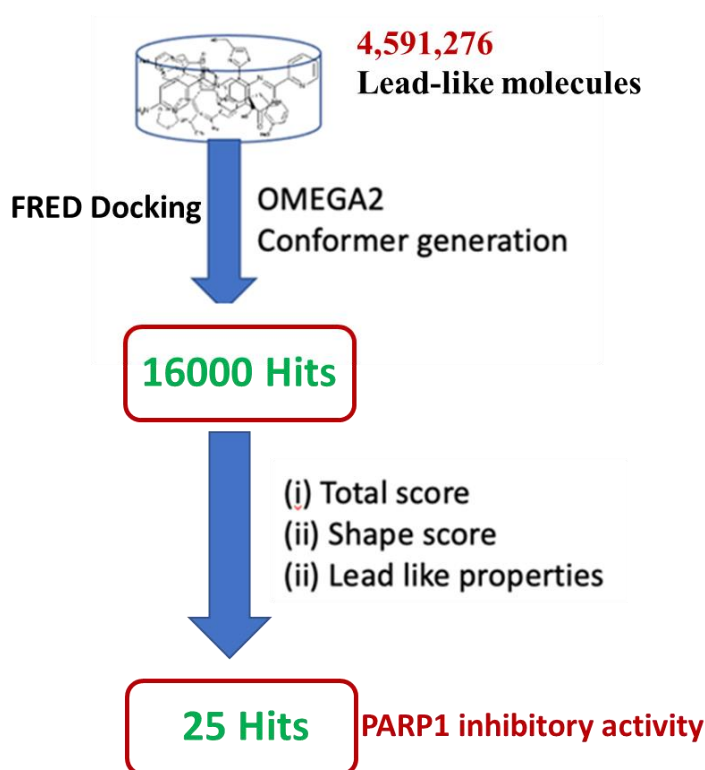


Figure 30: Schematic Representation of PARP1 *in vitro* study

The IC_{50} values of the strong inhibitors were calculated, and the values are noted in Table 6 from figure 32. Hit 22 has the best IC_{50} value of 1.4767. The chemical structure of Hit 22 has not been reported for a PARP1 inhibitor, making its scaffold novel. It was also the only hit from the molecular dynamics studies that also showed strong inhibition in the colorimetric assay. This difference in results could be for several reasons. There could be differences because of the nature of the study. Preliminary analysis using virtual high throughput screening can vary depending on the programs used. Furthermore, molecular dynamics looks at the binding stability of the inhibitory complex and the backbone stability of the enzyme. Just because the binding is good does not equate with biological effect. Also, the other reasons like the solubility of the hit, accuracy of the colorimetric kit, or the stability could affect the results.

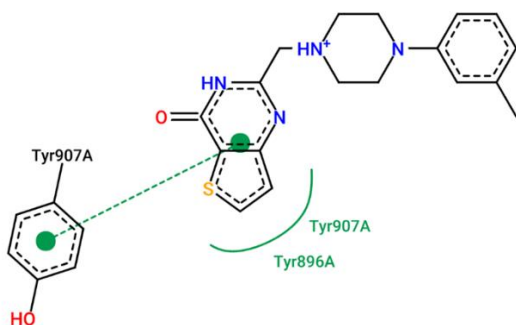
<i>Inhibition Activity</i>	Inhibition Percentage
<i>Inactive</i>	≥45%
<i>Weak</i>	46% to 65%
<i>Moderate</i>	66% to <80%
<i>Strong</i>	≥ 80%

Table 6: PARP1 Inhibitory Activity of hits

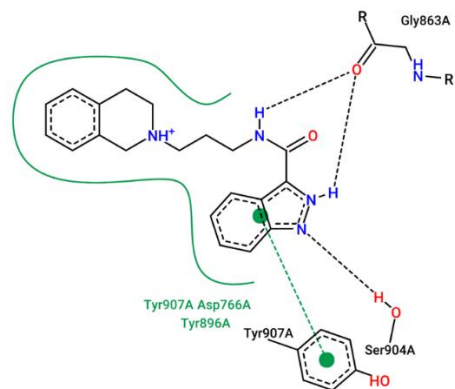
Hit	Inhibition Activity	Concentration (μM)
Z110096110	Moderate	50
Z225653548	Inactive	50
Z729248128	Weak	50
Z321249898	Inactive	50
Z167798216	Moderate	50
Z729231748	Inactive	50
Z990888126	Weak	50
Z224755122	Moderate	50
Z74715974	Moderate	50
Z1695739736	Strong	50
Z148570968	Moderate	50
Z28077285	Moderate	50
Z421514920	Weak	50
Z1037500644	Weak	50
Z1359552843	Strong	50
Z1695739736	Moderate	50
Z30644325	Moderate	50
Z195904178	Strong	50

Z421625134	Moderate	50
Z19572914	Moderate	50
Z372757196	Strong	50
Z32391921	Inactive	50
Z124826588	Weak	50
Z1021215630	Moderate	50
Z91830525	Moderate	50

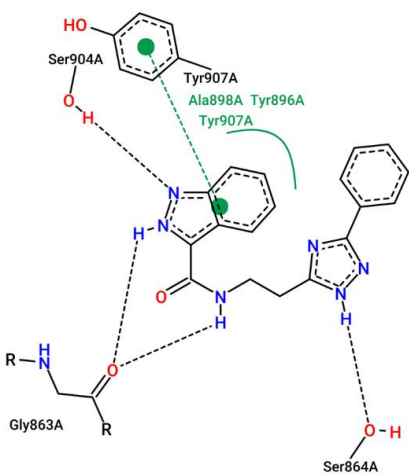
Hit 1 (Z195904178)



Hit 2 (Z372757196)



Hit 3 (Z1695739736)



Hit 4/Z03 (Z1359552843)

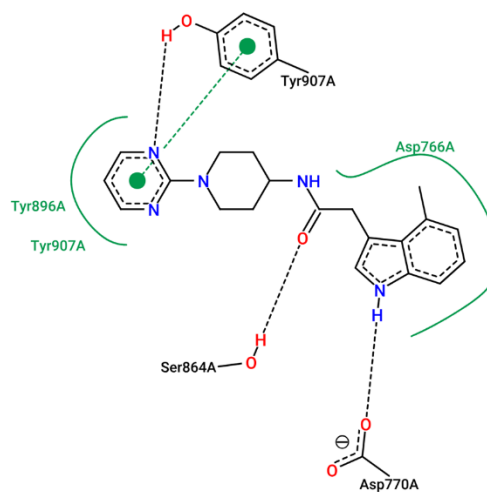
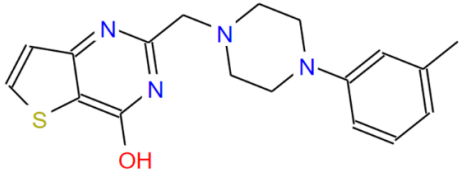
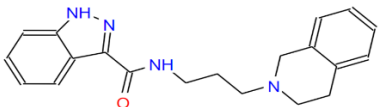
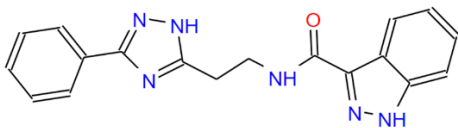
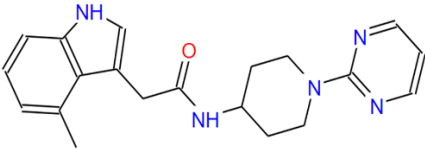


Figure 31: Chemical Structures and interactions of the top hits from PARP1 inhibitory study. Dashes indicate bond formation with red elements being hydrogen bond acceptors, blue elements hydrogen bond donors, and green dots indicating π - π stacking formation, and green, solid lines indicating Van der Waals interactions, and minus symbol indication ionic interactions.

Table 7: The IC₅₀ values of selected hits, chemical structure, and heterocyclic ring classification

Compound	IC ₅₀ (μM)	Structure	Heterocyclic Ring
Z195904178 [Hit 17]	5.3518		Thienopyrimidine
Z372757196 [Hit 10]	6.3031		Benzopyrazole Isoquinoline
Z1695739736 [Hit 24]	7.4533		Benzopyrazole
Z1359552843 [Hit 22]	1.4767		Indole Pyrimidine

Key

Hit	Color
17	Blue
10	Red
24	Green
22	Yellow

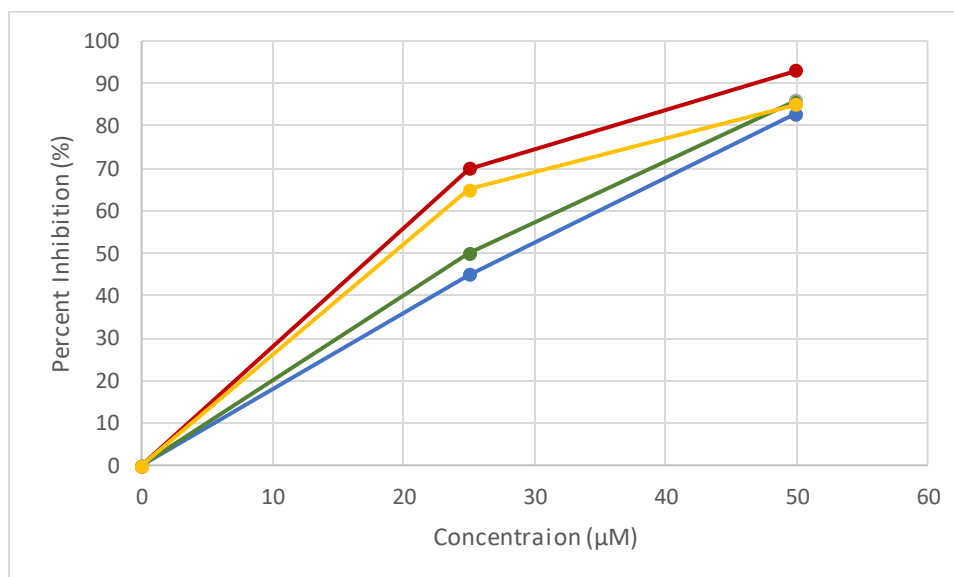
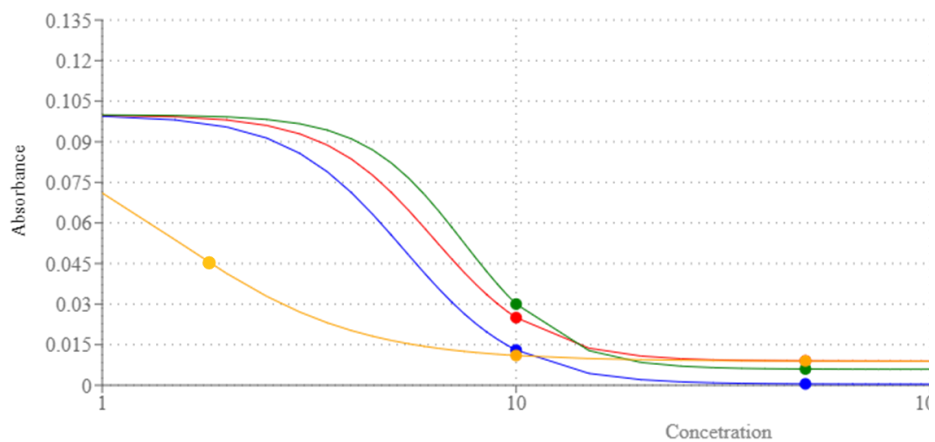


Figure 32: PARP1 inhibitory activity of selected hits

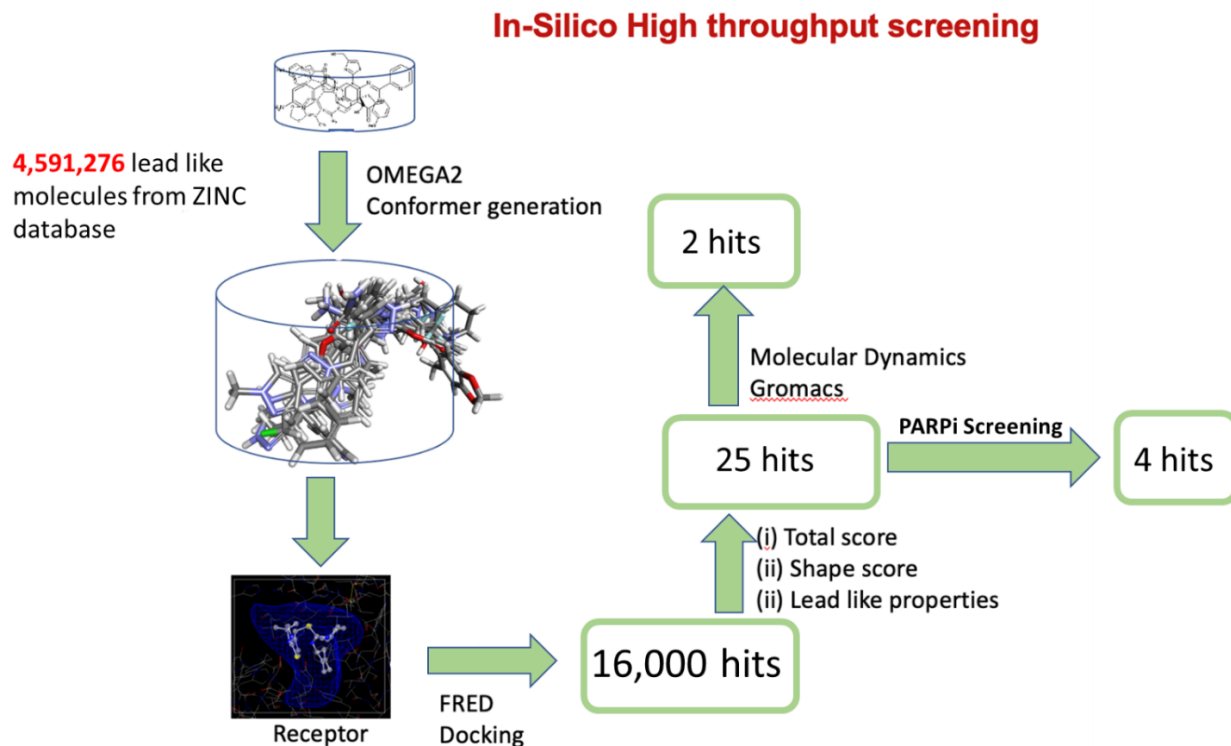


Figure 33: Summary of *In-Silico* High Throughput Screening Result

In summary, we started with 4.5 million lead-like compounds from the zinc database and used OMEGA2 to generate the most stable 3D conformers (figure 33). Using PARP1 5A00 pdb file the receptor file was generated by using Openeye's Make Receptor program. The results from the docking helped us determine our 25 hits chosen for further analysis. We selected five of our hits for molecular docking. We tested our 25 hits for their PARP1 inhibitory effect and categorized them based on percent inhibition. From both MD simulations and inhibitory analysis, we found that hit 22 showed the best results.

CHAPTER 5

SUMMARY AND CONCLUSION

The PARP-1 protein's crystal structure, which can be found in Figure 1, was taken from the protein data bank with the PDB ID 5A00. The ZINC database was used to compile a library of 4.59 million lead-like substances and for the receptors, hydrogen atoms and the missing residues were inserted. We have successfully computed the binding poses of the target with our selected ligands using FRED docking, which is used to accomplish rigid docking of ligands into the active site of the protein. 4.59 million lead-like chemicals were docked with the targets' active sites. The top five most stable conformations were identified, and the protein-ligand complex interaction sites were investigated. The five selected compounds are Hit 8 (Z01), Hit 2 (Z02), Hit 18 (Z03), Hit 22 (Z04), Hit 13 (Z05).

The Protein Data Bank (PDB) was used to obtain a high-resolution crystallographic structure of human PARP1-inhibitor bound. The PDB binding interactions were compared to FDA authorized inhibitors (Olaparib, Rucaparib, Niraparib, and Talazoparib). The interactions with the residues Gly863, Ser904, and Arg878 were critical for hydrogen bonding. Hydrogen bonding requires an inhibitor with an amide functional group. Ionic interactions were discovered with Glu763 and Asp766 residues. Tyr896, Tyr907, Tyr889, and Arg878 are Van der Waals interactions residues. There is also π - π stacking interaction between Tyr907's benzene ring and the inhibitor's aromatic ring. The findings of the commercially available PARP1 inhibitors were comparable. Rucaparib and Niraparib both demonstrated ionic interactions with Glu763 and Asp766.

Hits were classified based on their heterocyclic ring. Out of the 25 hits, benzopyrimidine and indole were the most common heterocyclic ring with nine hits having this ring. Benzopyrazole and phthalazine each had three hits, two isoquinolone analogs, two benzopyrimidine analogs, and one piperazine. These functional groups are important for deciding the types of bonds formed with PARP1.

We conducted molecular dynamics simulations. We analyzed five hits and got three hit molecular dynamics hits exhibited good RMSD, RMSF, Rg, and MM/PBSA values. The RMSD plot demonstrates that the complexes of PARP-1 with Hits 8, 2, and 22 were impressively stable throughout the simulation, with average RMSD values ranging between 1.7 and 1.9 nm. PARP-1 complexes with Hit 22 (Z04) and Hit 13 (Z05), like the reference structure, have remained stable, with RMSD values of 0.2 nm. According to the RMSD results, the binding of these two drugs to PARP-1 is continuous. The average RMSF values of all PARP-1 complexes range from 0.10 to 0.13 nm. Since the RMSF values of the complexes do not significantly differ from one another, we draw the conclusion that they were all effectively stabilized throughout the MD simulation. All systems were found to have Rg values that were coherent with the RMSF system. This reveals that over the entire 100 ns, the protein-ligand complexes were stable and compressed. The H-bonding analysis of all the complexes shows that Hit 8 (Z01) and Hit 18 (Z03) have generated several H-bonded interactions with PARP-1, compared to the number of interactions formed by the other compounds, which is fewer in number.

Due to its strong vdW, electrostatic, and polar energies, Hit 22 (Z04) possesses the highest binding affinity to PARP-1, measuring -19.6 kcal/mol. Hit 2 (Z02) and Hit 18 (Z03) have a greater affinity for PARP-1 with an energy of -18.1 kcal/mol, and Z05 has an energy of 17.8 kcal/mol due to the predominating vdW, electrostatic, and polar energies. Z01 has the lowest binding energy to PARP-1, which is -12.6 kcal/mol.

Out of the top 25 hits, four hits showed strong inhibitory activity against PARP1 (Table 4 and 5). Twelve of the inhibitors had moderate inhibition of PARP1. Of the four strong inhibitors, two (Hit 10 and Hit 22) are benzopyrazole analogs. The benzopyrazole ring provides an amide group for hydrogen bonding and an aromatic ring for the π - π stacking interaction. Hit 22, which had good results in the molecular dynamics study, has ionic interactions with Asp770.

The IC_{50} values of the strong inhibitors were calculated, and the values are noted in Table 6. Hit 22 has the best IC_{50} value of 1.4767 μ M. The chemical structure of Hit 22 has not been reported for a PARP1 inhibitor, making its scaffold novel. Hit 22 was the only hit from the molecular dynamics studies that also showed strong inhibition in the colorimetric assay. This difference in results could be for several reasons. There could be differences because of the nature of the study. Preliminary analysis using virtual high throughput screening can vary depending on the programs used. Furthermore, molecular dynamics looks at the binding stability of the inhibitory complex and the backbone stability of the enzyme. Just because the binding is good does not equate with biological effect. Also, other reasons like the solubility of the hit, accuracy of the colorimetric kit, or the stability could affect the results. The PARP1 colorimetric test revealed Hit 22 also showed strong inhibition and has an IC_{50} value of 1.4767 μ M and is a good hit for hit to lead studies and lead optimization.

REFERENCES

- Aberle, L., Krüger, A., Reber, J. M., Lippmann, M., Hufnagel, M., Schmalz, M., Trussina, I. R. E. A., Schlesiger, S., Zubel, T., Schütz, K., Marx, A., Hartwig, A., Ferrando-May, E., Bürkle, A., & Mangerich, A. (2020). PARP1 catalytic variants reveal branching and chain length-specific functions of poly(ADP-ribose) in cellular physiology and stress response. *Nucleic Acids Research*, *48*(18), 10015–10033. <https://doi.org/10.1093/nar/gkaa590>
- Abeti, R., & Duchon, M. R. (2012). Activation of PARP by Oxidative Stress Induced by β -Amyloid: Implications for Alzheimer's Disease. *Neurochemical Research*, *37*(11), 2589–2596. <https://doi.org/10.1007/s11064-012-0895-x>
- Ai, L., Xu, A., & Xu, J. (2020). Roles of PD-1/PD-L1 Pathway: Signaling, Cancer, and Beyond. In J. Xu (Ed.), *Regulation of Cancer Immune Checkpoints: Molecular and Cellular Mechanisms and Therapy* (pp. 33–59). Springer. https://doi.org/10.1007/978-981-15-3266-5_3
- Alemasova, E. E., & Lavrik, O. I. (2019). Poly(ADP-ribosyl)ation by PARP1: Reaction mechanism and regulatory proteins. *Nucleic Acids Research*, *47*(8), 3811–3827. <https://doi.org/10.1093/nar/gkz120>
- Andrikopoulou, A., Zografos, E., Apostolidou, K., Kyriazoglou, A., Papatheodoridi, A.-M., Kaparelou, M., Koutsoukos, K., Liontos, M., Dimopoulos, M.-A., & Zagouri, F. (2022). Germline and somatic variants in ovarian carcinoma: A next-generation sequencing (NGS) analysis. *Frontiers in Oncology*, *12*, 1030786. <https://doi.org/10.3389/fonc.2022.1030786>
- Arimont, M., Sun, S.-L., Leurs, R., Smit, M., de Esch, I. J. P., & de Graaf, C. (2017). Structural Analysis of Chemokine Receptor–Ligand Interactions. *Journal of Medicinal Chemistry*, *60*(12), 4735–4779. <https://doi.org/10.1021/acs.jmedchem.6b01309>

- Arruri, V. K., Gundu, C., Khan, I., Khatri, D. K., & Singh, S. B. (2021). PARP overactivation in neurological disorders. *Molecular Biology Reports*, *48*(3), 2833–2841. <https://doi.org/10.1007/s11033-021-06285-1>
- Augustin, A., Spenlehauer, C., Dumond, H., Ménissier-De Murcia, J., Piel, M., Schmit, A.-C., Apiou, F., Vonesch, J.-L., Kock, M., Bornens, M., & De Murcia, G. (2003). PARP-3 localizes preferentially to the daughter centriole and interferes with the G1/S cell cycle progression. *Journal of Cell Science*, *116*(Pt 8), 1551–1562. <https://doi.org/10.1242/jcs.00341>
- Azbazdar, Y., Karabici, M., Erdal, E., & Ozhan, G. (2021). Regulation of Wnt Signaling Pathways at the Plasma Membrane and Their Misregulation in Cancer. *Frontiers in Cell and Developmental Biology*, *9*. <https://www.frontiersin.org/articles/10.3389/fcell.2021.631623>
- Baig, M. H., Ahmad, K., Roy, S., Ashraf, J. M., Adil, M., Siddiqui, M. H., Khan, S., Kamal, M. A., Provazník, I., & Choi, I. (2016). Computer Aided Drug Design: Success and Limitations. *Current Pharmaceutical Design*, *22*(5), 572–581. <https://doi.org/10.2174/1381612822666151125000550>
- Banerjee, S., Gonzalez-Martin, A., Harter, P., Lorusso, D., Moore, K. N., Oaknin, A., & Ray-Coquard, I. (2020). First-line PARP inhibitors in ovarian cancer: Summary of an ESMO Open - Cancer Horizons round-table discussion. *ESMO Open*, *5*(6), e001110. <https://doi.org/10.1136/esmoopen-2020-001110>
- Barati, S., Fabrizio, C., Strafella, C., Cascella, R., Caputo, V., Megalizzi, D., Peconi, C., Mela, J., Colantoni, L., Caltagirone, C., Termine, A., & Giardina, E. (2022). Relationship between Nutrition, Lifestyle, and Neurodegenerative Disease: Lessons from ADH1B, CYP1A2 and MTHFR. *Genes*, *13*(8), 1498. <https://doi.org/10.3390/genes13081498>
- Barbarulo, A., Iansante, V., Chaidos, A., Naresh, K., Rahemtulla, A., Franzoso, G., Karadimitris, A., Haskard, D. O., Papa, S., & Bubici, C. (2013). Poly(ADP-ribose) polymerase family member 14

- (PARP14) is a novel effector of the JNK2-dependent pro-survival signal in multiple myeloma. *Oncogene*, 32(36), Article 36. <https://doi.org/10.1038/onc.2012.448>
- Barchiesi, G., Roberto, M., Verrico, M., Vici, P., Tomao, S., & Tomao, F. (2021). Emerging Role of PARP Inhibitors in Metastatic Triple Negative Breast Cancer. Current Scenario and Future Perspectives. *Frontiers in Oncology*, 11, 769280. <https://doi.org/10.3389/fonc.2021.769280>
- Berx, G., & Roy, F. van. (2009). Involvement of Members of the Cadherin Superfamily in Cancer. *Cold Spring Harbor Perspectives in Biology*, 1(6), a003129. <https://doi.org/10.1101/cshperspect.a003129>
- Bhowmick, N. A., Neilson, E. G., & Moses, H. L. (2004). Stromal fibroblasts in cancer initiation and progression. *Nature*, 432(7015), Article 7015. <https://doi.org/10.1038/nature03096>
- Blagg, J., & Workman, P. (2014). Chemical biology approaches to target validation in cancer. *Current Opinion in Pharmacology*, 17, 87–100. <https://doi.org/10.1016/j.coph.2014.07.007>
- Boehler, C., Gauthier, L. R., Mortusewicz, O., Biard, D. S., Saliou, J.-M., Bresson, A., Sanglier-Cianferani, S., Smith, S., Schreiber, V., Boussin, F., & Dantzer, F. (2011). Poly(ADP-ribose) polymerase 3 (PARP3), a newcomer in cellular response to DNA damage and mitotic progression. *Proceedings of the National Academy of Sciences of the United States of America*, 108(7), 2783–2788. <https://doi.org/10.1073/pnas.1016574108>
- Boraei, A. T. A., Singh, P. K., Sechi, M., & Satta, S. (2019). Discovery of novel functionalized 1,2,4-triazoles as PARP-1 inhibitors in breast cancer: Design, synthesis and antitumor activity evaluation. *European Journal of Medicinal Chemistry*, 182, 111621. <https://doi.org/10.1016/j.ejmech.2019.111621>
- Buch-Larsen, S. C., Hendriks, I. A., Lodge, J. M., Rykær, M., Furtwängler, B., Shishkova, E., Westphall, M. S., Coon, J. J., & Nielsen, M. L. (2020). Mapping Physiological ADP-Ribosylation Using Activated

Ion Electron Transfer Dissociation. *Cell Reports*, 32(12), 108176.

<https://doi.org/10.1016/j.celrep.2020.108176>

Burkhardt, D. L., & Sage, J. (2008). Cellular mechanisms of tumour suppression by the retinoblastoma gene. *Nature Reviews Cancer*, 8(9), Article 9. <https://doi.org/10.1038/nrc2399>

Cancer Statistics—NCI (nciglobal,ncienterprise). (2015, April 2). [CgvArticle].

<https://www.cancer.gov/about-cancer/understanding/statistics>

Challa, S., Khulpateea, B. R., Nandu, T., Camacho, C. V., Ryu, K. W., Chen, H., Peng, Y., Lea, J. S., & Kraus, W. L. (2021). Ribosome ADP-ribosylation inhibits translation and maintains proteostasis in cancers. *Cell*, 184(17), 4531-4546.e26. <https://doi.org/10.1016/j.cell.2021.07.005>

Chang, H., Jung, W., Kim, A., Kim, H. K., Kim, W. B., Kim, J. H., & Kim, B. (2017). Expression and prognostic significance of programmed death protein 1 and programmed death ligand-1, and cytotoxic T lymphocyte-associated molecule-4 in hepatocellular carcinoma. *APMIS*, 125(8), 690–698.

<https://doi.org/10.1111/apm.12703>

Cho, S. H., Ahn, A. K., Bhargava, P., Lee, C.-H., Eischen, C. M., McGuinness, O., & Boothby, M. (2011). Glycolytic rate and lymphomagenesis depend on PARP14, an ADP ribosyltransferase of the B aggressive lymphoma (BAL) family. *Proceedings of the National Academy of Sciences*, 108(38), 15972–15977. <https://doi.org/10.1073/pnas.1017082108>

Choi, Y., Abdelmegeed, M. A., & Song, B.-J. (2017). Diet high in fructose promotes liver steatosis and hepatocyte apoptosis in C57BL/6J female mice: Role of disturbed lipid homeostasis and increased oxidative stress. *Food and Chemical Toxicology*, 103, 111–121.

<https://doi.org/10.1016/j.fct.2017.02.039>

Choo, A. Y., Kim, S. G., Vander Heiden, M. G., Mahoney, S. J., Vu, H., Yoon, S.-O., Cantley, L. C., & Blenis, J. (2010). Glucose Addiction of TSC Null Cells Is Caused by Failed mTORC1-Dependent Balancing

of Metabolic Demand with Supply. *Molecular Cell*, 38(4), 487–499.

<https://doi.org/10.1016/j.molcel.2010.05.007>

De Bono, J. S., Hussain, M., Thiery-Vuillemin, A., Mateo, J., Sartor, A. O., Chi, K. N., Fizazi, K., Twardowski, P., Agarwal, N., Sandhu, S. K., Olmos, D., Shore, N. D., Saad, F., Liu, S., Goessl, C. D., & Burgents, J. (2017). PROfound: A randomized Phase III trial evaluating olaparib in patients with metastatic castration-resistant prostate cancer and a deleterious homologous recombination DNA repair aberration. *Journal of Clinical Oncology*, 35(15_suppl), TPS5091–TPS5091.

https://doi.org/10.1200/JCO.2017.35.15_suppl.TPS5091

Demény, M. A., & Virág, L. (2021). The PARP Enzyme Family and the Hallmarks of Cancer Part 1. Cell Intrinsic Hallmarks. *Cancers*, 13(9), 2042. <https://doi.org/10.3390/cancers13092042>

DeNardo, D. G., & Ruffell, B. (2019). Macrophages as regulators of tumour immunity and immunotherapy. *Nature Reviews Immunology*, 19(6), Article 6. <https://doi.org/10.1038/s41577-019-0127-6>

Deshpande, A., Sicinski, P., & Hinds, P. W. (2005). Cyclins and cdks in development and cancer: A perspective. *Oncogene*, 24(17), Article 17. <https://doi.org/10.1038/sj.onc.1208618>

Domagala, P., Huzarski, T., Lubinski, J., Gugala, K., & Domagala, W. (2011). PARP-1 expression in breast cancer including BRCA1-associated, triple negative and basal-like tumors: Possible implications for PARP-1 inhibitor therapy. *Breast Cancer Research and Treatment*, 127(3), 861–869.

<https://doi.org/10.1007/s10549-011-1441-2>

Doman, T. N., McGovern, S. L., Witherbee, B. J., Kasten, T. P., Kurumbail, R., Stallings, W. C., Connolly, D. T., & Shoichet, B. K. (2002). Molecular Docking and High-Throughput Screening for Novel Inhibitors of Protein Tyrosine Phosphatase-1B. *Journal of Medicinal Chemistry*, 45(11), 2213–2221. <https://doi.org/10.1021/jm010548w>

- Du, T., Zhang, Z., Zhou, J., Sheng, L., Yao, H., Ji, M., Xu, B., & Chen, X. (2022). A Novel PARP Inhibitor YHP-836 For the Treatment of BRCA-Deficiency Cancers. *Frontiers in Pharmacology*, *13*, 865085. <https://doi.org/10.3389/fphar.2022.865085>
- Entzeroth, M., Flotow, H., & Condrón, P. (2009). Overview of high-throughput screening. *Current Protocols in Pharmacology*, Chapter 9, Unit 9.4. <https://doi.org/10.1002/0471141755.ph0904s44>
- Farmer, H., McCabe, N., Lord, C. J., Tutt, A. N. J., Johnson, D. A., Richardson, T. B., Santarosa, M., Dillon, K. J., Hickson, I., Knights, C., Martin, N. M. B., Jackson, S. P., Smith, G. C. M., & Ashworth, A. (2005). Targeting the DNA repair defect in BRCA mutant cells as a therapeutic strategy. *Nature*, *434*(7035), 917–921. <https://doi.org/10.1038/nature03445>
- Fernández-Marcelo, T., Gómez, A., Pascua, I., de Juan, C., Head, J., Hernando, F., Jarabo, J. -R., Calatayud, J., Torres-García, A.-J., & Iniesta, P. (2015). Telomere length and telomerase activity in non-small cell lung cancer prognosis: Clinical usefulness of a specific telomere status. *Journal of Experimental & Clinical Cancer Research: CR*, *34*(1), 78. <https://doi.org/10.1186/s13046-015-0195-9>
- Ferreira, L. G., Dos Santos, R. N., Oliva, G., & Andricopulo, A. D. (2015). Molecular docking and structure-based drug design strategies. *Molecules (Basel, Switzerland)*, *20*(7), 13384–13421. <https://doi.org/10.3390/molecules200713384>
- Franceschi, C., Garagnani, P., Morsiani, C., Conte, M., Santoro, A., Grignolio, A., Monti, D., Capri, M., & Salvioli, S. (2018). The Continuum of Aging and Age-Related Diseases: Common Mechanisms but Different Rates. *Frontiers in Medicine*, *5*. <https://www.frontiersin.org/articles/10.3389/fmed.2018.00061>
- Frantz, C., Stewart, K. M., & Weaver, V. M. (2010). The extracellular matrix at a glance. *Journal of Cell Science*, *123*(24), 4195–4200. <https://doi.org/10.1242/jcs.023820>

- Fu, M., Hu, Y., Lan, T., Guan, K.-L., Luo, T., & Luo, M. (2022). The Hippo signalling pathway and its implications in human health and diseases. *Signal Transduction and Targeted Therapy*, 7(1), Article 1. <https://doi.org/10.1038/s41392-022-01191-9>
- Geyer, C. E., Garber, J. E., Gelber, R. D., Yothers, G., Taboada, M., Ross, L., Rastogi, P., Cui, K., Arahmani, A., Aktan, G., Armstrong, A. C., Arnedos, M., Balmaña, J., Bergh, J., Bliss, J., Delaloge, S., Domchek, S. M., Eisen, A., Elsayf, F., ... Cho, E. K. (2022). Overall survival in the OlympiA phase III trial of adjuvant olaparib in patients with germline pathogenic variants in BRCA1/2 and high-risk, early breast cancer. *Annals of Oncology*, 33(12), 1250–1268. <https://doi.org/10.1016/j.annonc.2022.09.159>
- Ghafouri-Fard, S., Khoshbakht, T., Hussen, B. M., Dong, P., Gassler, N., Taheri, M., Baniahmad, A., & Dilmaghani, N. A. (2022). A review on the role of cyclin dependent kinases in cancers. *Cancer Cell International*, 22, 325. <https://doi.org/10.1186/s12935-022-02747-z>
- Gibson, B. A., & Kraus, W. L. (2012). New insights into the molecular and cellular functions of poly(ADP-ribose) and PARPs. *Nature Reviews Molecular Cell Biology*, 13(7), 411–424. <https://doi.org/10.1038/NRM3376>
- Gomez, M., Wu, J., Schreiber, V., Dunlap, J., Dantzer, F., Wang, Y., & Liu, Y. (2006). PARP1 is a TRF2-associated poly(ADP-ribose) polymerase and protects eroded telomeres. *Molecular Biology of the Cell*, 17(4), 1686–1696. <https://doi.org/10.1091/mbc.e05-07-0672>
- Greten, F. R., & Grivennikov, S. I. (2019). Inflammation and Cancer: Triggers, Mechanisms, and Consequences. *Immunity*, 51(1), 27–41. <https://doi.org/10.1016/j.immuni.2019.06.025>
- Grivennikov, S. I., Greten, F. R., & Karin, M. (2010). Immunity, Inflammation, and Cancer. *Cell*, 140(6), 883–899. <https://doi.org/10.1016/j.cell.2010.01.025>
- Guo, C., Zhang, F., Wu, X., Yu, X., Wu, X., Shi, D., & Wang, L. (2020). BTH-8, a novel poly (ADP-ribose) polymerase-1 (PARP-1) inhibitor, causes DNA double-strand breaks and exhibits anticancer

- activities in vitro and in vivo. *International Journal of Biological Macromolecules*, *150*, 238–245.
<https://doi.org/10.1016/j.ijbiomac.2020.02.069>
- Guo, T., Zuo, Y., Qian, L., Liu, J., Yuan, Y., Xu, K., Miao, Y., Feng, Q., Chen, X., Jin, L., Zhang, L., Dong, C., Xiong, S., & Zheng, H. (2019). ADP-ribosyltransferase PARP11 modulates the interferon antiviral response by mono-ADP-ribosylating the ubiquitin E3 ligase β -TrCP. *Nature Microbiology*, *4*(11), Article 11. <https://doi.org/10.1038/s41564-019-0428-3>
- Gupta, R., Srivastava, D., Sahu, M., Tiwari, S., Ambasta, R. K., & Kumar, P. (2021). Artificial intelligence to deep learning: Machine intelligence approach for drug discovery. *Molecular Diversity*, *25*(3), 1315–1360. <https://doi.org/10.1007/s11030-021-10217-3>
- Hanahan, D., & Weinberg, R. A. (2011). Hallmarks of Cancer: The Next Generation. *Cell*, *144*(5), 646–674.
<https://doi.org/10.1016/j.cell.2011.02.013>
- Hayat, R., Manzoor, M., & Hussain, A. (2022). Wnt signaling pathway: A comprehensive review. *Cell Biology International*, *46*(6), 863–877. <https://doi.org/10.1002/cbin.11797>
- He, J.-X., Wang, M., Huan, X.-J., Chen, C.-H., Song, S.-S., Wang, Y.-Q., Liao, X.-M., Tan, C., He, Q., Tong, L.-J., Wang, Y.-T., Li, X.-H., Su, Y., Shen, Y.-Y., Sun, Y.-M., Yang, X.-Y., Chen, Y., Gao, Z.-W., Chen, X.-Y., ... Miao, Z.-H. (2016). Novel PARP1/2 inhibitor mefuparib hydrochloride elicits potent in vitro and in vivo anticancer activity, characteristic of high tissue distribution. *Oncotarget*, *8*(3), 4156–4168. <https://doi.org/10.18632/oncotarget.13749>
- Hottiger, M. O., Hassa, P. O., Lüscher, B., Schüler, H., & Koch-Nolte, F. (2010). Toward a unified nomenclature for mammalian ADP-ribosyltransferases. *Trends in Biochemical Sciences*, *35*(4), 208–219. <https://doi.org/10.1016/j.tibs.2009.12.003>
- Hughes, J., Rees, S., Kalindjian, S., & Philpott, K. (2011). Principles of early drug discovery. *British Journal of Pharmacology*, *162*(6), 1239–1249. <https://doi.org/10.1111/j.1476-5381.2010.01127.x>

- Hurvitz, S. A., Gonçalves, A., Rugo, H. S., Lee, K.-H., Fehrenbacher, L., Mina, L. A., Diab, S., Blum, J. L., Chakrabarti, J., Elmeliegy, M., DeAnnuntis, L., Gauthier, E., Czibere, A., Tudor, I. C., Quek, R. G. W., Litton, J. K., & Ettl, J. (2020). Talazoparib in Patients with a Germline BRCA-Mutated Advanced Breast Cancer: Detailed Safety Analyses from the Phase III EMBRACA Trial. *The Oncologist*, 25(3), e439–e450. <https://doi.org/10.1634/theoncologist.2019-0493>
- Jackson, S. P., & Bartek, J. (2009). The DNA-damage response in human biology and disease. *Nature*, 461(7267), Article 7267. <https://doi.org/10.1038/nature08467>
- Jiménez, C., Hernández, C., Pimentel, B., & Carrera, A. C. (2002). The p85 Regulatory Subunit Controls Sequential Activation of Phosphoinositide 3-Kinase by Tyr Kinases and Ras*. *Journal of Biological Chemistry*, 277(44), 41556–41562. <https://doi.org/10.1074/jbc.M205893200>
- Jubin, T., Kadam, A., Jariwala, M., Bhatt, S., Sutariya, S., Gani, A. R., Gautam, S., & Begum, R. (2016). The PARP family: Insights into functional aspects of poly (ADP-ribose) polymerase-1 in cell growth and survival. *Cell Proliferation*, 49(4), 421–437. <https://doi.org/10.1111/cpr.12268>
- Kallingal, A., Olszewski, M., Maciejewska, N., Brankiewicz, W., & Baginski, M. (2023). Cancer immune escape: The role of antigen presentation machinery. *Journal of Cancer Research and Clinical Oncology*. <https://doi.org/10.1007/s00432-023-04737-8>
- Kanai, M., Uchida, M., Hanai, S., Uematsu, N., Uchida, K., & Miwa, M. (2000). Poly(ADP-ribose) polymerase localizes to the centrosomes and chromosomes. *Biochemical and Biophysical Research Communications*, 278(2), 385–389. <https://doi.org/10.1006/bbrc.2000.3801>
- Karplus, M., & McCammon, J. A. (2002). Molecular dynamics simulations of biomolecules. *Nature Structural Biology*, 9(9), Article 9. <https://doi.org/10.1038/nsb0902-646>
- Karpova, Y., Wu, C., Divan, A., McDonnell, M. E., Hewlett, E., Makhov, P., Gordon, J., Ye, M., Reitz, A., Childers, W. E., Skorski, T., Kolenko, V., & Tulin, A. V. (2019). Non-NAD-like PARP-1 inhibitors in

- prostate cancer treatment. *Biochemical Pharmacology*, *167*, 149–162.
<https://doi.org/10.1016/j.bcp.2019.03.021>
- Kastan, M. B. (2008). DNA Damage Responses: Mechanisms and Roles in Human Disease: 2007 G.H.A. Clowes Memorial Award Lecture. *Molecular Cancer Research*, *6*(4), 517–524.
<https://doi.org/10.1158/1541-7786.MCR-08-0020>
- Kirby, I. T., Sanderson, D. J., & Cohen, M. S. (2021). PASTA: PARP activity screening and inhibitor testing assay. *STAR Protocols*, *2*(1), 100344. <https://doi.org/10.1016/j.xpro.2021.100344>
- Koelman, E. M. R., Yeste-Vázquez, A., & Grossmann, T. N. (2022). Targeting the interaction of β -catenin and TCF/LEF transcription factors to inhibit oncogenic Wnt signaling. *Bioorganic & Medicinal Chemistry*, *70*, 116920. <https://doi.org/10.1016/j.bmc.2022.116920>
- Koni, M., Pinnarò, V., & Brizzi, M. F. (2020). The Wnt Signalling Pathway: A Tailored Target in Cancer. *International Journal of Molecular Sciences*, *21*(20), Article 20.
<https://doi.org/10.3390/ijms21207697>
- Kraus, W. L. (2015). PARPs and ADP-Ribosylation: 50 Years ... and Counting. *Molecular Cell*, *58*(6), 902–910. <https://doi.org/10.1016/j.molcel.2015.06.006>
- Kumar, V., Kumar, A., Mir, K. U. I., Yadav, V., & Chauhan, S. S. (2021). Pleiotropic role of PARP1: An overview. *3 Biotech*, *12*(1), 3. <https://doi.org/10.1007/s13205-021-03038-6>
- Kwon, Y., Vinayagam, A., Sun, X., Dephoure, N., Gygi, S. P., Hong, P., & Perrimon, N. (2013). The Hippo Signaling Pathway Interactome. *Science*, *342*(6159), 737–740.
<https://doi.org/10.1126/science.1243971>
- Lee, M., Je, I.-G., Kim, J. E., Yoo, Y., Lim, J.-H., Jang, E., Lee, Y., Song, D. K., Moon, A.-N., Kim, J.-A., Jeong, J., Park, J.-T., Lee, J. W., Yang, J.-H., Hong, C.-H., Park, S.-Y., Park, Y.-W., Baek, N. S., Lee, S., ... Lee, W. S. (2023). Venadaparib Is a Novel and Selective PARP Inhibitor with Improved

- Physicochemical Properties, Efficacy, and Safety. *Molecular Cancer Therapeutics*, 22(3), 333–342. <https://doi.org/10.1158/1535-7163.MCT-22-0068>
- Lemmon, M. A., & Schlessinger, J. (2010). Cell Signaling by Receptor Tyrosine Kinases. *Cell*, 141(7), 1117–1134. <https://doi.org/10.1016/j.cell.2010.06.011>
- Lheureux, S., Gourley, C., Vergote, I., & Oza, A. M. (2019). Epithelial ovarian cancer. *Lancet (London, England)*, 393(10177), 1240–1253. [https://doi.org/10.1016/S0140-6736\(18\)32552-2](https://doi.org/10.1016/S0140-6736(18)32552-2)
- Li, H., Liu, Z.-Y., Wu, N., Chen, Y.-C., Cheng, Q., & Wang, J. (2020). PARP inhibitor resistance: The underlying mechanisms and clinical implications. *Molecular Cancer*, 19(1), 107. <https://doi.org/10.1186/s12943-020-01227-0>
- Li, Y., Li, Y., Huang, S., He, K., Zhao, M., Lin, H., Li, D., Qian, J., Zhou, C., Chen, Y., & Huang, C. (2017). Long non-coding RNA growth arrest specific transcript 5 acts as a tumour suppressor in colorectal cancer by inhibiting interleukin-10 and vascular endothelial growth factor expression. *Oncotarget*, 8(8), 13690–13702. <https://doi.org/10.18632/oncotarget.14625>
- Lipinski, C. A., Lombardo, F., Dominy, B. W., & Feeney, P. J. (1997). Experimental and computational approaches to estimate solubility and permeability in drug discovery and development settings. *Advanced Drug Delivery Reviews*, 23(1), 3–25. [https://doi.org/10.1016/S0169-409X\(96\)00423-1](https://doi.org/10.1016/S0169-409X(96)00423-1)
- Liu, P., Cheng, H., Roberts, T. M., & Zhao, J. J. (2009). Targeting the phosphoinositide 3-kinase (PI3K) pathway in cancer. *Nature Reviews. Drug Discovery*, 8(8), 627–644. <https://doi.org/10.1038/nrd2926>
- Lord, C. J., & Ashworth, A. (2017). PARP inhibitors: Synthetic lethality in the clinic. *Science (New York, N.Y.)*, 355(6330), 1152–1158. <https://doi.org/10.1126/science.aam7344>
- Miricescu, D., Totan, A., Stanescu-Spinu, I.-I., Badoiu, S. C., Stefani, C., & Greabu, M. (2020). PI3K/AKT/mTOR Signaling Pathway in Breast Cancer: From Molecular Landscape to Clinical

Aspects. *International Journal of Molecular Sciences*, 22(1), 173.

<https://doi.org/10.3390/ijms22010173>

Mukhopadhyay, P., Horváth, B., Rajesh, M., Varga, Z. V., Gariani, K., Ryu, D., Cao, Z., Holovac, E., Park, O., Zhou, Z., Xu, M.-J., Wang, W., Godlewski, G., Paloczi, J., Nemeth, B. T., Persidsky, Y., Liaudet, L., Haskó, G., Bai, P., ... Pacher, P. (2017). PARP inhibition protects against alcoholic and non-alcoholic steatohepatitis. *Journal of Hepatology*, 66(3), 589–600.

<https://doi.org/10.1016/j.jhep.2016.10.023>

Palavalli Parsons, L. H., Challa, S., Gibson, B. A., Nandu, T., Stokes, M. S., Huang, D., Lea, J. S., & Kraus, W. L. (2021). Identification of PARP-7 substrates reveals a role for MARYlation in microtubule control in ovarian cancer cells. *ELife*, 10, e60481. <https://doi.org/10.7554/eLife.60481>

Papaliagkas, V., Anogianaki, A., Anogianakis, G., & Ilonidis, G. (2007). The proteins and the mechanisms of apoptosis: A mini-review of the fundamentals. *Hippokratia*, 11(3), 108–113.

PARP1 Chemiluminescent Assay Kit. (n.d.). Retrieved December 8, 2023, from

<https://bpsbioscience.com/parp1-chemiluminescent-assay-kit-80551>

Putri, J. F., Bhargava, P., Dhanjal, J. K., Yaguchi, T., Sundar, D., Kaul, S. C., & Wadhwa, R. (2019).

Mortaparib, a novel dual inhibitor of mortalin and PARP1, is a potential drug candidate for ovarian and cervical cancers. *Journal of Experimental & Clinical Cancer Research : CR*, 38, 499.

<https://doi.org/10.1186/s13046-019-1500-9>

Qin, W., Wu, H.-J., Cao, L.-Q., Li, H.-J., He, C.-X., Zhao, D., Xing, L., Li, P.-Q., Jin, X., & Cao, H.-L. (2019).

Research Progress on PARP14 as a Drug Target. *Frontiers in Pharmacology*, 10, 172.

<https://doi.org/10.3389/fphar.2019.00172>

Rasmussen, M., Tan, S., Somisetty, V. S., Hutin, D., Olafsen, N. E., Moen, A., Anonsen, J. H., Grant, D. M., & Matthews, J. (2021). PARP7 and Mono-ADP-Ribosylation Negatively Regulate Estrogen

Receptor α Signaling in Human Breast Cancer Cells. *Cells*, 10(3), Article 3.

<https://doi.org/10.3390/cells10030623>

Richard, I. A., Burgess, J. T., O'Byrne, K. J., & Bolderson, E. (2022). Beyond PARP1: The Potential of Other Members of the Poly (ADP-Ribose) Polymerase Family in DNA Repair and Cancer Therapeutics. *Frontiers in Cell and Developmental Biology*, 9.

<https://www.frontiersin.org/articles/10.3389/fcell.2021.801200>

Rozario, T., & DeSimone, D. W. (2010). The extracellular matrix in development and morphogenesis: A dynamic view. *Developmental Biology*. <https://doi.org/10.1016/j.ydbio.2009.10.026>

Rudolph, J., Roberts, G., & Luger, K. (2021). Histone Parylation factor 1 contributes to the inhibition of PARP1 by cancer drugs. *Nature Communications* 2021 12:1, 12(1), 1–11.

<https://doi.org/10.1038/s41467-021-20998-8>

Sakthivel, S., & Habeeb, S. K. M. (2018). *Journal of Biomolecular Structure and Dynamics Combined pharmacophore, virtual screening and molecular dynamics studies to identify Bruton's tyrosine kinase inhibitors Combined pharmacophore, virtual screening and molecular dynamics studies to identify Bruton's tyrosine kinase inhibitors*. <https://doi.org/10.1080/07391102.2017.1415821>

Sasidharan Nair, V., & Elkord, E. (2018). Immune checkpoint inhibitors in cancer therapy: A focus on T-regulatory cells. *Immunology & Cell Biology*, 96(1), 21–33. <https://doi.org/10.1111/imcb.1003>

Shah, S., Rachmat, R., Enyoma, S., Ghose, A., Revythis, A., & Boussios, S. (2021). BRCA Mutations in Prostate Cancer: Assessment, Implications and Treatment Considerations. *International Journal of Molecular Sciences*, 22(23), 12628. <https://doi.org/10.3390/ijms222312628>

Sherr, C. J., & McCormick, F. (2002). The RB and p53 pathways in cancer. *Cancer Cell*, 2(2), 103–112.

[https://doi.org/10.1016/S1535-6108\(02\)00102-2](https://doi.org/10.1016/S1535-6108(02)00102-2)

- Shukla, S., Saxena, S., Singh, B. K., & Kakkar, P. (2017). BH3-only protein BIM: An emerging target in chemotherapy. *European Journal of Cell Biology*, *96*(8), 728–738.
<https://doi.org/10.1016/j.ejcb.2017.09.002>
- Siegel, R. L., Miller, K. D., Fuchs, H. E., & Jemal, A. (2022). Cancer statistics, 2022. *CA: A Cancer Journal for Clinicians*, *72*(1), 7–33. <https://doi.org/10.3322/caac.21708>
- Siegel, R. L., Miller, K. D., Wagle, N. S., & Jemal, A. (2023). Cancer statistics, 2023. *CA: A Cancer Journal for Clinicians*, *73*(1), 17–48. <https://doi.org/10.3322/caac.21763>
- Simbulan-Rosenthal, C. M., Rosenthal, D. S., Boulares, A. H., Hickey, R. J., Malkas, L. H., Coll, J. M., & Smulson, M. E. (1998). Regulation of the expression or recruitment of components of the DNA synthesome by poly(ADP-ribose) polymerase. *Biochemistry*, *37*(26), 9363–9370.
<https://doi.org/10.1021/bi9731089>
- Smith, S., & De Lange, T. (1999). Cell cycle dependent localization of the telomeric PARP, tankyrase, to nuclear pore complexes and centrosomes. *Journal of Cell Science*, *112*(21), 3649–3656.
<https://doi.org/10.1242/jcs.112.21.3649>
- Stewart, M. D., Merino Vega, D., Arend, R. C., Baden, J. F., Barbash, O., Beaubier, N., Collins, G., French, T., Ghahramani, N., Hinson, P., Jelinic, P., Marton, M. J., McGregor, K., Parsons, J., Ramamurthy, L., Sausen, M., Sokol, E. S., Stenzinger, A., Stires, H., ... Allen, J. (2022). Homologous Recombination Deficiency: Concepts, Definitions, and Assays. *The Oncologist*, *27*(3), 167–174.
<https://doi.org/10.1093/oncolo/oyab053>
- Sun, X., Zhang, Y., Chu, M., Wang, L., Shen, H., Zhang, Z., Hu, J., Yi, W., Yang, W., & Ma, X. (2018). PARP6 acts as an oncogene and positively regulates Survivin in gastric cancer. *International Journal of Clinical and Experimental Pathology*, *11*(5), 2364–2371.
- Talazoparib: MedlinePlus Drug Information*. (n.d.). Retrieved August 25, 2023, from <https://medlineplus.gov/druginfo/meds/a618070.html>

- Tian, C., Wei, Y., Li, J., Huang, Z., Wang, Q., Lin, Y., Lv, X., Chen, Y., Fan, Y., Sun, P., Xiang, R., Chang, A., & Yang, S. (2022). A Novel CDK4/6 and PARP Dual Inhibitor ZC-22 Effectively Suppresses Tumor Growth and Improves the Response to Cisplatin Treatment in Breast and Ovarian Cancer. *International Journal of Molecular Sciences*, 23(5), 2892. <https://doi.org/10.3390/ijms23052892>
- Tice, R. R., Agurell, E., Anderson, D., Burlinson, B., Hartmann, A., Kobayashi, H., Miyamae, Y., Rojas, E., Ryu, J. C., & Sasaki, Y. F. (2000). Single cell gel/comet assay: Guidelines for in vitro and in vivo genetic toxicology testing. *Environmental and Molecular Mutagenesis*, 35(3), 206–221. [https://doi.org/10.1002/\(sici\)1098-2280\(2000\)35:3<206::aid-em8>3.0.co;2-j](https://doi.org/10.1002/(sici)1098-2280(2000)35:3<206::aid-em8>3.0.co;2-j)
- Torretta, A., Chatzicharalampous, C., Ebenwaldner, C., & Schüler, H. (2023). PARP14 is a writer, reader, and eraser of mono-ADP-ribosylation. *Journal of Biological Chemistry*, 299(9). <https://doi.org/10.1016/j.jbc.2023.105096>
- Tuncel, H., Tanaka, S., Oka, S., Nakai, S., Fukutomi, R., Okamoto, M., Ota, T., Kaneko, H., Tatsuka, M., & Shimamoto, F. (2012). PARP6, a mono(ADP-ribosyl) transferase and a negative regulator of cell proliferation, is involved in colorectal cancer development. *International Journal of Oncology*, 41(6), 2079–2086. <https://doi.org/10.3892/ijo.2012.1652>
- Vyas, S., Chesarone-Cataldo, M., Todorova, T., Huang, Y.-H., & Chang, P. (2013). A systematic analysis of the PARP protein family identifies new functions critical for cell physiology. *Nature Communications*, 4(1), Article 1. <https://doi.org/10.1038/ncomms3240>
- Vyas, S. (Sejal K. (2014). *Cellular functions and enzymatic activity of the poly(ADP-ribose) polymerase protein family* [Thesis, Massachusetts Institute of Technology]. <https://dspace.mit.edu/handle/1721.1/87464>
- Walters, W. P. (2012). Going further than Lipinski's rule in drug design. *Expert Opinion on Drug Discovery*, 7(2), 99–107. <https://doi.org/10.1517/17460441.2012.648612>

- Wang, L., Zhang, S., Yu, X., & Guo, C. (2020). Novel Poly(ADP-ribose) Polymerase-1 Inhibitor DDHCB Inhibits Proliferation of BRCA Mutant Breast Cancer Cell In Vitro and In Vivo through a Synthetic Lethal Mechanism. *Chemical Research in Toxicology*, 33(7), 1874–1881.
<https://doi.org/10.1021/acs.chemrestox.0c00087>
- Wang, T., Zhang, D., Guo, C., & Zhu, W. (2022). Novel PARP Inhibitor DDPF-20 Induces DNA Damage and Inhibits Angiogenesis through the PI3K/Akt/VEGF Pathway. *Anti-Cancer Agents in Medicinal Chemistry- Anti-Cancer Agents*, 22(13), 2468–2476.
<https://doi.org/10.2174/1871520622666220221115007>
- Wang, Z., Grosskurth, S. E., Cheung, T., Petteruti, P., Zhang, J., Wang, X., Wang, W., Gharahdaghi, F., Wu, J., Su, N., Howard, R. T., Mayo, M., Widzowski, D., Scott, D. A., Johannes, J. W., Lamb, M. L., Lawson, D., Dry, J. R., Lyne, P. D., ... Chen, H. (2018). Pharmacological Inhibition of PARP6 Triggers Multipolar Spindle Formation and Elicits Therapeutic Effects in Breast Cancer. *Cancer Research*, 78(23), 6691–6702. <https://doi.org/10.1158/0008-5472.CAN-18-1362>
- Warshel, A. (2002). Molecular Dynamics Simulations of Biological Reactions. *Accounts of Chemical Research*, 35(6), 385–395. <https://doi.org/10.1021/ar010033z>
- Welsby, I., Hutin, D., Gueydan, C., Kruys, V., Rongvaux, A., & Leo, O. (2014). PARP12, an Interferon-stimulated Gene Involved in the Control of Protein Translation and Inflammation *. *Journal of Biological Chemistry*, 289(38), 26642–26657. <https://doi.org/10.1074/jbc.M114.589515>
- Yabroff, K. R., Wu, X.-C., Negoita, S., Stevens, J., Coyle, L., Zhao, J., Mumphrey, B. J., Jemal, A., & Ward, K. C. (2022). Association of the COVID-19 Pandemic With Patterns of Statewide Cancer Services. *JNCI: Journal of the National Cancer Institute*, 114(6), 907–909.
<https://doi.org/10.1093/jnci/djab122>
- Yu, M., Schreek, S., Cerni, C., Schamberger, C., Lesniewicz, K., Poreba, E., Vervoorts, J., Walsemann, G., Grötzinger, J., Kremmer, E., Mehraein, Y., Mertsching, J., Kraft, R., Austen, M., Lüscher-Firzlaff, J.,

- & Lüscher, B. (2005). PARP-10, a novel Myc-interacting protein with poly(ADP-ribose) polymerase activity, inhibits transformation. *Oncogene*, *24*(12), Article 12.
<https://doi.org/10.1038/sj.onc.1208410>
- Yuan, B., Ye, N., Song, S.-S., Wang, Y.-T., Song, Z., Chen, H.-D., Chen, C.-H., Huan, X.-J., Wang, Y.-Q., Su, Y., Shen, Y.-Y., Sun, Y.-M., Yang, X.-Y., Chen, Y., Guo, S.-Y., Gan, Y., Gao, Z.-W., Chen, X.-Y., Ding, J., ... Miao, Z.-H. (2017). Poly(ADP-ribose)polymerase (PARP) inhibition and anticancer activity of simmiparib, a new inhibitor undergoing clinical trials. *Cancer Letters*, *386*, 47–56.
<https://doi.org/10.1016/j.canlet.2016.11.010>
- Yue, W., Zheng, X., Lin, Y., Yang, C. S., Xu, Q., Carpizo, D., Huang, H., DiPaola, R. S., & Tan, X.-L. (2015). Metformin combined with aspirin significantly inhibit pancreatic cancer cell growth in vitro and in vivo by suppressing anti-apoptotic proteins Mcl-1 and Bcl-2. *Oncotarget*, *6*(25), 21208–21224.
- Zhang, H., Dai, Z., Wu, W., Wang, Z., Zhang, N., Zhang, L., Zeng, W.-J., Liu, Z., & Cheng, Q. (2021). Regulatory mechanisms of immune checkpoints PD-L1 and CTLA-4 in cancer. *Journal of Experimental & Clinical Cancer Research*, *40*(1), 184. <https://doi.org/10.1186/s13046-021-01987-7>
- Zhang, Y., & Zheng, J. (2020). Functions of Immune Checkpoint Molecules Beyond Immune Evasion. In J. Xu (Ed.), *Regulation of Cancer Immune Checkpoints: Molecular and Cellular Mechanisms and Therapy* (pp. 201–226). Springer. https://doi.org/10.1007/978-981-15-3266-5_9
- Zhu, K., Wu, Y., He, P., Fan, Y., Zhong, X., Zheng, H., & Luo, T. (2022). PI3K/AKT/mTOR-Targeted Therapy for Breast Cancer. *Cells*, *11*(16), 2508. <https://doi.org/10.3390/cells11162508>